

# Mechanical behaviour of brain tissue for injury prediction : characterisaton and modelling

**Citation for published version (APA):**

Hrapko, M. (2008). *Mechanical behaviour of brain tissue for injury prediction : characterisaton and modelling*. [Phd Thesis 1 (Research TU/e / Graduation TU/e), Mechanical Engineering]. Technische Universiteit Eindhoven. <https://doi.org/10.6100/IR634775>

**DOI:**

[10.6100/IR634775](https://doi.org/10.6100/IR634775)

**Document status and date:**

Published: 01/01/2008

**Document Version:**

Publisher's PDF, also known as Version of Record (includes final page, issue and volume numbers)

**Please check the document version of this publication:**

- A submitted manuscript is the version of the article upon submission and before peer-review. There can be important differences between the submitted version and the official published version of record. People interested in the research are advised to contact the author for the final version of the publication, or visit the DOI to the publisher's website.
- The final author version and the galley proof are versions of the publication after peer review.
- The final published version features the final layout of the paper including the volume, issue and page numbers.

[Link to publication](#)

**General rights**

Copyright and moral rights for the publications made accessible in the public portal are retained by the authors and/or other copyright owners and it is a condition of accessing publications that users recognise and abide by the legal requirements associated with these rights.

- Users may download and print one copy of any publication from the public portal for the purpose of private study or research.
- You may not further distribute the material or use it for any profit-making activity or commercial gain
- You may freely distribute the URL identifying the publication in the public portal.

If the publication is distributed under the terms of Article 25fa of the Dutch Copyright Act, indicated by the "Taverne" license above, please follow below link for the End User Agreement:

[www.tue.nl/taverne](http://www.tue.nl/taverne)

**Take down policy**

If you believe that this document breaches copyright please contact us at:

[openaccess@tue.nl](mailto:openaccess@tue.nl)

providing details and we will investigate your claim.

**Mechanical behaviour of brain tissue  
for injury prediction:  
characterisation and modelling**

Matej Hrapko

This research was conducted within the APROSYS Integrated Project supported by the European Commission.

CIP-DATA LIBRARY TECHNISCHE UNIVERSITEIT EINDHOVEN

Hrapko, Matej

Mechanical behaviour of brain tissue for injury prediction:  
characterisation and modelling

Eindhoven University of Technology, 2008.  
Proefschrift.

A catalogue record is available from the Eindhoven University of Technology Library.  
ISBN: 978-90-386-1268-3

Copyright © 2008 by Matej Hrapko. All rights reserved.

This thesis is prepared with  $\text{\LaTeX}$  2 $\epsilon$

Cover design: Martijn Sanders, Matej Hrapko and Michelle Tjelpa – *OranjeVormgevers.nl*

Picture on cover: Mark Hess – *HessDesignWorks.com*

Printed by the Universiteitsdrukkerij TU Eindhoven, Eindhoven, The Netherlands.

**Mechanical behaviour of brain tissue  
for injury prediction:  
characterisation and modelling**

Proefschrift

ter verkrijging van de graad van doctor  
aan de Technische Universiteit Eindhoven,  
op gezag van de Rector Magnificus, prof.dr.ir. C.J. van Duijn,  
voor een commissie aangewezen door het College voor Promoties  
in het openbaar te verdedigen op  
maandag 2 juni 2008 om 16.00 uur

door

**Matej Hrapko**

geboren te Bratislava, Slowakije

Dit proefschrift is goedgekeurd door de promotor:

prof.dr.ir. J.S.H.M. Wismans

Copromotoren:

dr.ir. G.W.M. Peters

en

dr.ir. J.A.W. van Dommelen

# Contents

---

<b>Summary</b>	<b>ix</b>
<b>Notation</b>	<b>xi</b>
<b>I Introduction</b>	<b>I</b>
I.1 Head injury . . . . .	I
I.2 Head and brain anatomy . . . . .	I
I.3 Head injury criteria . . . . .	2
I.4 Objective . . . . .	4
I.5 Outline of thesis . . . . .	5
<b>2 Influence of test conditions</b>	<b>7</b>
2.1 Introduction . . . . .	8
2.2 Materials and methods . . . . .	11
2.2.1 Effect of temperature . . . . .	12
2.2.2 Differences caused by anisotropy . . . . .	13
2.2.3 Effect of compression prior to shear measurements . . . . .	14
2.3 Results . . . . .	14
2.3.1 Effect of temperature . . . . .	14
2.3.2 Differences caused by anisotropy . . . . .	15
2.3.3 Effect of compression prior to shear measurements . . . . .	17
2.4 Discussion and conclusions . . . . .	18
2.A Overview of experimental studies . . . . .	20
<b>3 Effects of post-mortem time and sample preparation</b>	<b>25</b>
3.1 Introduction . . . . .	26
3.2 Materials and methods . . . . .	26
3.3 Results . . . . .	30
3.4 Discussion and conclusions . . . . .	31
<b>4 Characterisation in shear</b>	<b>33</b>
4.1 Introduction . . . . .	34
4.2 Materials and methods . . . . .	35

4.3	Results . . . . .	37
4.4	Constitutive model . . . . .	39
4.5	Model application . . . . .	42
4.6	Discussion and conclusions . . . . .	44
<b>5</b>	<b>Validation in compression</b>	<b>47</b>
5.1	Introduction . . . . .	48
5.2	Materials and methods . . . . .	49
5.2.1	Effect of test conditions . . . . .	50
5.2.2	Effect of friction . . . . .	51
5.2.3	Model validation . . . . .	51
5.3	Results . . . . .	52
5.3.1	Effect of test conditions . . . . .	52
5.3.2	Effect of friction . . . . .	53
5.3.3	Model validation . . . . .	56
5.4	Discussion and conclusions . . . . .	57
5.A	Summary of results from compression experiments . . . . .	59
<b>6</b>	<b>Influence of constitutive modelling in a 3D head model</b>	<b>61</b>
6.1	Introduction . . . . .	62
6.2	Methods . . . . .	63
6.2.1	Effect of the skull-brain interface conditions . . . . .	63
6.2.2	Effect of different constitutive models . . . . .	66
6.3	Results . . . . .	66
6.3.1	Effect of the skull-brain interface conditions . . . . .	66
6.3.2	Effect of different constitutive models . . . . .	69
6.4	Discussion and conclusions . . . . .	72
6.A	Model performances . . . . .	74
6.B	Influence of constitutive models for varying loading conditions . . . . .	74
<b>7</b>	<b>Effect of brain heterogeneity</b>	<b>77</b>
7.1	Introduction . . . . .	78
7.2	Materials and methods . . . . .	79
7.3	Results . . . . .	81
7.3.1	Strain fields . . . . .	81
7.3.2	Reproducibility . . . . .	86
7.4	Discussion and conclusions . . . . .	86
<b>8</b>	<b>Discussion, conclusions and recommendations</b>	<b>91</b>
8.1	Discussion and conclusions . . . . .	91
8.2	Recommendations . . . . .	94
<b>A</b>	<b>Finite element implementation</b>	<b>97</b>
A.1	Compressible viscoelastic model for brain tissue . . . . .	98
A.2	Numerical implementation . . . . .	101

---

<b>Samenvatting</b>	<b>II5</b>
<b>Bibliography</b>	<b>II5</b>
<b>Acknowledgements</b>	<b>II7</b>
<b>Curriculum Vitae</b>	<b>II9</b>





# Summary

---

## **Mechanical behaviour of brain tissue for injury prediction: characterisation and modelling**

The head is the most vulnerable part of the body during crash situations and is often involved in life-threatening injuries. To be able to understand and predict the deformation of brain tissue causing injuries, it is necessary to know the mechanical behaviour of brain tissue. A mathematical description of this behaviour can subsequently be used in Finite Element simulations to predict the mechanical response of the contents of the head to a prescribed loading history. The mechanical properties of brain tissue have been studied since the 1960's, however they are still not well understood. Moreover, results from different studies are orders of magnitude different.

The main objective of this study was to characterise the large strain mechanical behaviour of brain tissue for different deformation modes and to develop a constitutive model for this material to be used in finite element predictions of the response of the brain in crash situations. Furthermore, the influences of constitutive non-linearities of brain tissue in numerical head model simulations were investigated.

To characterise the linear and large strain viscoelastic response of brain tissue in different deformation modes, porcine brain tissue was chosen as a substitute for human brains because of the availability and the possibility to minimise the post-mortem time during testing. Both shear and compression experiments were performed on an ARES II rotational rheometer in a plate-plate configuration. For shear measurements, samples were placed eccentrically to increase the measured signal and to obtain an approximately homogeneous deformation.

The effects of different test conditions on the measured mechanical response of brain tissue were examined. Particularly, the effects of sample preparation, post-mortem time, temperature, pre-compression prior to shear measurements and differences caused by anisotropy were investigated. Also, the influence of a fluid layer surrounding the sample and the effect of friction were examined and were found to play an important role during compression measurements.

Subsequently, the response of brain tissue to large strain shear deformation has been

studied. No significant immediate mechanical damage was observed for shear deformation up to strains of 0.45. Moreover, the material behaviour during complex loading-unloading histories was characterised. Based on these experimental results, a new differential non-linear constitutive model has been developed. The model was validated using a data set obtained by combining measurements performed in shear and compression for the same samples.

A compressible version of the constitutive model is implemented in the crash simulation code MADYMO, using an explicit integration procedure. Simulations are performed using the newly developed non-linear version of the constitutive model, a simplified version of this model and a non-linear model from literature within a three-dimensional finite element head model, to investigate the sensitivity of closed head impact simulations to the incorporation of constitutive non-linearities for brain tissue.

Furthermore, two-dimensional brain slice experiments have been conducted. In these experiments, a digital image correlation technique was used to obtain high-resolution field information. The experiments demonstrate the importance of the brain heterogeneity for the mechanical response of the brain and therefore for the mechanism of traumatic brain injury. This heterogeneity might be incorporated in the next generation of injury assessment tools.

# Notation

---

In the following definitions, a Cartesian coordinate system with unit vector base  $\{\vec{e}_1, \vec{e}_2, \vec{e}_3\}$  applies and following the Einstein summation convention, repeated indices are summed from 1 to 3.

## Quantities

scalar	$a$
vector	$\vec{a} = a_i \vec{e}_i$
tensor	$\mathbf{A} = A_{ij} \vec{e}_i \vec{e}_j$

## Operations

transpose	$\mathbf{A}^T = A_{ji} \vec{e}_i \vec{e}_j$
inverse	$\mathbf{A}^{-1}$
determinant	$\det(\mathbf{A}) = (\mathbf{A} \cdot \vec{e}_1) \cdot (\mathbf{A} \cdot \vec{e}_2) \times (\mathbf{A} \cdot \vec{e}_3)$
trace	$\text{tr}(\mathbf{A}) = \mathbf{A} : \vec{e}_i \vec{e}_i = A_{ii}$
isochoric part	$\tilde{\mathbf{A}} = \det(\mathbf{A})^{-\frac{1}{3}} \mathbf{A}$
deviatoric part	$\mathbf{A}^d = \mathbf{A} - \frac{1}{3} \text{tr}(\mathbf{A}) \mathbf{I}$
first invariant	$I_1 = \text{tr}(\mathbf{A})$
second invariant	$I_2 = \frac{1}{2} [\text{tr}(\mathbf{A})^2 - \text{tr}(\mathbf{A}^2)]$
third invariant	$I_3 = \det(\mathbf{A})$

---

time derivative	$\dot{A}$
multiplication	$c = ab$
	$\vec{c} = a\vec{b}$
	$\mathbf{C} = a\mathbf{B}$
dyadic product	$\mathbf{C} = \vec{a}\vec{b} = a_i b_j \vec{e}_i \vec{e}_j$
cross product	$\vec{c} = \vec{a} \times \vec{b}$
inner product	$c = \vec{a} \cdot \vec{b} = a_i b_i$
	$\mathbf{C} = \mathbf{A} \cdot \mathbf{B} = A_{ij} B_{jk} \vec{e}_i \vec{e}_k$
double inner product	$c = \mathbf{A} : \mathbf{B} = A_{ij} B_{ji}$

## CHAPTER ONE

# Introduction

---

### 1.1 Head injury

According to the World Health Organization approximately 1.2 million fatalities occur on the world's roads each year. Up to 50 million people sustain injuries, with many suffering from permanent disabilities [1]. More than one third of all injuries are traumatic brain injuries (TBI) which represent also one of the major causes of death resulting from traffic accidents [2]. Despite the major advances in prevention and treatment, head injury remains a major health and social problem.

TBI can be caused when the head is suddenly struck by an object with or without the object penetrating the skull and the brain. These injuries can be divided into primary injuries, which occur at the moment of impact, and secondary injuries, which develop at a later stage. The majority of brain injuries are caused by diffuse axonal injury (DAI) characterised by microscopic damage of axons. DAI can occur without any direct impact on the head, as it can be the result of rapid acceleration/deceleration. DAI is thought to be the most common and important pathology in mild, moderate, and severe traumatic brain injury [3]. It may develop over a period of hours or even a days after an accident.

### 1.2 Head and brain anatomy

The brain together with the spinal cord forms the central nervous system which controls and regulates all body activity. This makes the brain one of the most important parts of the body. The brain is enclosed by the pia mater and the arachnoid mater, which are separated from the dura mater, the skull and the skin, by a subarachnoid space that is filled by cerebrospinal fluid (CSF), see Figure 1.1. The brain consists of three main parts, the cerebrum, the cerebellum, and the brain stem which connects the brain to the spinal cord. The cerebrum is connected through the hypothalamus, thalamus, and brainstem

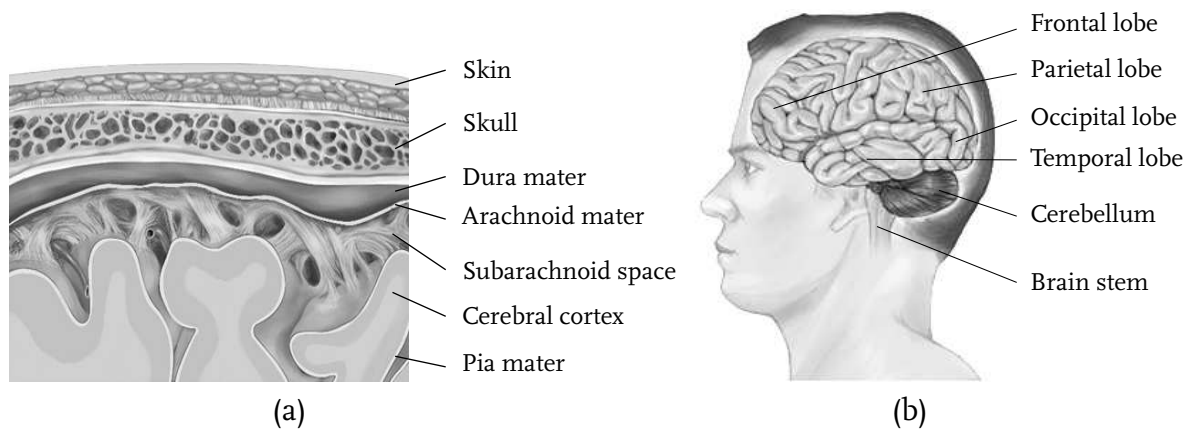


**Figure 1.1:** (a) Cross-section of the skull and the meninges, (b) main regions of the brain [4].

(midbrain, pons, and medulla oblongata) to the spinal cord, see Figure 1.2. The cerebrum consists mainly of the left and right cerebral hemisphere which are connected together by the corpus callosum. The cerebral hemispheres are separated by the falx cerebri which is an invagination of the dura mater. Each of these hemispheres has an outer layer of grey matter called the cerebral cortex that is supported by an inner layer of white matter called the corona radiata. Grey matter consists of nerve cell bodies (neurons), glial cells, capillaries, and short nerve cell extensions/processes (axons and dendrites). White matter is composed of myelinated nerve cell processes (axons), which connect various grey matter areas and carry nerve impulses between neurons [5].

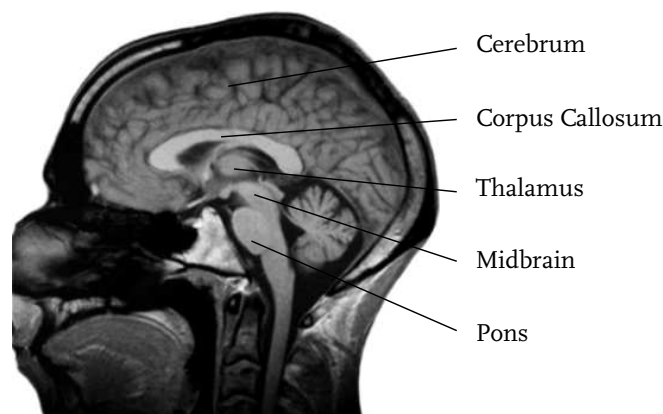


**Figure 1.2:** Cross-sectional image of the head obtained by magnetic resonance scanning [6].

### 1.3 Head injury criteria

The occurrence and consequences of TBI can be reduced by the development of improved injury protective measures. The application of macroscopic biomechanical models for

injury assessment has already led to a substantial decrease of head injuries. To assess the likelihood of head injury, in the early sixties, the Head Injury Criterion (HIC) was developed [7] based on the Wayne State Tolerance Curve [8]:

$$\text{HIC} = \left\{ (t_2 - t_1) \left( \frac{1}{t_2 - t_1} \int_{t_1}^{t_2} a(t) dt \right)^{2.5} \right\}_{\max} \quad (1.1)$$

in which  $a(t)$  denotes the translational head acceleration in g's as a function of time, and  $t_1$  and  $t_2$  represent the initial and final times of an interval that maximises this function. Although this criterion is still used in most current test standards, it suffers from a number of drawbacks, one of which is that it is based on linear head acceleration only. Moreover, it does not allow for a distinction between different injury mechanisms. Macroscopic head injury criteria which also account for rotational acceleration have been proposed as well, e.g. the Generalized Acceleration Model for Brain Injury Threshold (GAMBIT) [9] and Head Injury Power (HIP) [10,11]. All these macroscopic criteria provide a direct relation between the kinematics of the head and the possible occurrence of injury, as is schematically shown in Figure 1.3.

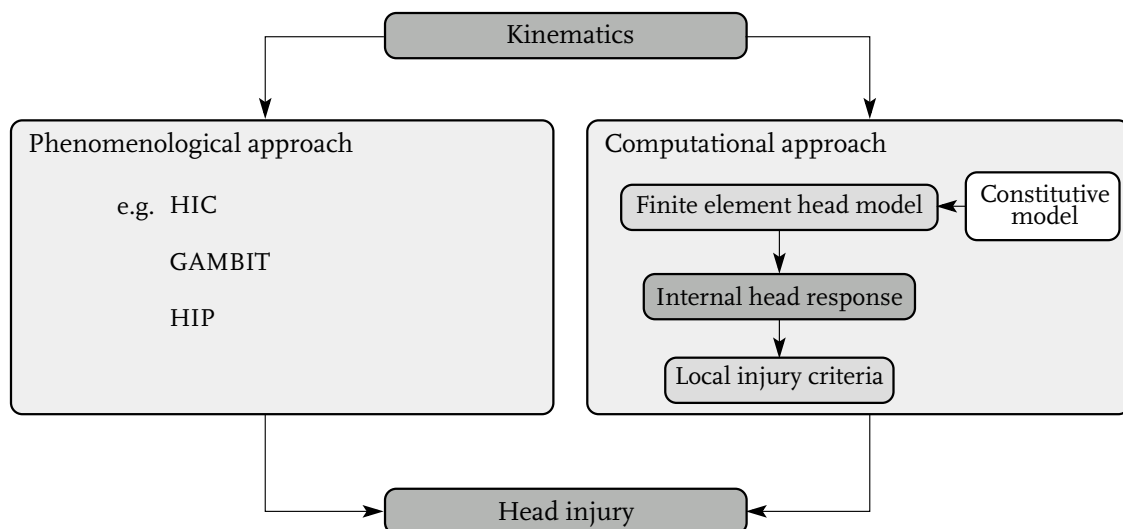


**Figure 1.3:** Assessment of brain injury by macroscopic and computational injury criteria.

Recent safety research focuses on so-called next-generation injury assessment tools for use in future regulations for injury protection devices. During a crash the head is exposed to external mechanical loading which causes an internal mechanical response of the brain tissue. Above a certain strain or a strain rate, damage of the brain tissue can occur. In order to predict the mechanical response of the contents of the head during impact, Finite Element (FE) models are being developed. The various aspects involved in the development of a finite element head model are shown in Figure 1.4. Current FE head models contain a somewhat detailed geometrical description of various anatomical components of the head but often lack accurate validated descriptions of the mechan-



ical behaviour of brain tissue. Without an accurate representation of the constitutive behaviour of the various components, the predictive capabilities of head models may be limited.

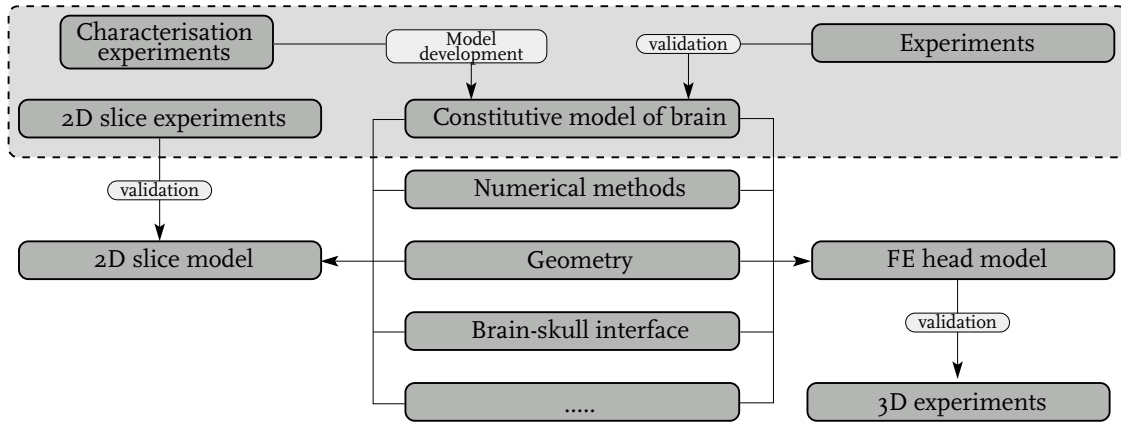


**Figure 1.4:** Schematic representation of various aspect involved in the development of a reliable finite elements head model. The dashed box indicates the aspects considered in this study.

Brain tissue has been studied with a variety of techniques and a number of constitutive models were proposed. However, large discrepancies exist in published data, which makes a comparison of results difficult. Consequently, up to now, no universally accepted data set for the constitutive response of brain tissue exists. Moreover, existing constitutive models were not validated to describe the influence of non-linear behaviour during complex loading histories and to describe the response to large deformations in different deformation modes. The ability of a constitutive model to describe this complex mechanical response may be important for reliable simulations of head injury. Therefore, a consistent data set involving large strains obtained from different deformation modes is required. Ideally, the same sample should be used for different deformation modes to reduce the effect of inter-sample variation. A material model, which is able to describe large deformations, complex loading histories, and different deformation modes is needed.

## 1.4 Objective

The main objective of this work was to characterise the large strain mechanical behaviour of brain tissue for different deformation modes and to develop a constitutive model for this material to be used in finite element predictions of the response of the brain in crash situations. To achieve this goal, the following aspects have been addressed:

- possible reasons for discrepancies found in literature,
- reliable testing protocols for different measurements,

- characterisation of the mechanical behaviour of brain tissue for large deformations, complex loading histories, and different deformation modes,
- development of a constitutive model for describing the non-linear viscoelastic behaviour of brain tissue for large deformations, complex loading histories, and different deformation modes,
- the influence of using different constitutive models for brain tissue when used in a 3-D FE head model,
- the effect of structural heterogeneities on the mechanical response of the brain for impact conditions.

## 1.5 Outline of thesis

In this thesis, an experimental study on the characterisation of the mechanical behaviour of brain tissue and a new constitutive model to describe this behaviour are presented. The role of this study in the development of a 3D finite element head model for injury assessment is schematically indicated in Figure 1.4.

In Chapter 2, an overview of studies on the mechanical properties of brain tissue is given, focusing on testing methods. The influence of some important test conditions (temperature, pre-compression, anisotropy) is experimentally determined for shear on porcine brain tissue. An improved method for rotational shear experiments was used producing an approximately homogeneous strain field and enhancing accuracy. Small strain oscillatory shear experiments were used to determine the linear mechanical behaviour of brain tissue in shear deformation. The effects of the sample preparation procedure and of post-mortem time on the mechanical response of brain tissue are examined in Chapter 3.

In Chapter 4, two types of large strain shear experiments are used to characterise the non-linear time-dependent mechanical behaviour of porcine brain tissue. Subsequently, a new non-linear viscoelastic material model in a differential framework, that is based on these experimental results, is presented.

In Chapter 5, the mechanical behaviour of porcine brain tissue in compressive deformation is examined. Two measurement protocols and two testing parameters affecting compression measurements are examined. A consistent data set containing the response to both compression and shear deformation is obtained for the same samples. These results are used to validate the non-linear viscoelastic constitutive model of brain tissue.

In Chapter 6, the influences of constitutive non-linearities of brain tissue in numerical head model simulations are investigated by comparing the performance of the newly developed non-linear constitutive model with its simplified version and with a previously developed constitutive model [12]. For this purpose, a head model with a sliding interface is used which is compared with a previously developed head model with a tied interface.

To assess the influence of heterogeneities in the brain, an experimental procedure is developed in which high-resolution strain fields in planar sections of brain tissue are

measured during translational acceleration in Chapter 7. The brain slices containing both grey and white matter as well as the complex folding structure are encapsulated in a cavity filled with artificial cerebrospinal fluid. This cavity with the enclosed slice is subjected to an acceleration of 80 - 100 g. By using a high-speed video camera and a digital image correlation technique, strain fields are obtained and Von Mises strains are calculated.

Finally, a discussion and conclusions drawn from this work as well as recommendations for future work are presented in Chapter 8.

In Appendix A a compressible version of the non-linear viscoelastic constitutive model developed in Chapter 4 is presented and the implementation of this model in an explicit FE code is discussed.

## CHAPTER TWO

Influence of test conditions<sup>I</sup>

---

**Abstract**

To understand brain injuries better, the mechanical properties of brain tissue have been studied for fifty years, however no universally accepted data set exists. The variation in material properties reported may be caused by differences in testing methods and protocols used. An overview of studies on the mechanical properties of brain tissue is given, focusing on testing methods. Moreover, the influence of important test conditions such as temperature, anisotropy and pre-compression was experimentally determined for shear deformation. Results measured at room temperature show a stiffer response than those measured at body temperature. By applying time-temperature superposition, a horizontal shift factor  $a_T = 8.5-11$  was found, which is in agreement with values found in literature. Anisotropy of samples from the corona radiata was investigated by measuring the shear resistance for different directions in the sagittal, the coronal and the transverse plane. Results measured in the coronal and the transverse plane were 1.3 and 1.25 times stiffer than results obtained from the sagittal plane. The variation caused by anisotropy within the same plane of individual samples was found to range from 25 to 54%. The effect of pre-compression on shear results was investigated and was found to stiffen the sample response. Combinations of these and other factors (post-mortem time, donor age, donor type, etc.) lead to large differences among different studies, depending on the different test conditions.

---

<sup>I</sup> *Reproduced from: M. Hrapko, J. A. W. van Dommelen, G. W. M. Peters, J. S. H. M. Wismans, (2008). The Influence of Test Conditions on Characterization of the Mechanical Properties of Brain Tissue. Journal of Biomechanical Engineering, 130(3).*

## 2.1 Introduction

Of all body parts, the head is the most vulnerable and is often involved in life-threatening injury [13]. To predict the mechanical response of the contents of the head during impact, FE models are employed. They contain a somewhat detailed geometrical description of anatomical components but lack accurate descriptions of the mechanical behaviour of the brain tissue. Since the early 1960's, researchers have been studying the material properties of brain tissue using a variety of testing techniques. The reported mechanical properties, such as the storage modulus ( $G'$ ) and loss modulus ( $G''$ ), describing linear viscoelastic behaviour are orders of magnitude different, see Figure 2.1. This may be caused by the broad range of testing methods and protocols used, which makes a comparison of results difficult. Several authors have presented an overview of available literature on the constitutive properties of brain tissue [14–17]. An overview of the methods and the conditions of materials tested in previous studies is given in Table 2.1. The studies were divided into groups depending on the type of experiment and are summarised in Table 2.6 and Table 2.7 in Appendix 2.A. In addition to these studies, some investigators have used techniques like magnetic resonance elastography [18–22] and ultrasound [23–27], however these are not included in the tables.

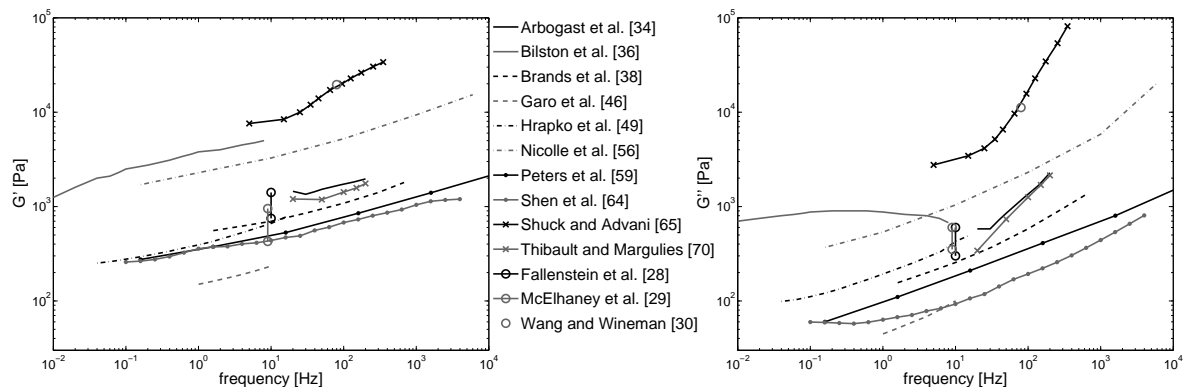


**Figure 2.1:** Summary of the linear viscoelastic properties of brain tissue reported in literature. Notice that Fallenstein et al. [28], McElhaney et al. [29] and Wang and Wineman [30] have reported data for one frequency only.

Animal brains are often used as a substitute for human brains. The main reasons are that animal brains are easily available and that the post-mortem time can be minimised. Human brains have been obtained from autopsies or lobotomies on epileptic patients. In the study of Prange and Margulies [63], human and porcine brain samples subjected to shear stress relaxation tests were compared. The human samples were on average 29% stiffer than the porcine samples. Takhounts et al. [68] found human brain tissue samples to be 40% stiffer than bovine samples in stress relaxation experiments. This conclusion was obtained from the linear stress relaxation function. In contrast, Nicolle et al. [56,57] concluded from dynamic frequency sweep tests that the storage modulus of porcine brain tissue was 17% higher than that of human brain tissue, whereas the loss modulus was

**Table 2.1:** Overview of previous studies on the mechanical properties of brain tissue.

	donor	state	region	load	test
Arbogast et al. [31–34]	PB	vtr	Bs,Cb,T,CR	S	DE,SR,CSR
Bilston et al. [35,36]	BB	vtr	CC	S	DE,SR,CSR
Brands et al. [37,38,12]	PB	vtr	T	S	DE,SR
Cheng and Bilston [39]	BB	vtr	CR	C	SR,CSR
Darvish and Crandall [40]	BB	vtr	CR	S	DE
Dodgson [41]	RMB	vtr	–	C	Cr
Donnelly and Medige [42]	HB	vtr	CC,Mb	S	CSR
Estes and McElhaney [43]	HB,MB	vtr	CR	C	CSR
Fallenstein et al. [28]	HB,MB	vv,vtr	Cb	S,C	DE,PI
Franceschini et al. [44]	HB	vtr	Cb,CC,T	T,C	CSR,Cr
Galford and McElhaney [45]	HB,MB	vtr	Cb	C	DE,SR,Cr
Garo et al. [46]	PB	vtr	T	S	DE,CSR
Gefen et al. [47,48]	PB,RMB	vv,vtr	CGM	C	PI
Hrapko et al. [49,50]	PB	vtr	CC	S,C	DE,SR,CSR
Koeneman [51]	RB,RMB,PB	vtr	Cb	C	DE,Cr
McElhaney et al. [29]	HB,MB	vv,vtr	Cb,CGM	S,C	DE,CSR,PI
Metz et al. [52]	MB	vv,vtr	CGM	C	ECE
Miller et al. [53–55]	PB	vv,vtr	Cb,CGM	C,T	CSR,PI
Nicolle et al. [56,57]	PB,HB	vtr	CR,T	S	DE,SR
Ning et al. [58]	PB	vtr	Bs	S	CSR,SR
Ommaya [14]	MB,CB	vtr	CGM	C	PI
Peters et al. [59]	BB	vtr	CR,Mb	S	DE,SR
Prange et al. [60–63]	PB,HB	vtr	CR,CC,T	S,C	SR
Shen et al. [64]	PB	vtr	Cb	S,C	DE,SR,CSR
Shuck and Advani [65]	HB	vtr	CR,T	S	DE
Velardi et al. [66]	PB	vtr	CR,CC,CGM	T	CSR
Takhounts et al. [67,68]	BB,HB	vtr	Cb	S	SR
Thibault and Margulies [69,70]	PB	vtr	Cb	S	DE
Wang and Wineman [30]	MB	vv,vtr	CGM	C	DE,PI

Donor: PB – porcine, BB – bovine, HB – human, RB – rabbit, RMB – rat or mouse, MB – monkey, CB – cat. State: vv – in vivo, vtr – in vitro. Loading condition: C – compression, S – shear, T – tension. Type of test: DE – dynamic experiment (strain/frequency sweep), SR – stress relaxation test, CSR – constant strain rate test, PI – probe indentation, Cr – creep, ECE – elastic cylinder expansion. Brain region: Cb – cerebrum (white and grey), CC – corpus callosum (white), CR – corona radiata (white), T – thalamus (grey), Mb – midbrain (grey), Bs – brainstem (grey), CGM – cortical grey matter.

similar in both materials. The differences between human and animal brains are often considered relatively small which enables animal brains to be a good substitute for human brains.

Some parts of the brain may show anisotropic behaviour because of the underlying microstructure. Whereas grey tissue was found to be nearly isotropic, white matter was found to be anisotropic with different degrees of anisotropy [63]. Based on its highly organised structure the most anisotropic region is expected to be the corpus callosum (white

matter). Arbogast et al. [31,34] tested the anisotropy of the brainstem in 2.5% strain dynamic frequency sweep experiments in three different orientations based on the fibre direction. The differences for dynamic moduli were found to be up to 30%. Prange et al. [62,63] identified the anisotropy of brain tissue at large strains (up to 50%) shear experiments on white and grey matter samples. White matter behaviour was more anisotropic (31–48% difference), while grey matter was nearly isotropic (12% difference). By studying inter-regional differences, grey matter from the thalamus was found to be approximately 40% and 12.5% stiffer than white matter from the corpus callosum and the corona radiata, respectively. Nicolle et al. [56,57] investigated anisotropy within the corona radiata (white matter). However, their observations did not allow any conclusion on the anisotropy.

Besides differences in the material tested, the test conditions also give rise to differences in the results. The method used to attach the sample to the plates of a setup for shear deformation can also have a role in the variation in results. Some authors [40,42,56,57,67,68] have used glue to attach samples to the plates, whereas others [32,34,31,35–38,12,49,46,61,63,60,62,69,70,64] have used a roughened surface (glass or sandpaper) to avoid slip. Arbogast et al. [31] and Brands et al. [38] have found no difference in results when either sandpaper or glue was used to fix the sample to the plates. On the other hand, Nicolle et al. [56,57] have found the dynamic modulus to be dependent on the sample thickness when the samples were not fixed, whereas no variation was achieved when samples were glued to the plates. A drawback of using the adhesive, is the unknown adhesive thickness. However, when a roughened surface is used the sample must be uniaxially loaded prior to the shear test which may affect the results of the shear measurements.

The tissue and also its mechanical properties may degenerate with increasing post-mortem time due to various reasons (e.g. autolytic processes, completion of rigor mortis, osmotic swelling, etc.). This degeneration effect may be temperature dependent in that the rate of degeneration possibly decreases with decreasing temperatures. Some authors [65,40,42,56,57,59,67,68] have tested samples days post-mortem, whereas others [34,70,38,36,63,49] within a few hours post-mortem. Metz et al. [52] have reported a 30–70% decrease of the tissue response to the inflation of a balloon catheter, from live to 3/4 hour post-mortem. No change of measured properties caused by higher post-mortem time was found by McElhaney et al. [29] up to 15 hours post-mortem and by Darvish and Crandall [40] in 3–16 days. Nicolle et al. [56,57] compared samples measured at 24 and 48 hours post-mortem and found only a 6% increase of dynamic modulus. Shen et al. [64] examined samples up to 7 days post-mortem, and reported only a small variation of the material properties. Garo et al. [46] found the onset of stiffening of the shear modulus by approximately 27 Pa/h to be after 6 hours post-mortem.

All of these aspects can have an effect on the mechanical properties measured and a combination of these and other aspects has led to a large variation of results reported in literature. In this study the effect of different test conditions on the mechanical response of brain tissue is examined. Specifically, the effect of different temperatures and the effect of pre-compression on linear and large strain results are examined. Also, differences caused by anisotropy are investigated for samples from the corona radiata in the sagittal,

the coronal, and the transverse plane. As opposed to previous studies, here the variation of mechanical properties for a full range of orientations ( $0^\circ$ – $360^\circ$ ) for shearing within certain planes of individual samples is studied. For this study, a new modification was made to the eccentric rheometric methodology developed by Van Turnhout et al. [71]. Each of these topics is investigated in otherwise comparable conditions.

## 2.2 Materials and methods

Brain halves were obtained from six months old pigs in a local slaughterhouse. To slow down their degradation and dehydration they were transported in a solution of Phosphate Buffered Saline (PBS) in a box filled with ice. Samples were prepared from tissue located in the corona radiata region within 3 hours after sacrifice. The post-mortem time was minimised to reduce sample degradation, see Chapter 3. Using a vibrating-blade microtome (Leica VT 1000S), approximately 2 mm thick slices were cut parallel to the plane of testing chosen. From these slices, samples with a diameter of 8 to 12 mm were cut out by a cork bore. Until the start of the tests, the samples were preserved in PBS at  $4^\circ\text{C}$ . The testing conditions for each topic of this study are summarised in Table 2.2.

**Table 2.2:** Experimental conditions for studying different aspects of testing brain tissue.

	Temperature [ $^\circ\text{C}$ ]	Testing plane	Normal force [mN]	Post-mortem time [h]	No. of samples
Temperature	7–37	sagittal	5	2–7	3
Anisotropy	23	sagittal, coronal transversal	5	2–7	5, 4 4
Pre-compression	23	sagittal	0–28	2–7	3

A rotational rheometer (ARES II, Advanced Rheometric Expansion System) with a 10GM FRT transducer was used to test the samples in shear. An eccentric test configuration was used [71] to improve the signal to noise ratio. In this configuration, the measured torque is increased and an approximately homogeneous shear field is obtained. Sandpaper was attached to the top and the bottom plate to prevent slipping of the samples. The height of the samples was estimated by lowering the top plate with constant velocity ( $\approx 0.008 \text{ mm s}^{-1}$ ) until touching the top of the sample and measuring a maximum axial force of 5 mN. During testing, a moist chamber was used to prevent dehydration of the sample and the temperature was controlled by a Peltier heat pump. Because of the heterogeneity of brain tissue, samples of small dimensions were used. Care was taken to test all samples in the same orientation (the shear direction corresponding to the anterior-posterior direction) to minimise any possible effect of anisotropy of the material on the properties measured, except for the study of anisotropy which is discussed further on.



Samples were tested in shear deformation in dynamic frequency sweep tests (DFS) and subsequently in stress relaxation tests (SR). It is important to notice that no preconditioning of samples was made prior to testing. However, all experiments started with a dynamic frequency sweep test. In these tests, the properties of brain tissue in the linear viscoelastic regime (which for brain tissue is limited to 1% strain [37,56]) were measured after a steady state was obtained. The tests consisted of a sinusoidal shear strain of 1% imposed on the sample, with a range of frequencies from 1 Hz to 10 Hz. For each frequency, the storage modulus  $G'$  and the loss modulus  $G''$  were determined. Subsequently, the same sample was subjected to a SR test which consisted of a ramp-and-hold test to a strain of 10%. The strain rate during the loading phase was  $1 \text{ s}^{-1}$  and the strain  $\gamma$  was held for 10 s during which the stress  $\tau$  was recorded from which the relaxation modulus  $G(t) = \tau(t)/\gamma$  was obtained. Afterwards, the strain was released with the same constant strain rate as in the loading phase. Then, the sample was left to recover for a period of at least 100 s during which the tissue response was recorded as well. This testing protocol was used to assess the effect of different experimental aspects. Therefore, for each aspect certain conditions were varied which will be discussed in subsequent sections.

### 2.2.1 Effect of temperature

Although the effect of temperature is an important issue, only few studies have been published in the literature [59,38,64]. Therefore, the purpose of this study is to determine the effect of temperature on the mechanical properties measured for brain tissue. Particularly important is the difference between room temperature (approximately  $23^\circ\text{C}$ ) and body temperature (approximately  $37^\circ\text{C}$ ), to be able to scale results obtained at those different conditions. In addition, the results can be used to extend the frequency/time range of measured data by applying time-temperature superposition.

Three samples from the posterior side of the corona radiata were measured at 37, 30, 23, 15, and  $7^\circ\text{C}$ . DFS tests and SR tests were conducted to obtain data in the linear and large strain regime, respectively. To characterise the temperature dependence of brain tissue time-temperature superposition (TTS) was applied. This method was previously used for brain tissue by Peters et al. [59], Brands et al. [38], and recently by Shen et al. [64]. For different temperatures, sets of isothermal characteristics were obtained within an equal frequency/time range. These characteristics were shifted along the frequency/time axis, to form a master curve. In the current study, the reference temperature  $T_0$  was chosen to be  $37^\circ\text{C}$ . The horizontal shift depends only on the difference between the reference temperature and the temperature of the shifted characteristic and can be described by the horizontal shift factor  $a_T(T, T_0)$  [72]. Besides the horizontal shift factor, also a vertical shift, characterised by the shift factor  $b_T(T, T_0)$  has to be applied. First, the horizontal shift factor  $a_T$  is determined from the phase angle  $\delta$ , only, to satisfy:

$$\delta(\omega, T) = \delta(a_T\omega, T_0). \quad (2.1)$$

After applying this shift to the dynamic modulus  $G^*$ , the vertical shift factor  $b_T$  is deter-

mined to satisfy:

$$G^*(\omega, T) = \frac{1}{b_T} G^*(a_T \omega, T_0). \quad (2.2)$$

In the case of the SR experiments, the shift factors are determined to satisfy:

$$G(t, T) = \frac{1}{b_T} G\left(\frac{t}{a_T}, T_0\right). \quad (2.3)$$

### 2.2.2 Differences caused by anisotropy

Samples from the corona radiata were tested in three planes (sagittal, coronal, transverse) in shear. The corona radiata region was chosen, because of easy sample preparation and the expected amount of anisotropy due to its structural organisation. In the sagittal plane, 5 samples were tested, whereas in the coronal and the transverse plane, 4 samples each were tested. To facilitate a change of the sample orientation during the measurement, the bottom plate of the rotational rheometer was extended with an additional rotating disc which was placed eccentrically, see Figure 2.2. The sample was placed in the cen-

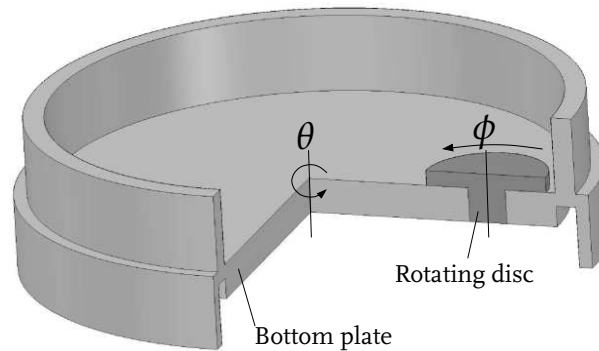


**Figure 2.2:** Eccentric test configuration. Samples are placed on an eccentric disc which can rotate to change the orientation  $\phi$  in order to study anisotropy. Shear strain is applied to the sample by an angular displacement  $\theta$  of the bottom plate. The upper wall of the plate is designed to carry a moist chamber whereas the lower wall provides the attachment to the original setup.

tre of this eccentric disc which can be rotated by an angle  $\phi$ , changing the orientation of the sample with respect to the shear direction. After each sequence of shear tests, the top plate was detached from the sample and the eccentric disc was rotated to a new orientation and subsequently fixed. Then, the top plate was lowered to the original height and a new sequence of shear tests was conducted. The order of orientation angles was randomly chosen so that eventually the range of  $0-360^\circ$  was covered by  $30^\circ$  increments. The first and last sequences of tests corresponded both with the zero degree orientation to observe any changes caused by post-mortem time. The whole set of shear measurements took up to one hour. The random way of varying orientations was chosen to enable

a separation of the time dependent changes from the measured orientation dependent properties. For this purpose, it was assumed that  $G(t, \phi) = C_t(t)G_\phi(\phi)$ . A linear function  $C_t(t) = (At + 1)$  was fitted to the data by a least-squares error method assuming  $G_\phi$  to be constant. Subsequently, the data was corrected for a possible post-mortem time dependence according to  $G_\phi(\phi) = G(t, \phi)/(At + 1)$ . Therefore, only data depending on the rotation angle  $\phi$  are presented.

### 2.2.3 Effect of compression prior to shear measurements

It is hypothesised that the compression force which has to be imposed to the sample prior to shear tests, affects the measured mechanical properties obtained for the material. To the author's knowledge, this effect was not studied in a systematical way before. To support the hypothesis, shear measurements were conducted on three samples with varying amounts of compression for each sample.

The height of each sample  $h_0$  was estimated during an initial constant strain rate compression test ( $\dot{h}/h_0 \approx 0.05 \text{ s}^{-1}$ ), starting without the top plate touching the sample. Before any compression started, the sample was loaded in tension due to its spontaneous adhesion to the top plate caused by a thin fluid layer. The height of each sample  $h_0$  was defined as the height where the normal force  $F_N$  was equal to zero. Due to viscoelastic behaviour of the material, this estimated sample height can be compression rate dependent. After each sequence of shear tests, the distance between the plates was decreased stepwise, causing the normal force  $F_N$  to increase. For each height, a DFS test and a SR test were performed as described in the general methodology section.

## 2.3 Results

### 2.3.1 Effect of temperature

The mean dynamic modulus and the mean phase angle obtained for three samples of brain tissue at  $23^\circ\text{C}$  and  $37^\circ\text{C}$  are shown in Figure 2.3. The maximum standard deviations are 30% for both quantities.

Measured results were found to be clearly temperature dependent with a horizontal shift factor  $a_T$  between  $23^\circ\text{C}$  and  $37^\circ\text{C}$  of up to 11, whereas the vertical shift factor  $b_T$  was close to one. Results for DFS tests and for SR tests at different temperatures in the range  $7\text{--}37^\circ\text{C}$  are given for an individual sample in Figure 2.4. These data have been used to obtain master curves for an extended range of frequencies and relaxation times, which are given in Figure 2.4 as well. For both tests, it is visible that stiffening of the sample response is obtained with decreasing temperature.

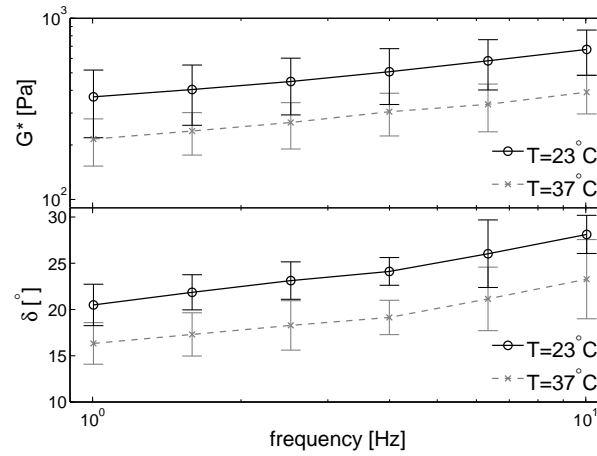


**Figure 2.3:** Dynamic modulus  $G^*$  and phase angle  $\delta$  for DFS tests at  $23^\circ\text{C}$  and  $37^\circ\text{C}$ .

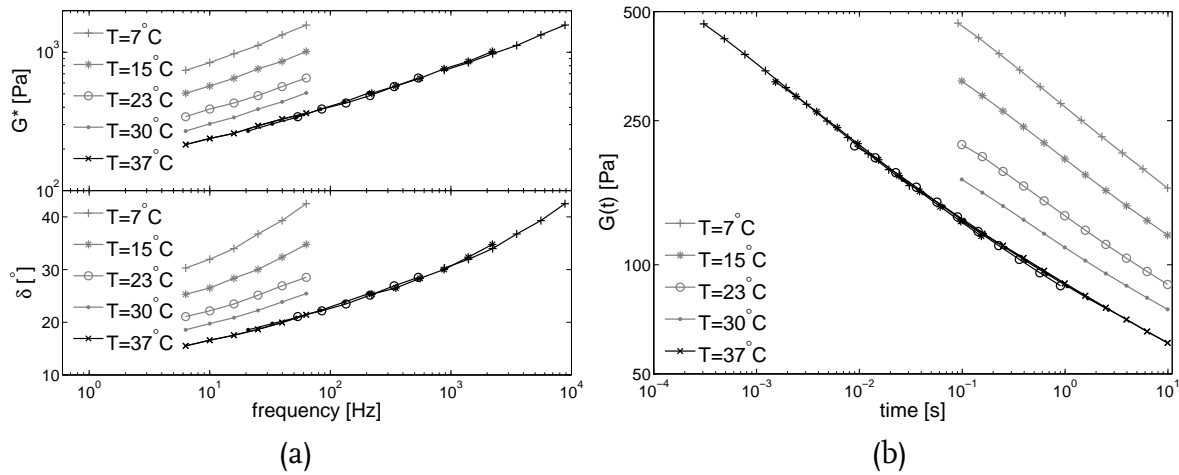


**Figure 2.4:** (a) Measured DFS data for one sample before applying TTS (grey lines) and master curve after applying TTS (black lines). (b) Measured SR data of 20% strain for one sample before applying TTS (grey lines) and master curve after applying TTS (black lines).

### 2.3.2 Differences caused by anisotropy

Anisotropy of brain tissue samples from the corona radiata was examined in the sagittal, the coronal, and the transverse plane by DFS and SR tests. Moreover, results are also compared among these planes. The variation caused by anisotropy for shear tests in different directions within the plane of testing was highest in the sagittal plane, whereas the smallest variation was found to be in the coronal plane, except for the relaxed response, see Table 2.3. By comparing the SR results it can be observed that the amount of anisotropy increases with strain, which is also observed by comparing SR (large strain) with DFS (small strain) results. In Figure 2.5a the results from a DFS test are given in a polar plot for one individual sample, whereas in Figure 2.5b the results from a SR test on the same sample are shown. In most cases, the shape of the measured stress response in a po-

**Table 2.3:** Anisotropy within different planes of testing. Average ratios of maximum and minimum response measured are given.

	No. of samples	DFS		SR		
		$G_{max}^*/G_{min}^*$		$G_{max}/G_{min}$		
		$f = 1 \text{ Hz}$	$f = 10 \text{ Hz}$	$\gamma = 4.5\%$	$\gamma = 8\%$	$t = 10 \text{ s}$
sagittal	5	1.40	1.38	1.44	1.54	1.40
coronal	4	1.26	1.23	1.33	1.42	1.36
transverse	4	1.37	1.34	1.39	1.46	1.32

lar plot was elliptical. Only in some cases the polar plot had the shape of an equilateral triangle. Whereas the directions corresponding to the maximum and minimum sample response were consistent among measurements on individual samples, they varied between samples.

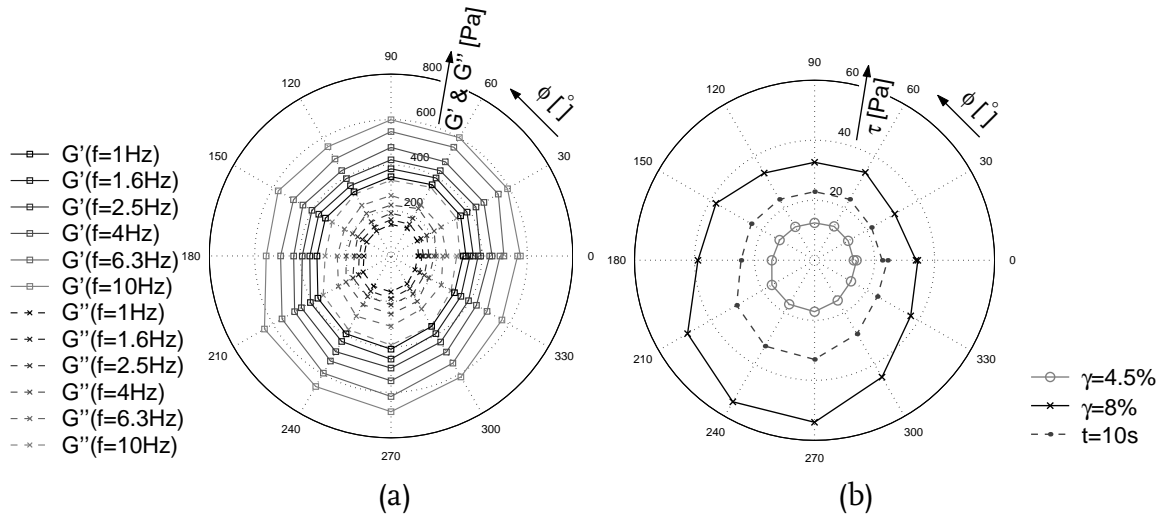


**Figure 2.5:** Polar plots of (a)  $G'$  (solid lines) and  $G''$  (dashed lines) from DFS tests, (b) stress at 4.5% strain (grey line), 8% strain (solid line), and stress after 10 seconds of relaxation (dashed line) during a SR test.

The variations caused by anisotropy between the planes are presented in Figure 2.6 where the error bars represent the average differences between the maximum and minimum found within the plane of testing. Whereas the results measured in the coronal and the transverse plane were statistically indistinguishable, they were 1.3 and 1.25 times stiffer, respectively, than the results obtained in the sagittal plane. These differences were similar for the DFS (Figure 2.6a) and the SR tests (Figure 2.6b, c). The variation caused by anisotropy within the planes was found to increase with increasing strain for SR tests, whereas it was found to decrease with increasing frequency for DFS tests. Standard deviations for these tests were found to be up to 26%.

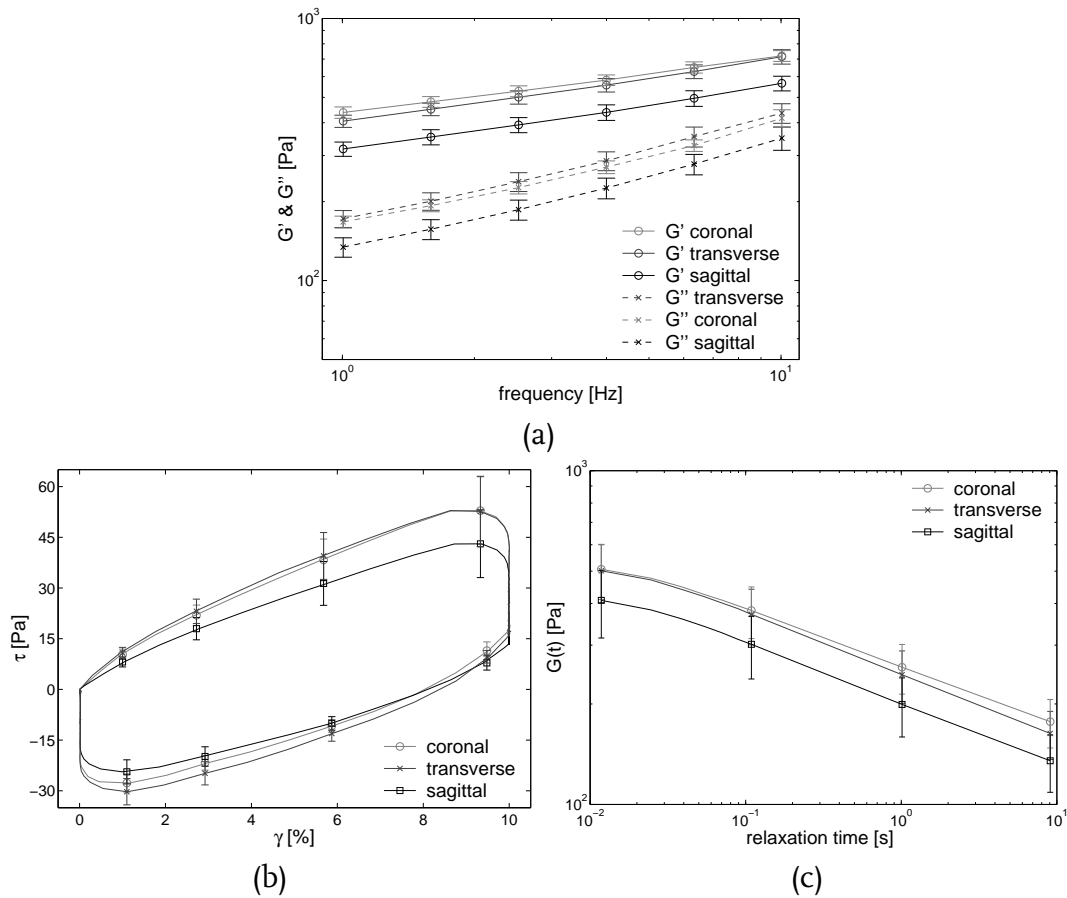


**Figure 2.6:** Mean shear properties for each anatomical plane with bars representing the variation caused by anisotropy (a) DFS test, (b, c) SR test.

### 2.3.3 Effect of compression prior to shear measurements

Results of DFS and SR tests with different amounts of pre-compression are given in Figure 2.7. From these results it is visible that the response in shear stiffens with decreasing gap, i.e. with increasing pre-compression force. The differences caused by different pre-compression forces are summarised in Table 2.4. In the case of DFS tests, for a pre-compression force of 10 mN the stress response is 11.6% ( $f = 10$  Hz) to 21.5% ( $f = 1$  Hz) stiffer, than for a pre-compression force of 5 mN. The difference was decreasing with increasing frequencies. For the SR tests with a pre-compression force of 10 mN the response is 12.5% (during loading) to 18.5% (after relaxation) stiffer, than for a pre-compression force of 5 mN. The difference was higher after relaxation than during the loading phase. Moreover, during the loading part of the SR tests the differences were independent of strain.

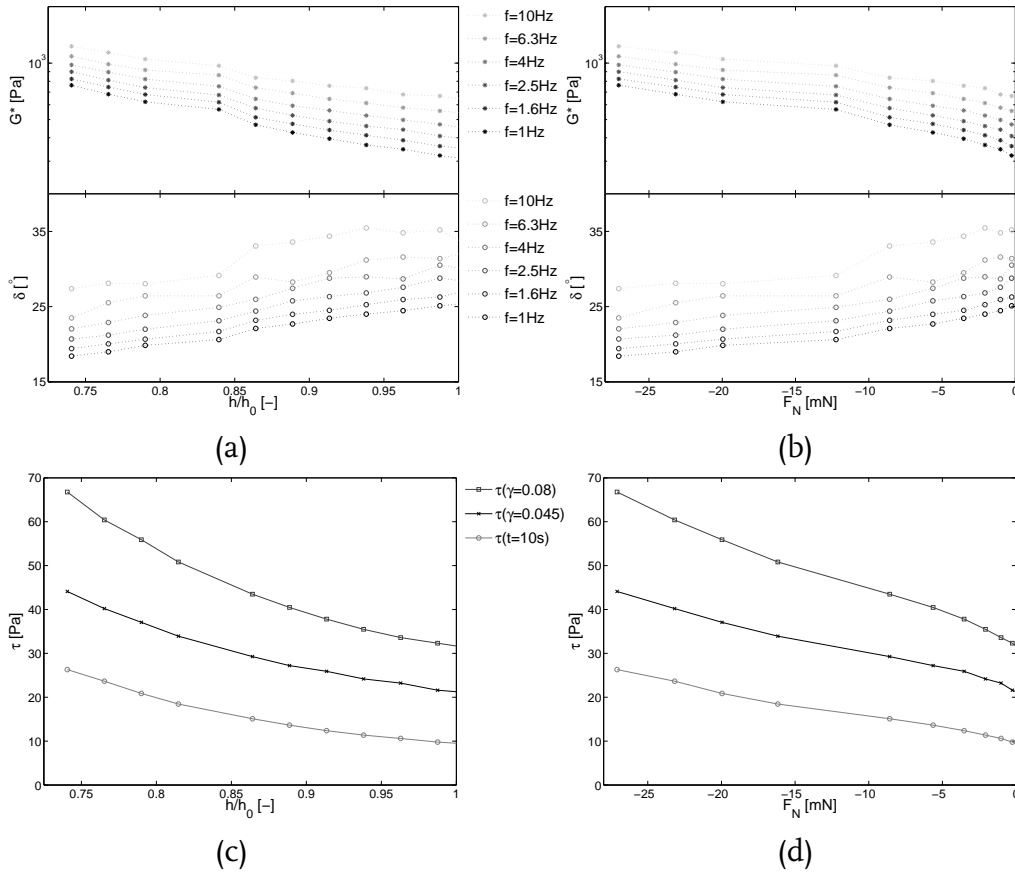


**Figure 2.7:** Dynamic frequency sweep results as a function of (a) height of the gap between plates, (b) normal force. Stress relaxation results as a function of (c) height of the gap between plates, (d) normal force.

**Table 2.4:** Variations caused by pre-compression forces measured in shear tests. Data measured for a pre-compression force of 0, -5, and -10 mN are compared.

	DFS		SR		
	$G_{f=1\text{Hz}}^*$	$G_{f=10\text{Hz}}^*$	$\tau_{\gamma=4.5\%}$	$\tau_{\gamma=8\%}$	$\tau_{t=10\text{s}}$
$F_N = -10\text{ mN}/F_N = 0\text{ mN}$	1.622	1.357	1.414	1.419	1.650
$F_N = -5\text{ mN}/F_N = 0\text{ mN}$	1.336	1.216	1.253	1.263	1.395
$F_N = -10\text{ mN}/F_N = -5\text{ mN}$	1.215	1.116	1.124	1.129	1.183

## 2.4 Discussion and conclusions

The constitutive properties of soft tissues as obtained in mechanical characterisation experiments are particularly sensitive to a number of experimental conditions. In this study, the influence of some of these conditions has been investigated by keeping all other conditions unchanged. In particular, the consequences of differences in temperature, material anisotropy and the chosen amount of pre-compression in shear measurements have been investigated.

**Effect of temperature:** Mechanical test results of brain tissue have been shown to be clearly temperature dependent and can be scaled by a horizontal shift factor  $a_T$  and a negligible vertical shift factor  $b_T$ . There is only one study [73] where the results were found to be independent of temperature. Current results compare well with results previously published by Peters et al. [59], Brands et al. [38], and Shen et al. [64] (see Table 2.5). Data measured at room temperature are recommended to be shifted by a horizontal factor of  $a_T = 8.5-11$  to obtain the values representative for body temperature. Because the vertical factor  $b_T$  is close to one, no vertical shift is required.

**Table 2.5:** Shift factors  $a_T$  and  $b_T$  for scaling results from 23°C to 37°C.

	No. of samples	Type of test	Mean	
			$a_T$	$b_T$
current study	3	DFS, SR	8.5-11	1.3-0.99
Brands et al. [38]	4	DFS	5.5	1.03
Peters et al. [59]	5	DFS, SR	6.7	2.6
Shen et al. [64]	-	DFS	~5	1

**Differences caused by anisotropy:** Anisotropy of brain tissue can also play a role in results of mechanical tests. In the current study, the average differences between the maximum and minimum found within the testing plane from DFS and SR tests are 25% to 40% and 32% to 54%, respectively. The ratios between the results from the coronal/sagittal and transverse/sagittal planes were approximately 1.3, whereas results from coronal and transverse planes were statistically indistinguishable. There have been only a few studies investigating the mechanical anisotropy of brain tissue. Arbogast et al. [31,34] tested the anisotropy of the brainstem in 2.5% strain DFS tests in three different orientations and found differences to be up to 30%. Prange and Margulies [63] identified the anisotropy of brain tissue at large strains (up to 50%) from (translational) shear experiments on white matter samples from the corona radiata. They have found a ratio of 1.35-1.5 between two preferred directions in the sagittal plane. This compares well with results obtained within each plane (1.4-1.54) in the current study. Contrary, Nicolle et al. [56,57] studied anisotropy within the corona radiata (white matter) in three planes but did not find any statistical difference between the results. However, since this conclusion does not exclude the possibility of anisotropy, it is not necessarily in disagreement with the current observations.

**Effect of compression prior to shear measurements:** When sandpaper is used to prevent slip in shear experiments, samples should be compressed prior to testing. This can be avoided by gluing the sample to the plates. However, in that case the thickness of the glue layer is unknown and therefore the real height of the sample is unknown. As a consequence, also in case of glue the sample is often uniaxially loaded prior to shear measurements. The amount of pre-compression was found to significantly affect the mechanical properties obtained in shear measurements. Although a sufficient amount of pre-compression is required to prevent the occurrence of slip in subsequent shear measurements, an increasing amount of compression force will yield the deformation state to



be a combination of shear and compression rather than pure shear. Furthermore, the friction created between the sample and the plate will lead to a non-homogeneous state with an enlarged cross-sectional area in the middle plane of the sample. The dependence of the shear properties obtained from the measurement on the amount of pre-compression, results from a combination of these effects, all leading to an increasing apparent shear modulus with increasing pre-compression. In the current study, a 20% increase of the shear modulus observed was found when increasing the pre-compression force from 5 to 10 mN. Contrary, Nicolle et al. [57] have found a 24% decrease of shear modulus in the linear range with pre-compression increasing from 1% to 3%.

Additionally, the effect of post-mortem time has been studied for comparable conditions as well, see Chapter 3. An increase of approximately 27 Pa/h was found for moduli measured at a strain of 4.5% for tests exceeding the threshold time of 6 hours post-mortem. The post-mortem time, sample preparation and mechanical history of the tissue were highlighted as important aspects for interpreting the results of mechanical characterisation studies on brain tissue.

Because of availability and the possibility to test at relatively short post-mortem times, porcine brains were used in this work. Porcine brain tissue has been used in many previous studies on the mechanical properties of brain tissue as well (see Table 2.1). Although differences between human and porcine brain tissue do exist, these differences are considered to be small compared to differences due to the effect of post-mortem time [63]. Furthermore, the donor animals used in this study were not full grown (approximately six months). However, the composition (water content, DNA-P level, cholesterol) of porcine brain tissue has been found to change significantly only during the first four months [74]. Therefore, the mechanical properties of this material can be considered to remain unchanged after this age.

The considerable differences in mechanical properties as reported in literature may be caused by variations in the material tested, test conditions, testing protocols, and by other reasons. Generally, a combination all of these experimental aspects will determine the mechanical properties measured. Therefore, in experimental studies aimed at determining the mechanical behaviour of soft tissues like brain tissue, the experimental conditions should be carefully controlled and documented. In this study, the effect of some of these aspects was systematically investigated by using otherwise consistent conditions, which can be considered as a step towards obtaining a consistent data set describing the mechanical properties of brain tissue. However, notice that the spread in absolute values of comparable results (see Figure 2.1 and Figure 2.8 in Appendix 2.A) from these studies is about two decades, much more than the variation found due to anisotropy, post-mortem time, temperature and pre-compression.

## 2.A Overview of experimental studies

The data available in literature were divided into groups depending on the type of experiment. An overview of measurements in shear deformation is given in Table 2.6, whereas

Table 2.7 includes measurements in uniaxial deformation.

In general, dynamic tests were done by applying an oscillatory sinusoidal strain with a certain amplitude with or without varying the strain/frequency. Note that the linear viscoelastic properties should be determined from dynamic tests in the linear regime, which was found to be limited to 1% shear strain by Brands et al. [37] and Nicolle et al. [56]. Dynamic tests include also free vibration experiments. Constant strain rate tests consist of loading the sample by keeping a constant strain rate up to a certain strain level. In stress relaxation tests, the subsequent relaxation of the mechanical response is measured. A summary of stress relaxation and constant strain rate experiments is given in Figure 2.8. Creep test were done by applying a certain load on the sample and recording the strain response.

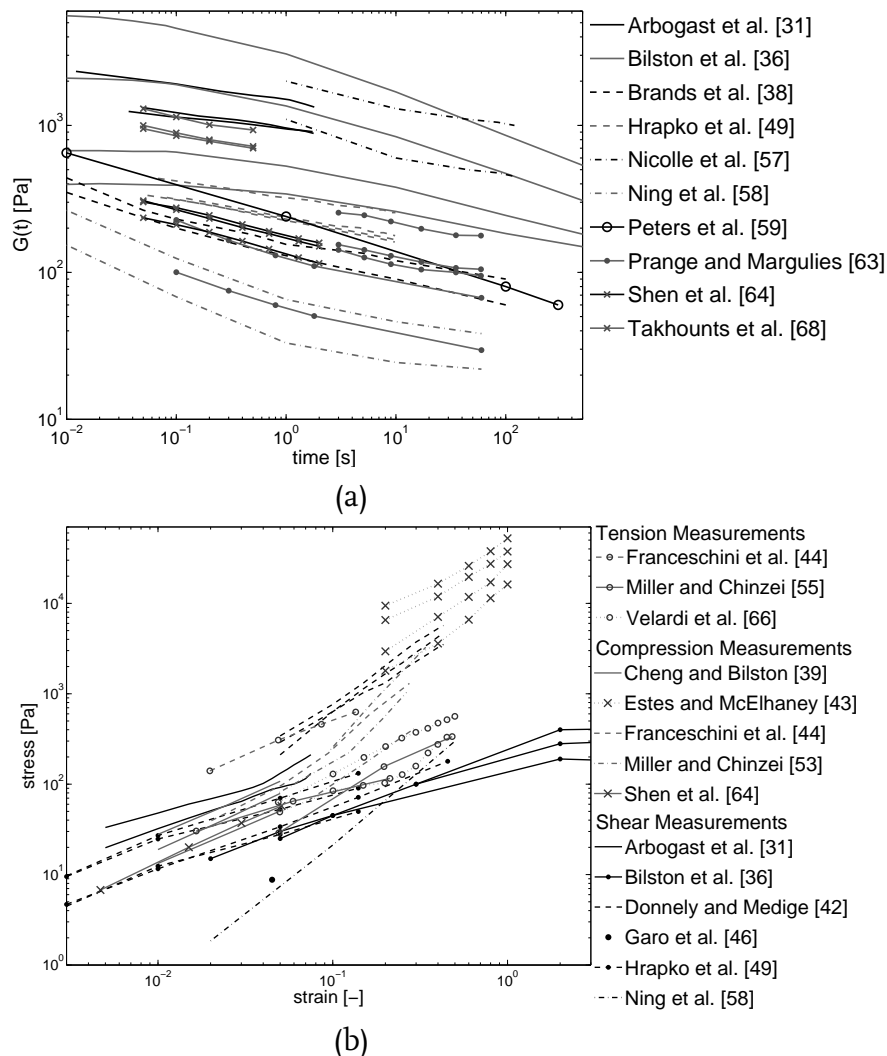


**Figure 2.8:** (a) Summary of shear stress relaxation experiment results reported in literature. (b) Summary of constant strain rate experiment results reported in literature, for shear (black) and uniaxial (grey) deformation.

**Table 2.6:** Overview of experimental studies on brain tissue in shear.

Dynamic tests						
	donor age	post-mortem time [h]	attach. method	$T$ [°C]	frequency [Hz]	strain [%]
Arbogast et al. [31,32,34]	p,fg	4	no,g,rs	5-25	20-200	2.5,5,7.5
Bilston et al. [35,36]	-	8	sp	37	0.01-20	0.015-2
Brands et al. [37,38]	nfg	4	sp,no,g	4-38	0.1-16	0.1-10
Darvish and Crandall [40]	nfg	72-288	g	37	0.5-200	1-20
Fallenstein et al. [28]	fg	2.5-62	g,rs	37	9-10	7-24.5
Garo et al. [46]	nfg	2-10	sp	37	1-10	1
Hrapko et al. [49]	nfg	5	sp	37	0.04-16	1
McElhaney et al. [29]	fg	2.5-15	no	37	9-10	-
Nicolle et al. [56,57]	nfg	24-48	g	37	0.1-9000	0.01-10
Peters et al. [59]	nfg	27-51	-	7-37	0.016-16	0.2-5
Shuck and Advani [65]	fg	-	-	37	5-350	1.23
Thibault and Margulies[69,70]	p,fg	3	no	~25	20-200	2.5,5
Stress relaxation tests						
	donor age	post-mortem time [h]	attach. method	$T$ [°C]	strain [%]	relax. time [s]
Arbogast et al. [31]	p	4	no	~25	2.5,5,7.5	1.8
Bilston et al. [35,36]	-	8	sp	37	0.001-15	3000
Brands et al. [38]	nfg	4	sp	38	5-20	100
Hrapko et al. [49]	nfg	5	sp	37	1-20	10
Nicolle et al. [56,57]	nfg	24-48	g	37	0.1-50	300
Ning et al. [58]	p	5	no	-	2.5-50	60
Peters et al. [59]	nfg	27-51	-	7-37	1	300
Prange et al. [60-63]	p,nfg,fg	3-5	no	~25	2.5-50	60
Shen et al. [64]	fg	48-120	sp	10-37	0.5,5,10,20	2
Takhounts et al. [67,68]	fg	48	g	~25	12.5-50	0.5
Constant strain rate tests						
	donor age	post-mortem time [h]	attach. method	$T$ [°C]	strain rate [s <sup>-1</sup> ]	strain [%]
Arbogast et al. [31]	p	4	no	~25	-	8
Bilston et al. [36]	-	8	sp	37	0.055,0.2335,0.947	2000
Donnelly and Medige [42]	fg	72-96	g	~25	30,60,90,120,180	0.28-12.5
Garo et al. [46]	nfg	2-10	sp	37	1	5
Hrapko et al. [49]	nfg	5	sp	37	1,1.5	1-50
Ning et al. [58]	p	5	no	-	20-25	50

Donor age: p – paediatric, nfg – not full grown, fg – full grown. Attachment method: no – no glue, g – glue, sp – sandpaper, rs – roughened surface.  $T$  – test temperature.

**Table 2.7:** Overview of experimental studies of brain tissue in uniaxial deformation.

Dynamic tests						
	donor age	post-mortem time [h]	attach. method	$T$ [°C]	strain [-]	frequency [Hz]
Galford and McElhaney[45]	fg	1-12	no	37	-	31,34
Koeneman [51]	-	0.5-3	no	22	$\sim 10^{-5}$	80-350
McElhaney et al. [29]	fg	2.5-15	no	37	-	31,34
Stress relaxation tests – Compression						
	donor age	post-mortem time [h]	attach. method	$T$ [°C]	strain [-]	relax. time [s]
Cheng and Bilston [39]	nfg	-	no,g	-	-0.05	3500
Galford and McElhaney[45]	fg	1-12	no	37	-	80
Prange et al. [62]	fg	5	no	$\sim 25$	-0.05,-0.3,-0.5	60
Constant strain rate tests						
	donor age	post-mortem time [h]	attach. method	$T$ [°C]	strain [-]	strain rate [ $s^{-1}$ ]
Compression						
Cheng and Bilston [39]	nfg	-	no,g	-	-0.05	$1 \times 10^{-2}$ - $1 \times 10^{-4}$
Estes and McElhaney [43]	fg	1-12	no	37	-1	0.08,0.8,8,40
Franceschini et al. [44]	fg	-	g	37	-0.26	$5.5-9.3 \times 10^{-3}$
McElhaney et al. [29]	fg	2.5-15	no	37	-1.2	0.1,1,10,65
Miller and Chinzei [53]	nfg	-	no	$\sim 22$	-0.34	$64 \times 10^{-2}$ - $64 \times 10^{-7}$
Shen et al. [64]	fg	48-120	no	-	-0.05	0.01
Tension						
Franceschini et al. [44]	fg	-	g	37	1.335	$5.5-9.3 \times 10^{-3}$
Miller and Chinzei [55]	nfg	-	g	$\sim 22$	0.48	$64 \times 10^{-2}$ - $64 \times 10^{-4}$
Velardi et al. [66]	fg	5-6	g	20-25	0.6	0.01
Creep tests – Compression						
	donor age	post-mortem time [h]	attach. method	$T$ [°C]	load [N,Pa]	time [s]
Dodgson et al. [41]	-	-	-	16-26	0.2N	15-90000
Franceschini et al. [44]	fg	-	no	$\sim 25$	2-12N	54000
Galford and McElhaney[45]	fg	1-12	no	37	3447,6895Pa	1000
Koeneman [51]	-	0.5-3	-	22	-	0.2-200

Donor age: p – paediatric, nfg – not full grown, fg – full grown. Attachment method: no – no glue, g – glue, sp – sandpaper, rs – roughened surface. T – test temperature.



# Effects of post-mortem time and sample preparation<sup>I</sup>

---

## Abstract

Since the early seventies, the material properties of brain tissue have been studied using a variety of testing techniques. However, data reported in literature show large discrepancies even in the linear viscoelastic regime. In the current study, the effect of the sample preparation procedure and of post-mortem time on the mechanical response of porcine brain tissue is examined. Samples from the thalamus region were prepared with different techniques and were tested for different loading histories. Each sample was tested in oscillatory shear tests (1% strain amplitude, 1–10 Hz frequencies) followed by sequences of 5% strain loading-unloading cycles. The stress response to the loading-unloading cycles showed a clear dependency on post-mortem time, becoming more stiff with increasing time. This dependency was affected by the mechanical history induced by the preparation procedure.

---

<sup>I</sup> *Reproduced from:* A. Garo, M. Hrapko, J. A. W. van Dommelen, G. W. M. Peters, (2007). Towards a reliable characterisation of the mechanical behaviour of brain tissue: the effects of post-mortem time and sample preparation. *Biorheology*, 44(1), p. 51–58.

### 3.1 Introduction

Injuries due to car accidents, specifically head injuries which are often fatal, remain a major problem in traffic safety. In order to understand and prevent traumatic brain injuries, the mechanical behaviour of brain tissue must be understood. Many studies have been performed in the last decades to characterise various aspects of this complex tissue, such as its dynamic response and its large strain behaviour [65,59,34,70,38,36,56,49,64]. However, no universally accepted data exists that describes its linear viscoelastic behaviour. The differences in the reported viscoelastic properties may be due to a combination of several reasons, such as regional differences, anisotropy, differences between species but also test conditions such as post-mortem time and sample preparation. Prange and Margulies [63] showed that the difference between white matter from the corpus callosum and grey matter from the thalamus region is up to 30%. Human samples obtained from temporal lobectomies performed on epileptic patients, were on average 29% stiffer than porcine samples. Moreover, they reported that differences attributed to anisotropy of grey matter and white matter were up to 10% and up to 50%, respectively. The results of the various studies are orders of magnitude different. Such differences cannot be attributed entirely to regional, donor or to anisotropy variations. Several studies have commented on degeneration effects resulting from post-mortem time. Metz et al. [52] have reported a 30-70% decrease of the tissue response to the inflation of a balloon catheter, from live to 3/4 hour post-mortem. McElhaney et al. [29] have reported no significant changes in sample properties up to 15 hours post-mortem and Nicolle et al. [56] have reported only a 6% increase of shear modulus between samples measured at 24 and 48 hours post-mortem. However, many authors [34,70,38,36,63] suggested that the tissue would degenerate with increasing post-mortem time due to various reasons (e.g. autolytic processes, completion of rigor mortis, osmotic swelling, etc.).

The purpose of this study is to determine the effects of sample preparation and post-mortem time on the measured mechanical properties of brain tissue. It is hypothesised that both the mechanical history that is imposed during the preparation procedure and the total post-mortem time affect the mechanical properties of the material.

### 3.2 Materials and methods

The experiments were performed on porcine brains from six months old pigs obtained from a local slaughterhouse. Brain halves were transported in a solution of Phosphate Buffered Saline (PBS) in a box filled with ice to prevent dehydration and to slow down their degradation. The samples were prepared from tissue located in the thalamus region within 3 hours after sacrifice. This region of the central nervous system is a homogeneous mixture of white and grey matter and is particularly important because it is the relay station to higher cortical areas.

Two different methods were employed to prepare 1.5 to 3.5 mm thick slices:

- The first procedure consisted of using a vibrating-blade microtome, (Leica VT 1000S). Slices were cut from the thalamus with a speed of 0.05 - 0.1 mm/s and a frequency of 100 Hz. The surface of the blade was set to be parallel with the cutting plane. The advantage of this method is the high dimensional accuracy.
- The second procedure involved a standard rotating-disk vertical slicer (Bizerba) with which slices were cut from brain halves.

The slices were cut parallel to the sagittal plane in the superior-inferior direction. From these slices, samples with a diameter of 10 to 13 mm were cut using a cork bore. Until the start of the tests, the samples were preserved in PBS at 4°C.

The samples were tested in shear with the rotational rheometer ARES II (Advanced Rheometric Expansion System). Sandpaper was glued by double layer tape on the upper and lower plate to prevent slippage of the samples. In order to measure the height of the samples, the upper plate was lowered until touching the top of the sample and measuring a maximum axial force of 50 mN. During testing, the temperature was kept at 37°C and a moist chamber was used to prevent dehydration of the brain tissue samples. The tests were conducted at post-mortem times ranging from 2.5 to 10 hours, with the start of the tests corresponding to 2.5 to 8 hours. Because of the heterogeneity of brain tissue, samples of small dimensions were used. In order to minimise any possible effect of anisotropy of the material on the measured properties, all samples were tested in the same orientation (the shear direction corresponding to the anterior-posterior direction). To improve the signal to noise ratio, an eccentric test configuration was used [71]. In this configuration, the sample is placed at the edge of the bottom plate, leading to an increase of the measured torque. Moreover, an approximately homogeneous shear field is obtained.

A series of loading-unloading cycles was applied to the samples in two different test sequences. Each test sequence was preceded by a dynamic frequency sweep test in which the sinusoidal shear strain imposed on the sample had an amplitude of 1% corresponding to the linear range of brain tissue [37,56], and the frequency was ranging from 1 Hz to 10 Hz. For each frequency, the storage and loss moduli were determined. Subsequently, a series of loading-unloading cycles at a constant shear rate of  $1 \text{ s}^{-1}$  was applied. The purpose of these tests was to determine the presence of any potential evolution of mechanical properties due to either increasing post-mortem time or mechanical history of the sample. The test sequences differed in the shear strain amplitude of the loading-unloading cycles:

- In test sequence A (see Figure 3.1a), the samples were subjected to loading-unloading cycles to a strain of 5%, which is in the non-linear range of the material. Between each cycle, a period of 10 minutes was left in order to let the material recover at zero strain. This waiting period was chosen as a convenient division of post-mortem time for measurements.
- In test sequence B (see Figure 3.1b), 5% strain loading-unloading cycles were applied every 10 minutes during 1 hour. Thereafter, a 20% loading-unloading cycle



was applied, followed by again a series of 5% strain loading-unloading cycles every 10 minutes during 2 hours.

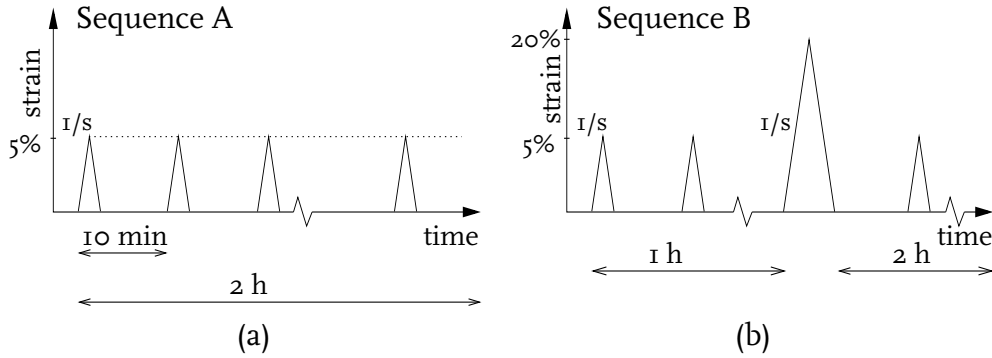


**Figure 3.1:** Different sequences of transient tests.

In Hrapko et al. [49], it was demonstrated that the strain level chosen in this study does not lead to changes in the mechanical behaviour at short times (up to 30 minutes). Sequence B was designed to study the effect of a large strain mechanical history on the response of brain tissue at longer times.

Three different test protocols have been used in this study, consisting of different combinations of sample preparation method and test sequence:

- Protocol 1: the samples were prepared with the microtome and subjected to test sequence A.
- Protocol 2: the samples were prepared using the vertical slicer and subjected to test sequence A.
- Protocol 3: the samples were prepared using the vertical slicer and tested according to test sequence B.

Table 3.1 gives the main features of the samples tested.

The aim of the first two test protocols was to investigate a possible effect of the cutting procedure on the mechanical response of the samples. The preparation procedure could potentially affect the mechanical behaviour of the material due to the mechanical history applied during this procedure. The third test protocol was applied with the goal to investigate the effect of a well-defined mechanical history on the mechanical response of the tissue at a relatively long time scale.

In the eccentric rotational shear configuration [71], the shear stress  $\tau$  and shear strain  $\gamma$  were calculated from the measured torque  $M$  and angle  $\theta$  by:

$$\tau = \frac{Mr}{2\pi r_1^2 \left( \frac{(r-r_1)^2}{2} + \frac{r_1^2}{8} \right)}, \quad \gamma = \theta \frac{r}{h}, \quad (3.1)$$

**Table 3.1:** Sample details and test matrix. The post-mortem time corresponds to the start of the test.

sample No.	protocol No.	cutting device	test sequence	diameter [mm]	height [mm]	post-mortem time [min]
1	1	Leica VT 1000S	A	12.1	1.40	300
2				11.1	1.79	465
3				10.2	1.41	450
4				11.3	3.14	480
5	2	VS Bizerba	A	13.0	3.47	180
6				12.7	2.93	380
7				10.5	1.79	180
8				10.3	1.81	340
9	3	VS Bizerba	B	12.2	2.71	180
10				10.6	2.86	390
11				12.6	3.32	150
12				10.6	3.33	360

where  $r$  is the radius of the plate,  $r_1$  is the sample radius and  $h$  is the sample height. It is assumed that the effect of the free boundaries can be neglected since the sample thickness is much smaller than the sample diameter.

During the dynamic frequency sweep tests, an oscillatory shear strain  $\gamma(t) = \gamma_0 \sin(\omega t)$  was applied to the sample. Since for these tests, the shear strain magnitude was within the linear viscoelastic limit [37,56], linear viscoelastic material behaviour can be assumed. Consequently, the shear response  $\tau(t)$  can be written as:

$$\tau = G^* \gamma_0 \sin(\omega t + \delta) = \gamma_0 [G' \sin(\omega t) + G'' \cos(\omega t)]. \quad (3.2)$$

The material response during the frequency sweep tests is reported in terms of the storage modulus  $G'$  and the loss modulus  $G''$ .

Since the strain magnitude of the loading-unloading cycles that were applied in this study are outside the linear viscoelastic regime, no constitutive assumption is made for the interpretation of the test results. The material response of these tests is characterised in terms of the modulus at  $\gamma^* = 0.045$  shear strain during the loading phase:

$$G(\gamma^*) = \frac{\tau(\gamma^*)}{\gamma^*}. \quad (3.3)$$

The strain magnitude was chosen below the amplitude of the loading-unloading cycle. At this stage of the loading phase, a constant and reproducible strain rate of  $1 \text{ s}^{-1}$  is obtained.

To assess a possible dependence of the modulus at 4.5% strain on post-mortem time, linear correlation coefficients ( $R$ ) are determined for the results obtained in two different stages of the test series. Furthermore, the probability ( $P$ ) value for the hypothesis of no correlation is determined. To define the threshold time  $t_0$ , which separates the post-mortem time  $t$  into two stages, the function  $G = C_1 + C_2(t - t_0)H(t - t_0)$  was fitted by

a least-squares error method to all measured data. Coefficients  $C_1$  and  $C_2$  represent the modulus [Pa] before  $t_0$  and the increase of modulus with time [Pa/min] after  $t_0$ , respectively, and  $H$  is the Heaviside step function.

### 3.3 Results

The storage and loss moduli of all samples are given in Figure 3.2, and it is evident that they increase with frequency. The average standard deviations for the storage modulus and the loss modulus are 17% and 19%, respectively. These results are close to those found by Brands et al. [37] and Peters et al. [59] using a centered plate-plate configuration.

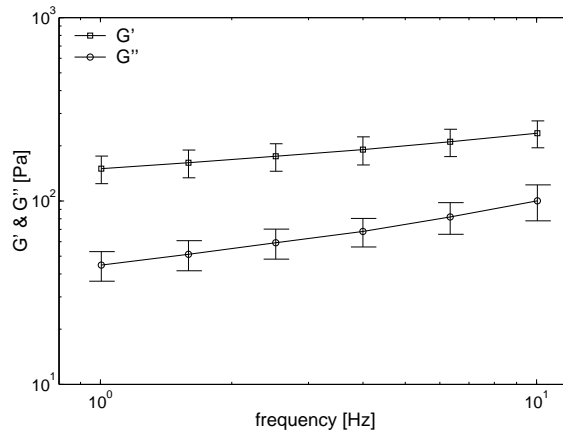


**Figure 3.2:** Average storage modulus  $G'$  and loss modulus  $G''$  for all samples and standard deviations.

Figure 3.3 shows the instantaneous modulus calculated from the shear stress level at 4.5% strain (Equation 3.3) versus the post-mortem time for all three protocols. It should be noted that at the end of the test, the samples were still visibly wet. The results of protocol 1 show the same trend: the behaviour of the brain tissue remains relatively constant during the first 40 minutes of the test and then the response increases during the remainder of the test. It should be noted that the samples were tested at post-mortem times exceeding 300 minutes. For protocol 2 the responses of 3 samples did not evolve with time as strongly as the samples subjected to protocol 1. The modulus remained approximately constant over time, even for post-mortem times longer than 300 minutes. Because of the good reproducibility of the test with samples prepared with the slicer, this preparation technique was also used in the third protocol, in which a shear strain of 20% was applied, after which the evolution of the mechanical response was again monitored. For protocol 3, it was observed that the stress response tended to increase when the post-mortem time exceeds 300 minutes. The stiffness increases after the 20% loading-unloading cycle for three of the samples. By comparing results of protocol 3 with protocol 2 it can be concluded that the 20% loading-unloading cycle accelerates the changes in the mechanical behaviour, even for post-mortem times smaller than 300 minutes.

Figure 3.3 shows that the moduli at 4.5% strain range from approximately 195 Pa for post-mortem times smaller than the threshold time to approximately 305 Pa for post-mortem times up to 10 hours. In general, the measured material response tends to increase with post-mortem time for post-mortem times exceeding the threshold time  $t_0 \approx 6$  hours. No correlation was found ( $R < 0.01$ ,  $P = 0.95$ ) between the modulus and post-mortem time up to 6 hours post-mortem. Contrary, for post-mortem times larger than 6 hours, a strong correlation was found ( $R = 0.61$ ,  $P = 0.00$ ) between modulus and post-mortem time. The mean modulus for the first stage was found to be  $C_1 = 195$  Pa, whereas the modulus increase during the second stage was found to be  $C_2 = 0.45$  Pa/min. The standard deviation found in the measured moduli at 4.5% strain is up to 25%.

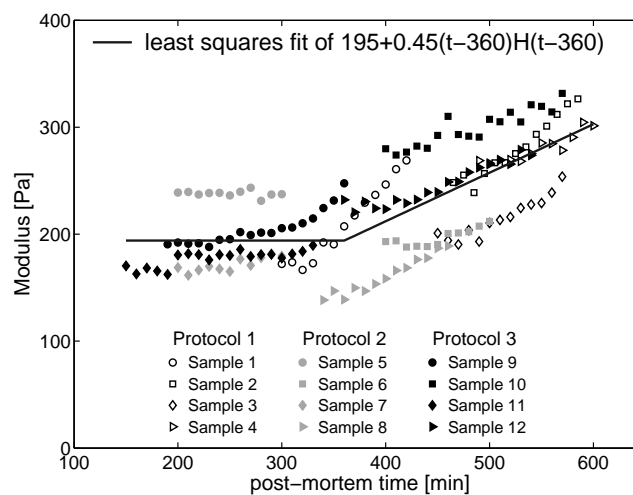


Figure 3.3: Modulus at 4.5% strain versus post-mortem time.

### 3.4 Discussion and conclusions

Studies on the characterisation of brain properties by different laboratories using different testing protocols have yielded a wide range of results. Concerning the results of the dynamic frequency sweep tests, all the samples show the same behaviour: the storage and loss moduli increase with frequency, however, the results are orders of magnitude different. Current results are similar to the data found by Peters et al. [59], Brands et al. [37], and Shen et al. [64] but smaller than the results of Arbogast and Margulies [34], Thibault and Margulies [70], Bilston et al. [36], and Nicolle et al. [56]. The differences between various studies cannot be attributed entirely to species, regional variation or to anisotropy. Among other factors, a possible source for differences in reported properties may be the preparation techniques used and the difference in post-mortem times. Therefore, the effect of the sample preparation and post-mortem time on the measured mechanical properties of brain tissue was investigated.

To investigate the possible effect of the cutting procedure, samples prepared with dif-

ferent techniques were subjected to identical series of tests. Furthermore, an additional test sequence, with a well-defined strain history was applied. From the results of these protocols a number of observations can be made. Most importantly, the mechanical response of brain tissue stiffens with increasing post-mortem time, if this post-mortem time exceeds a threshold value. The onset of changes in the mechanical behaviour with increasing post-mortem time appears to depend on the mechanical history of the tissue. Furthermore, this mechanical history may be affected by the sample preparation procedure. Mechanical loading during sample preparation can accelerate the evolution of mechanical properties with advancing post-mortem time. Moreover, for reproducible results, brain tissue should generally be tested within a post-mortem time of 6 hours. The average deviation for tests exceeding the threshold of 6 hours post-mortem was found to be approximately 27 Pa/h (for moduli computed at a strain of 4.5%). It appears that sample preparation and in particular post-mortem time are important aspects for interpreting the results of mechanical characterisation studies on brain tissue. For studies in which the tissue is tested at relatively longer post-mortem times, the mechanical properties obtained can be expected to be relatively stiff.

Those authors [34,70,38,36,63] who measured their results on shorter post-mortem times argued that this minimises deviations caused by higher post-mortem times. However, also several studies were made with larger post-mortem times. No deviation of measured results caused by higher post-mortem time was found by McElhaney et al. [29] for times up to 15 hours. Nicolle et al. [56] compared samples measured at 24 and 48 hours post-mortem and found only a 6% increase in linear viscoelastic response. It should be mentioned that they have stored the samples at 6°C to minimise the changes. Darvish and Crandall [40] have prepared their samples 24 hours post-mortem, stored them in a solution of physiological saline and bovine serum and tested them in 3-16 days. No correlation was found between time and variation in mechanical properties. Also, Shen et al. [64] have used samples from porcine brains (one week post-mortem), and reported only a small variation of the material properties.

By investigating different aspects of testing and preparation procedures, the differences between the results of different studies can be partially explained. Although the results of this study are not conclusive, clear trends can be observed, which can be considered as a step towards a reliable characterisation of the mechanical behaviour of brain tissue.

# Characterisation in shear<sup>I</sup>

---

## Abstract

The non-linear mechanical behaviour of porcine brain tissue in large shear deformations is determined. An improved method for rotational shear experiments is used, producing an approximately homogeneous strain field and leading to an enhanced accuracy. Results from oscillatory shear experiments with a strain amplitude of 0.01 and frequencies ranging from 0.04 to 16 Hz are given. The immediate loss of structural integrity, due to large deformations, influencing the mechanical behaviour of brain tissue, at the time scale of loading, is investigated. No significant immediate mechanical damage is observed for these shear deformations up to strains of 0.45. Moreover, the material behaviour during complex loading histories (loading-unloading) is investigated. Stress relaxation experiments for strains up to 0.2 and constant strain rate experiments for shear rates from 0.01 to 1 s<sup>-1</sup> and strains up to 0.15 are presented.

A new differential viscoelastic model is used to describe the mechanical response of brain tissue. The model is formulated in terms of a large strain viscoelastic framework and considers non-linear viscous deformations in combination with non-linear elastic behaviour. This constitutive model is applicable in three-dimensional head models in order to predict the mechanical response of the intra-cranial contents due to an impact.

---

<sup>I</sup> *Reproduced from:* M. Hrapko, J. A. W. van Dommelen, G. W. M. Peters, J. S. H. M. Wismans, (2006). The mechanical behaviour of brain tissue: large strain response and constitutive modelling. *Biorheology*, 43(5), p. 623–636.

## 4.1 Introduction

The head is often considered as the most critical region of the human body for life-threatening injuries sustained in accidents. The social costs of these accidents were estimated at 180 billion Euros per year in the European Union alone [75]. From 1995 to 2001 an average of 1.4 million cases of traumatic brain injury occurred in the United States each year, of which 20% resulted from motor vehicle accidents [2]. In order to develop effective protective measures, a better understanding of the process of injury development in the brain is required.

During a crash the head is exposed to external mechanical loading which causes an internal mechanical response of the brain tissue. Above a certain strain or a strain rate brain tissue damage can occur. To assess the likelihood of head injury, in the early sixties, the Head Injury Criterion was developed [7] and is still used in most current test standards. However it suffers from a number of drawbacks, one of which is that it is based on linear head acceleration only. Moreover, it does not allow for a distinction between different injury mechanisms. Nowadays, FE models are being developed, in order to predict the mechanical response of the contents of the head during impact. Current FE head models contain a somewhat detailed geometrical description of various anatomical components of the head but lack accurate descriptions of the mechanical behaviour of brain tissue. Without an accurate representation of the constitutive behaviour of the various components, the predictive capabilities of head models may be limited. Therefore, brain tissue has been studied with a variety of techniques and a number of constitutive models were proposed. The mechanical behaviour of brain tissue has been tested mostly *in vitro* in shear [34,36,38,40,42,45,56,59,65,68,70,63], compression [63,43,53] and tension [55]. Moreover, some results from *in vivo* measurements have been reported as well [48,54]. However, no consensus exists on the linear viscoelastic properties and on the nature of the non-linear behaviour. Reported properties of brain tissue vary more than an order of magnitude. Several reasons for this scatter may exist, such as differences in testing protocols, different donor species, anisotropy, and the non-homogeneous nature of brain tissue. Post-mortem times vary from a few hours [34,36,38,63] to a few days [40,42,56]. Animal brain tissue is frequently used as a substitute for the human brain in experiments to characterise the mechanical behaviour. The main reasons are that animal brains are easily available and can be tested at short post-mortem times. In most studies involving human brains, material was obtained from autopsies with the consequence of longer post-mortem times. The mechanical response of fresh human brain tissue was reported to be approximately 30% stiffer than that of porcine brain tissue [63]. Similar results have been presented for bovine brain tissue [68].

A number of constitutive models were developed to describe the mechanical behaviour of brain tissue. Many researchers used an integral model, often in combination with Ogden hyper-elasticity to describe the viscoelastic behaviour of brain tissue [40,76,77,56,63,68], and some propose a differential constitutive equation [36,12,42]. However, these existing models were not validated to describe the influence of non-linear behaviour on complex loading histories. The ability of a constitutive model to describe this complex mechanical response is crucial for reliable simulations of head injury. Therefore a model is re-

quired that is able to describe the response to large deformations in different deformation modes.

This paper presents experimental data on the mechanical response of brain tissue subjected to large deformations. The occurrence of mechanical damage is investigated by a series of constant shear rate experiments with an increasing strain amplitude. Moreover, results from a series of loading-unloading cycles for different shear rates are presented. Stress relaxation and recovery upon unloading of brain tissue are investigated in shear. Based on the experimental results, a new non-linear viscoelastic material model is formulated using a differential framework which is suitable for large deformations. Experience with many other materials has indicated that non-linearity often originates from the viscous part of a viscoelastic model. Large shear strain experimental results have indicated a non-linearity of the viscous behaviour for brain tissue as well [36]. In the model presented here, a non-linear elastic mode is used in combination with a number of viscoelastic modes showing shear thinning behaviour. The model is fitted to the loading and the relaxation part of the stress relaxation data of shear experiments and is validated by its ability to describe the response during complex loading histories. It can be expected that if a model is applicable for the large strain response of porcine brain tissue, it can also be applied to human brain tissue after determining the appropriate parameters.

## 4.2 Materials and methods

Porcine brain tissue was tested in simple shear experiments. Porcine brain tissue was chosen as a substitute for human brains because of availability and the possibility to minimise the post-mortem time at testing. Fresh halves of porcine brains from approximately 6 month old pigs were obtained from a local slaughterhouse. Immediately after acquisition, they were placed in an ice cooled physiological saline solution to prevent dehydration and to slow down degradation of the tissue. Samples were prepared from the brain halves within 2 hours after sacrifice. Slices were cut by a Leica VT1000S Vibrating-blade microtome from the posterior side of the corona radiata region. Cylindrically shaped samples were obtained with a cork bore which was applied from the medial to the lateral side, such that the axis of the cylinder was at  $30^\circ$  from the axis perpendicular to the sagittal plane, see Figure 4.1. The samples had a diameter of 7-10 mm and a height of 1-3 mm. Immediately after sample preparation, the samples were placed in a physiological saline solution at  $7^\circ\text{C}$ , and subsequently were tested within a 0.5 to 3 hours. All samples were tested within post-mortem times ranging from 2.5 to 5 hours.

Shear experiments were performed on an ARES II rotational rheometer with a 10GM FRT transducer in a plate-plate configuration. Waterproof sandpaper (grain size 0.18 mm) was attached to the upper and lower plate of the rheometer to prevent slippage during the loading of the sample. This configuration was previously shown to be effective by Brands et al. [38]. During the test, samples were covered by a moist chamber to prevent dehydration and the samples were tested at a temperature of  $37^\circ\text{C}$ . An eccentric configuration was used, where the sample was placed at the edge of the plate [71], with a radius of



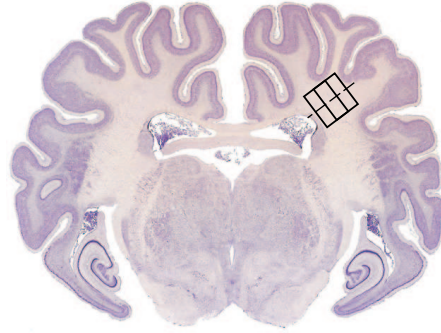


**Figure 4.1:** Sample location in a coronal section of a porcine brain [78].

25 mm, see Figure 4.2. The shear stress  $\tau$  and shear strain  $\gamma$  were then calculated from the measured torque  $M$  and angle  $\theta$  by:

$$\tau = \frac{Mr}{2\pi r_1^2 \left( \frac{(r-r_1)^2}{2} + \frac{r_1^2}{8} \right)}, \quad \gamma = \theta \frac{r}{h}, \quad (4.1)$$

where  $r$  is the radius of the plate,  $r_1$  is the sample radius and  $h$  is the sample height. It is assumed that the effect of the free boundaries can be neglected while the sample thickness is much smaller than the sample diameter. The advantages of shifting the sample to the edge of the plate are that the measured torque signal is increased and the deformation is more homogeneous than in the conventional centred configuration. Consequently, this configuration enables the study of the large strain response of the material.

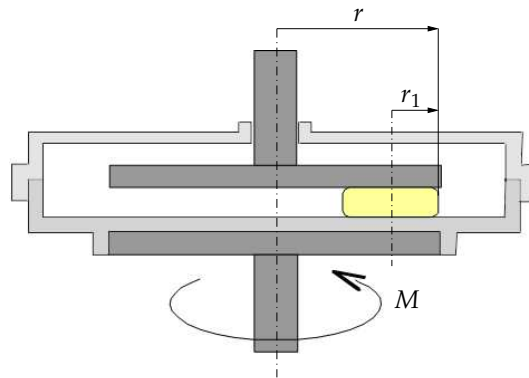


**Figure 4.2:** Eccentric configuration for rotational shear experiments.

All shear experiments were preceded by a 10 cycle sinusoidal preconditioning with a frequency of 0.16 Hz and a strain amplitude of 0.01, which was previously determined to be the linear viscoelastic limit [37,56]. This was confirmed by strain sweep measurements on the current setup. Thereafter, a dynamic sinusoidal strain was conducted with an amplitude of 0.01 and the frequency ranging from 0.04 to 16 Hz. For each frequency, the

storage modulus  $G'$  and the loss modulus  $G''$  were determined from cycle 2–6. Subsequently, the same sample was tested in either a series of stress relaxation experiments, constant shear rate experiments for different shear rates, or constant shear rate experiments with an increasing strain amplitude. The latter experiments were designed to investigate any potential damaging effect of a previous strain history on the immediate mechanical response. These loading-unloading tests were conducted with a constant shear rate of  $1 \text{ s}^{-1}$  and the strain was incrementally increased from  $0.01$  up to  $0.5$ , see Figure 4.3a. After each loading-unloading cycle the sample was left to recover at zero strain for at least  $10$  times the loading time. Thereafter, in the next cycle, the strain amplitude was increased. In another test sequence (Figure 4.3b), loading-unloading cycles with a strain amplitude of  $0.15$  were conducted with the constant shear rate per cycle increasing from  $0.01 \text{ s}^{-1}$  to  $1 \text{ s}^{-1}$ . Between two cycles, the sample was left to recover for at least  $10$  times the loading time. The stress relaxation experiments were composed of a series of ramp-and-hold tests at different strain levels, see Figure 4.3c. The strain rate during the loading phase was  $1 \text{ s}^{-1}$  and the strain was held for  $10 \text{ s}$  during which the relaxation of the material was recorded and the relaxation modulus  $G(t) = \tau(t)/\gamma$  was computed. Then, the strain was released with a constant strain rate of  $1 \text{ s}^{-1}$  and the sample was left to recover for a period of at least  $100 \text{ s}$  during which the tissue response was recorded as well. The test was repeated for different strain levels where the strains were chosen to be:  $0.01$ ,  $0.05$ ,  $0.1$ ,  $0.15$ ,  $0.2$ , respectively.

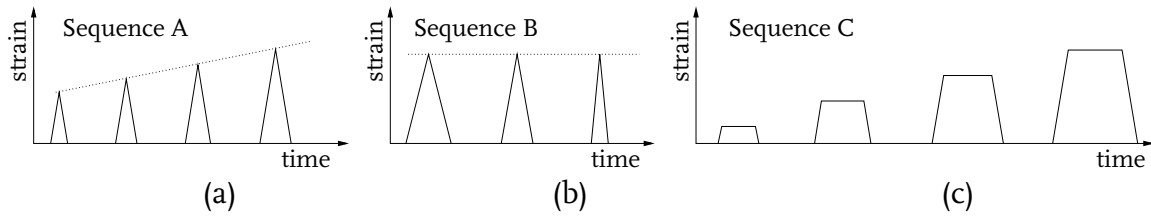


**Figure 4.3:** Schematic illustration of test sequences for large strain shear experiments.

## 4.3 Results

Dynamic frequency sweep results of 21 samples in terms of storage modulus  $G'$  and loss modulus  $G''$  with an average standard deviation of 28% are shown in Figure 4.4. This deviation may be caused by differences between the samples and the brains and by local anisotropy. The results compare well with those from [38].

Results from constant shear rate experiments with an increasing strain amplitude are presented for a representative sample in Figure 4.5. In Figure 4.5b, the  $0.01$  strain limit for linear behaviour is clearly visible in the beginning of each loading part. There was no yield or failure visible for the tested strain range. By comparing different loading-unloading cycles, which were all applied at an identical strain rate, it can be observed that there is no significant immediate mechanical damage affecting the stress-strain behaviour due to previous shear deformations (up to strains of  $0.45$ ) occurring at the time

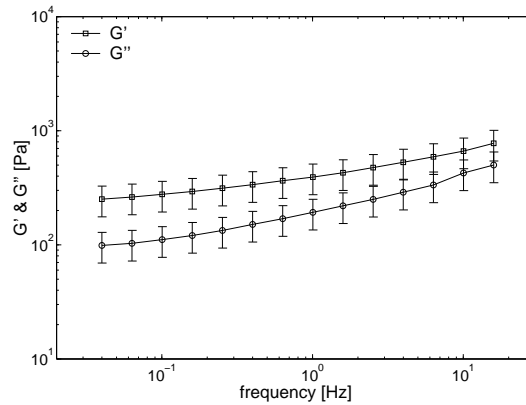


**Figure 4.4:** Storage modulus and loss modulus obtained in dynamic frequency sweep experiments.

scale of the experiment. However, at larger time scales, functional damage or the development of mechanical changes may still occur. For strains larger than 0.25, the stress-strain curve starts to decrease slightly which is caused by incomplete recovery after the unloading phase, although the time for recovery was more than 10 times the loading and unloading time. This can be attributed to non-linearities in the material behaviour. However, the results obtained prove that measurements up to a strain of 0.2 and a shear rate of  $1 \text{ s}^{-1}$  are reproducible for short time scales.

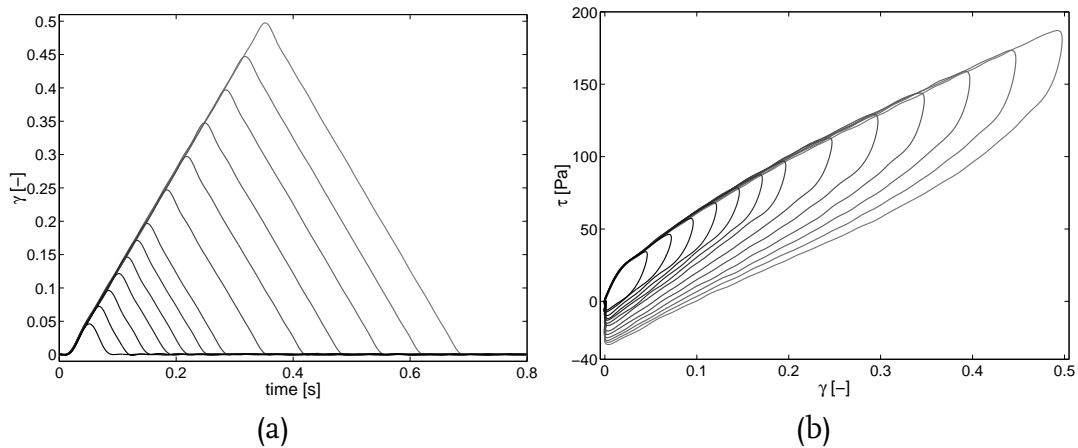


**Figure 4.5:** Results of constant shear rate experiment with increasing strain amplitude (test sequence A). (a) Applied shear strain with reproducible strain rate, (b) stress-strain response.

In Figure 4.6, results from constant shear rate experiments at different shear rates are shown. These tests were performed to show the non-linear strain rate sensitivity of brain tissue. The strain of 0.15 was chosen based on the results of test sequence A. From these results it can be observed that also in the non-linear range, the stress as a function of strain is strain rate dependent and that the response stiffens with increasing strain rate.

The linear strain limit seems to be the same for all strain rates.

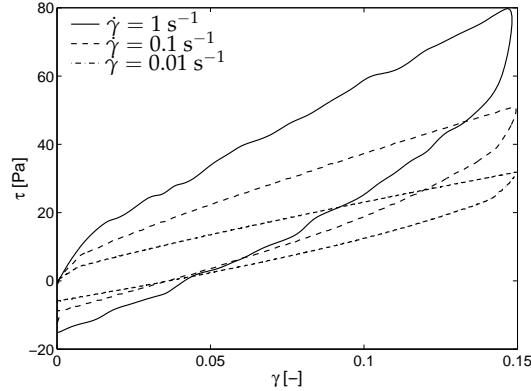


**Figure 4.6:** Stress-strain response obtained during constant shear rate experiments at different shear rates (test sequence B).

In Figure 4.7, results are shown from stress relaxation experiments on two samples. During the loading phase the stress response weakens above the linear viscoelastic strain limit and is identical for each stress relaxation test, Figure 4.7b. This confirms the conclusion from the constant strain rate tests that there is no immediate mechanical damage for these strain levels. During stress relaxation, the relaxation modulus does not reach a plateau value within the time range allowed, see Figure 4.7c. This is supported by the findings of other researchers who performed stress relaxation experiments [31,36,38,56,63,68]. As is seen from Figure 4.7c, the observed relaxation modulus decreases as a function of applied strain, where the difference becomes smaller for larger strains. This represents the true material behaviour and is in contrast with results of other researchers using a rotational rheometer with a concentric configuration. Here an approximately homogeneous shear field was obtained by placing the samples at the edge of the plate. Similar behaviour was observed in simple shear measurements on a translational shearing device by Prange and Margulies [63]. Stress relaxation curves for different strain values are nearly parallel. After unloading, the sample recovers completely for strains in the linear region. For strains above the linear viscoelastic limit, the sample does not recover completely, although the time for recovery was more than 10 times the relaxation time.

## 4.4 Constitutive model

A parallel arrangement of a number of viscoelastic modes and a non-linear elastic mode is chosen to model the mechanical behaviour of brain tissue. The total Cauchy stress tensor  $\boldsymbol{\sigma}$  is written as the summation of these contributions:

$$\boldsymbol{\sigma} = -p\mathbf{I} + \boldsymbol{\sigma}_e^d + \sum_{i=1}^N \boldsymbol{\sigma}_{ve_i}^d \quad (4.2)$$

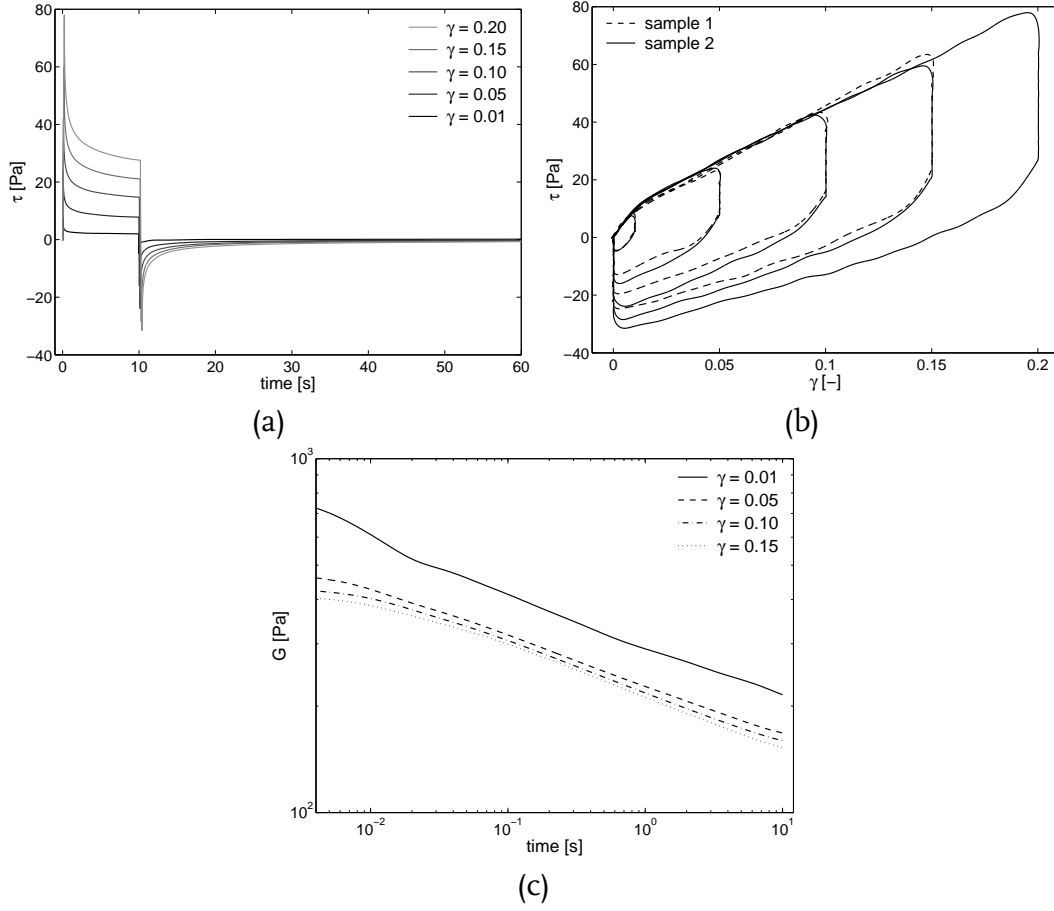


**Figure 4.7:** Results of stress relaxation experiments in shear (test sequence C). (a) Stress vs. time for one sample; (b) stress-strain behaviour for two samples; (c) average stress relaxation modulus from the two samples.

where the superscript “d” indicates that the extra stress is deviatoric and  $N$  represents the number of viscoelastic modes. In the current considerations, the material is assumed to be incompressible. A general differential framework is used to describe the viscoelastic modes [79]. It is based on a multiplicative decomposition of the deformation gradient tensor  $F$  into an elastic part and an inelastic part for each mode  $i$ , denoted by the subscripts “e” and “v”, respectively:

$$F = F_e \cdot F_v, \quad (4.3)$$

where for clarity, the subscript  $i$  has been omitted. This decomposition considers the concept of a local intermediate stress-free state which results from instantaneous elastic unloading of the current configuration. Accordingly, the velocity gradient tensor  $L = \dot{F} \cdot F^{-1}$  is decomposed as:

$$L = L_e + L_v \quad \text{with} \quad L_e = \dot{F}_e \cdot F_e^{-1} \quad \text{and} \quad L_v = F_e \cdot \dot{F}_v \cdot F_v^{-1} \cdot F_e^{-1}. \quad (4.4)$$

Furthermore, the inelastic deformations are chosen to be spin-free:  $\Omega_v = \frac{1}{2}(L_v - L_v^T) = O$ . Based on the kinematics of this framework, the following evolution equation for the

inelastic deformations can be derived:

$$\dot{\mathbf{C}}_v = \mathbf{F}^T \cdot \mathbf{B}_e^{-1} \cdot \left[ (\mathbf{L} - \mathbf{L}_e) \cdot \mathbf{B}_e + \mathbf{B}_e \cdot (\mathbf{L}^T - \mathbf{L}_e^T) \right] \cdot \mathbf{B}_e^{-1} \cdot \mathbf{F}, \quad (4.5)$$

where  $\mathbf{C}_v$  and  $\mathbf{B}_e$  represent the inelastic right Cauchy-Green deformation tensor and the elastic Finger tensor, respectively. An explicit integration procedure is used for this evolution equation. In each viscoelastic mode of the model, the deviatoric part of the extra stress tensor is assumed to be given by a relationship of the form  $\sigma_{ve}^d(\mathbf{F}_e)$ . Based on the relaxation behaviour of brain tissue, a two-parameter Mooney-Rivlin model is chosen, which reduces to a simple neo-Hookean model in shear and provides an extra parameter to adapt the model to different deformation modes. This model can alternatively be written as:

$$W_{ve} = \frac{1}{2} G_{ve} [aI_{e1} + (1-a)I_{e2} - 3] \rightarrow \sigma_{ve}^d = G_{ve} \left[ a\mathbf{B}_e^d - (1-a)(\mathbf{B}_e^{-1})^d \right], \quad (4.6)$$

with  $I_{e_i}$  the invariants of  $\mathbf{B}_e$  and  $W_{ve}(I_{e1}, I_{e2})$  the strain energy function. The inelastic flow in a mode is driven by the deviatoric elastic stress and is given by the associated flow rule:

$$\mathbf{D}_v = \frac{1}{2\eta(\tau)} \sigma_{ve}^d, \quad (4.7)$$

where the viscosity parameter  $\eta$  may depend on the equivalent stress measure  $\tau = \sqrt{\frac{1}{2} \sigma^d : \sigma^d}$ , where  $\sigma^d$  represents the deviatoric part of the total stress experienced by the material.

This framework was used by Brands et al. [12] for the modelling of the mechanical behaviour of brain tissue. They used 4 viscoelastic modes, each with a constant viscosity  $\eta_i$ . For the elastic part of the behaviour of each mode, a second order Mooney-Rivlin model was used, leading to artificial softening effects. Experience with many other materials has indicated that non-linearity often originates from the inelastic part. Here, the Ellis model is chosen to describe the stress-dependence of the viscosity:

$$\eta = \eta_\infty + \frac{\eta_0 - \eta_\infty}{1 + \left( \frac{\tau}{\tau_0} \right)^{n-1}}. \quad (4.8)$$

This model considers a powerlaw dependence, with a plateau value  $\eta_0$  for small stress levels and a value of  $\eta_\infty$  for infinite values of  $\tau$ . The latter is chosen here as  $\eta_\infty = k\eta_0$ .

A non-linear equilibrium mode is added to the viscoelastic modes. This mode is described by a Mooney-Rivlin-type model, modified with a non-linear prefactor:

$$\sigma_e^d = 2 \frac{\partial W_e}{\partial I_1} \mathbf{B}^d - 2 \frac{\partial W_e}{\partial I_2} (\mathbf{B}^{-1})^d, \quad (4.9)$$

with  $W_e = W_e(I_1, I_2)$  the strain energy function. The shape of the partial derivatives of the strain energy function is chosen based on the non-linear strain dependence of the equilibrated response to the shear relaxation tests:

$$W_e = G_e \left\{ -\frac{(1-A)}{C^2} [(Cx+1) \exp(-Cx) - 1] + \frac{1}{2} Ax^2 \right\}, \quad (4.10)$$

with

$$x = \sqrt{bI_1 + (1-b)I_2 - 3}. \quad (4.11)$$

With this strain energy function, the constitutive relation for the equilibrium mode can be written as:

$$\sigma_e^d = G_e \left[ (1-A) \exp\left(-C\sqrt{bI_1 + (1-b)I_2 - 3}\right) + A \right] \left[ b\mathbf{B}^d - (1-b)(\mathbf{B}^{-1})^d \right]. \quad (4.12)$$

The parameters  $a$  and  $b$  distinguish between the contribution of the first and the second invariant of  $\mathbf{B}_e$  and  $\mathbf{B}$ , respectively, to the strain energies and cannot be determined in shear experiments. Therefore, these parameters can, without other than experimental data in shear, be set to  $a = b = 1$ .

## 4.5 Model application

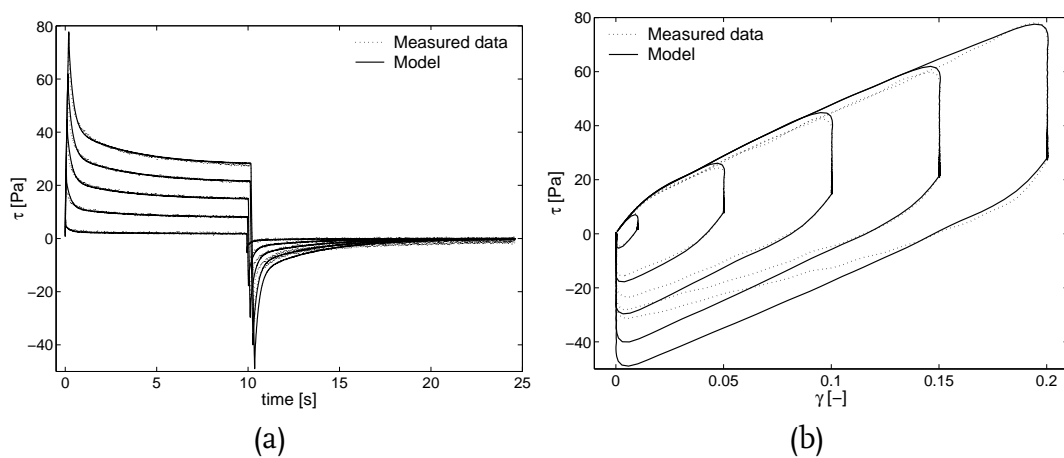
The model described in the previous section was fitted by a least-squares error method to the loading and relaxation part of a shear stress relaxation test (sample 2). The parameters obtained are given in Table 4.1. The coefficient  $\tau_0$  was chosen as the stress corresponding to the linear viscoelastic strain limit. The parameters  $A$ ,  $C$ , and  $G_e$  in the elastic spring contribution were fitted to the non-linear prefactor obtained from the end points of the relaxation part of the stress relaxation experiments at different strain levels. Then, the viscoelastic parameters  $G_i$ ,  $\lambda_i$  of 5 modes and the viscous parameters  $n$  and  $k$  were fitted to the loading and the relaxation part of the stress relaxation data for the test with a strain of 0.2. The coefficients  $a$  and  $b$  should be fitted to the results from measurements in

Table 4.1: Model parameters.

Elastic and viscous parameters	Viscoelastic parameters	
$G_e = 182.9 \text{ Pa}$	$G_1 = 835.5 \text{ Pa}$	$\lambda_1 = 0.012 \text{ s}$
$A = 0.73$	$G_2 = 231.2 \text{ Pa}$	$\lambda_2 = 0.35 \text{ s}$
$C = 15.6$	$G_3 = 67.1 \text{ Pa}$	$\lambda_3 = 4.62 \text{ s}$
$n = 1.65$	$G_4 = 3.61 \text{ Pa}$	$\lambda_4 = 12.1 \text{ s}$
$\tau_0 = 9.7 \text{ Pa}$	$G_5 = 2.79 \text{ Pa}$	$\lambda_5 = 54.3 \text{ s}$
$k = 0.39$		

other deformation modes such as compression. In the current study these parameters are arbitrarily chosen to be 1.

In Figure 4.8, the model fit, as well as predictions, are shown and are compared with experimental results. It can be seen that the model was fitted well to the loading and relaxation parts of the ramp-and-hold test with a strain of 0.2 and is able to predict the response of the remaining stress relaxation tests. The unloading and recovery parts are less well described. The determined parameter set was validated for the loading and unloading part of constant shear rate experiments on a different sample, see Figure 4.9. The model predicts the response of the loading-unloading cycles reasonably well, with a maximum deviation of 12.4%.



**Figure 4.8:** Model fit and prediction for stress relaxation experiments.

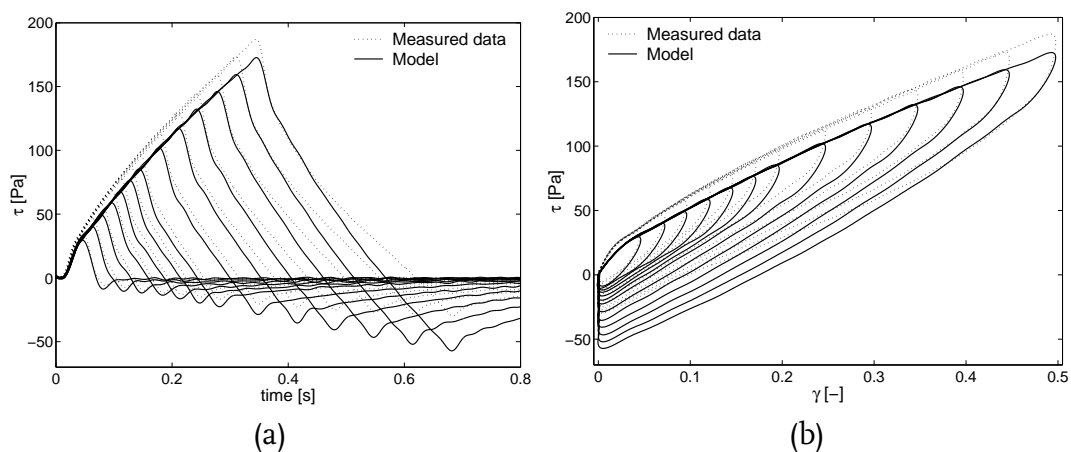


**Figure 4.9:** Model prediction for constant shear rate experiments on a different sample.



## 4.6 Discussion and conclusions

In this paper, the *in vitro* large strain mechanical response of porcine brain tissue in shear tests was investigated. An improved method for rotational shear experiments, with an eccentric sample placement, was used. The occurrence of slippage during measurements was previously investigated [38] on a similar experimental setup and was found to be absent. Also Bilston et al. [36] used sandpaper and reported no slip for strains up to 20 with similar shear rates as in the current study. Therefore, it is assumed that no slip was present.

Results from dynamic frequency sweep tests showed that the samples stiffen with increasing frequency. No cross point for the storage and loss modulus was found in the frequency range used in these measurements. When comparing the linear viscoelastic parameters with results presented by other authors, the values obtained in this study are in the lower part of the range reported in literature and are comparable with the data presented by Arbogast and Margulies [32,34], Brands et al. [38], Peters et al. [59] and Thibault and Margulies [70].

The occurrence of mechanical damage, defined as an immediate change of the mechanical response due to previous deformation, was investigated by a sequence of loading-unloading cycles. It was concluded that no significant immediate mechanical damage affecting the stress-strain behaviour due to previous shear deformations was observed up to a strain of 0.45. This conclusion is limited to the time scale of the experiment. At these strain levels, functional damage may still occur (as observed by for example Bain and Meaney [80] and Morrison III et al. [81]) and at larger time scales also mechanical changes could develop. This observation is in agreement with results of Prange and Margulies [63] who reported no change in long term modulus and no structural changes in the tissue during stress relaxation experiments up to a strain of 0.5 and shear rates of  $8.33 \text{ s}^{-1}$ . Moreover, it was found that for strains larger than 0.2 the sample did not recover completely after a loading-unloading cycle which indicates a non-linearity of the material behaviour. No maximum in the stress-strain response was found in the constant strain rate measurements even though the samples were tested up to a strain of 0.5. This is in agreement with the findings of Arbogast et al. [31], Bilston et al. [36], and Donnelly and Medige [42].

A decrease of the relaxation modulus with increasing strain was found in the stress relaxation measurements, which is in agreement with Arbogast et al. [31], Bilston et al. [36], Brands et al. [38], Nicolle et al. [56], Peters et al. [59] and Prange and Margulies [63]. This effect was decreasing with strain level for strains higher than the linear viscoelastic limit which differs from the results of Brands et al. [38] and Nicolle et al. [56]. This difference may be attributed to the non-homogeneous shear field in case of a conventional centred rotational shear setup. It was found that for strains in the non-linear regime, the sample did not recover completely.

Although the large strain experiments have been conducted on a limited number of samples, the experimental protocol, which was based on a well-defined series of repeated tests, allowed to determine the non-linear response of brain tissue. The large strain re-

sponse was found to be highly reproducible. In addition to the different samples used in the stress relaxation experiments showing almost identical behaviour, also the different samples used the test sequence to ascertain the absence of damage showed almost identical behaviour, as could be observed from the model prediction in Figure 4.9.

Based on the experimental results, a new differential constitutive model was formulated and subsequently fitted to the presented experimental data. The model predicts the response during the loading phase and the relaxation phase well but is not able to correctly predict the behaviour during unloading and recovery. Important for application in numerical head models is its ability to accurately predict the mechanical response in other deformation modes. The ability of the model to predict the mechanical response of brain tissue in compression is addressed in Chapter 5.

The constitutive model presented in this Chapter is applicable in three-dimensional head models, where the non-linear nature of the constitutive behaviour may have significant consequences for the predicted mechanical response [82]. However, it should be noted that the viscous non-linearities are moderate compared to many other materials.



# Validation in compression<sup>I</sup>

---

# 5

## Abstract

No validated, generally accepted dataset on the mechanical properties exists, not even for small strains. Most of the experimental and methodological issues have previously been addressed for linear shear loading. The objective of this work was to obtain a consistent data set for the mechanical response of brain tissue to either compression and shear. Results for these two deformation modes were obtained from the same samples to reduce the effect of inter-sample variation. Since compression tests are not very common, the influence of several experimental conditions for the compression measurements was analysed in detail. Results with and without initial contact of the sample with the loading plate were compared. The influence of a fluid layer surrounding the sample and the effect of friction were examined and were found to play an important role during compression measurements.

To validate the non-linear viscoelastic constitutive model of brain tissue that was developed in Chapter 4 and has shown to provide a good prediction of the shear response, the model has been implemented in the explicit FE code MADYMO. The model predictions were compared to compression relaxation results up to 15% strain of porcine brain tissue samples. Model simulations with boundary conditions varying within the physical ranges of friction, initial contact and compression rate are used to interpret the compression results.

---

<sup>I</sup> *Partly reproduced from:* M. Hrapko, J. A. W. van Dommelen, G. W. M. Peters, J. S. H. M. Wismans, (2008). Characterisation of the mechanical behaviour of brain tissue in compression and shear, submitted.

## 5.1 Introduction

The head is the most vulnerable part and it is often involved in life-threatening injury. Transport crashes in the EU caused up to 40 thousand deaths, over 3.3 million casualties and cost over 180 billion Euros in 2001 [75]. To develop protective measures, an accurate assessment of injury risk is required. In the early sixties, the currently used Head Injury Criterion was developed [7] based on the Wayne State Tolerance Curve [8]. However, it is based on linear head acceleration only and it does not allow for a distinction between different injury mechanisms. By using a detailed FE model of the head, the behaviour of the brain can be predicted and improved injury criteria can be developed and implemented into safety standards. These FE models often contain a detailed geometrical description of the anatomical components but lack accurate descriptions of the mechanical behaviour of the brain tissue.

The research on the behaviour of brain tissue started by Franke [83] by studying the response of porcine brain tissue to forced vibrations. The mechanical behaviour of brain tissue has been tested mostly *in vitro* in shear [34,36,38,46,58,59,63–65,70], but also in compression [39,43,53,84,63,64] and tension in some studies [44,55,66]. Although a large collection of data is available, studies on the characterisation of brain properties by different laboratories using different testing protocols have yielded a tremendously wide range of results, already for the linear viscoelastic properties (for a complete overview, see Chapter 2). As a consequence of the inconsistency in methods and results, these results cannot be combined to one data set that is covered by one (visco-elastic) constitutive model that can be used for multiple deformation modes. Ideally, the response to different types of deformation should be measured for the same sample to reduce the effect of inter-sample variation.

Various aspects of the experimental procedure may influence the sample response and subsequently affect the measurement result. In case of shear measurements, several aspects have been studied before, e.g. slip/no-slip boundary conditions, influence of the height of the sample, influence of different temperatures, effect of post-mortem time, etc. [36,38,57,46,85]. Also, the effect of the experimental conditions during compression measurements, such as frictional effects and consequences of different procedures for obtaining sample height, should be further evaluated. Miller and Chinzei [53] and Shen et al. [64] highlighted the tendency of a sample to adhere to the loading plate of a rheometer, which takes place even before touching the sample. This is caused by the surface tension of a thin fluid layer on top of the sample, and may affect the measurement results. This effect is examined in the current study, by comparing model predictions with measurement results using different compression protocols.

There are a few studies discussing the effect of friction between the sample and the loading plate. Wu et al. [86] has used data and an Ogden hyper-elastic model from Miller and Chinzei [53] in an FE model. They compared results for friction coefficients of 0 to 0.5, applying a Coulomb friction model, for different strain rates, and also different specimen aspect ratios (diameter/height). Different strain rates were found to have no effect on model predictions of the stress responses. However, they concluded that a higher

friction coefficient will increase the reaction force obtained during compression measurements. Also, the smaller the specimen aspect ratio, the smaller the friction effect on the measured results is. The difference in stress results of a 20% strain compression with friction coefficients of 0.1 and 0.3 versus frictionless compression was up to 10% and 60%, respectively. Miller [84] has investigated the effect of friction coefficients of 0-0.1 using an FE model. The stress increase for a 20% strain compression due to friction coefficients of 0.05 and 0.1 was up to 7.5% and 15%, respectively. Recently, Cheng and Bilston [39] compared experimental results and model predictions of pure slip, slip with friction coefficients of 0.1, 0.3 and 0.5, and a no-slip boundary condition in compression. The peak reaction force of a no-slip boundary condition obtained from numerical simulations were found to be 3 times stiffer than the experimental results. The equilibrium reaction force obtained from measurements with a no-slip boundary condition was found to be 1.64 times higher than those obtained with a slip boundary condition. Friction is apparently an important aspect which influences compression measurement results and therefore it is examined further in the current study. It will be shown that a Coulomb friction model is not valid.

A number of constitutive models have been developed to describe the mechanical behaviour of brain tissue. Some authors propose integral models [76,53,56,58,63,68] often in combination with Ogden hyper-elasticity, whereas others propose differential models [36,12,42,49,64]. Crucial for the use of these models to predict injury is the ability to correctly describe the non-linear behaviour for complex loading histories and large deformations in complex, mixed deformation modes. The ability of a model to describe the anisotropic behaviour of brain tissue may be of less importance, because of the relatively low anisotropy of brain tissue [57,63,66].

The objective of this study was to obtain a data set for the mechanical response of brain tissue in different deformation modes and to validate a non-linear viscoelastic constitutive model for brain tissue. The model developed in Chapter 4 has shown to provide a good prediction of the shear response. A consistent data set was obtained by combining measurements performed in shear and compression for the same samples. This way, variation caused by inter-sample differences in experimental conditions is reduced. Several aspects of the compression protocol are examined in order to correctly interpret the results to obtain reliable results.

## 5.2 Materials and methods

Fresh halves of porcine brains from approximately 6 months old pigs were obtained from a local slaughterhouse. At this age, tissue is considered to possess a fully developed micro-structure [70,63]. Porcine brain tissue was chosen as a substitute for human brains because of availability and the possibility to minimise the post-mortem time at testing. To prevent dehydration and to slow down degradation of the tissue, the brains were placed in an ice-cooled physiological saline solution immediately after acquisition. Samples were prepared from the brain halves within 2 hours post-mortem. Slices were cut by a Leica

VT1000S Vibrating-blade microtome in three different planes from the corona radiata region. From these slices, cylindrically shaped samples that were composed of white matter only were obtained with a cork bore. The diameter of the sample was 8 to 12 mm and the height was approximately 2 mm. Immediately after sample preparation, samples were placed in a physiological saline solution at 4 °C, and subsequently were tested within 0.5 to 5 hours. All samples were tested within post-mortem times ranging from 2.5 to 7 hours.

Both shear and compression experiments were performed on an ARES II rotational rheometer with a 10GM FRT transducer in a plate-plate configuration. For shear measurements, an eccentric configuration was used, in which the sample was placed at the edge of the plate [71]. The advantages of shifting the sample to the edge of the plate are the increased measured signal and a more homogeneous deformation than in the conventional centred configuration. Consequently, this configuration enables the study of the large strain response of the material. For shear tests, waterproof sandpaper with a grain size of 0.18 mm was attached to the top and the bottom plate of the rheometer to prevent slippage. This configuration was previously shown to be effective by Bilston et al. [36] and Brands et al. [38]. In compression experiments, Teflon tape was attached to the top and the bottom plate to minimise friction effects. During the test, samples were covered by a moist chamber to prevent dehydration and the samples were tested at a temperature of 23 °C.

The height of each sample  $h_0$  was estimated during an initial compression stress relaxation test at constant velocity ( $v_c = 0.1 \text{ mm/s}^{-1}$ ), starting without the top plate touching the sample. This constant velocity corresponds to a compression rate of approximately  $0.045 \text{ s}^{-1}$  which is dependent on the height of the sample. This procedure will be referred to as *protocol 1*, see Figure 5.1a.



**Figure 5.1:** Compression protocol (a) without initial contact, (b) with initial contact.

### 5.2.1 Effect of test conditions

It is hypothesised that the difference in results obtained with the two compression protocols is caused by adhesion of the sample to the top plate of the rheometer before touching the sample in protocol 1. This is caused by the surface tension of a thin fluid layer on the top of the sample. The results of the two compression protocols were compared with model predictions to test this hypothesis. The deformations applied in protocols 1 and 2 were reproduced and used as input for the constitutive model. In the first part of the

loading history, the material was loaded in tension (mimicking the attachment of the fluid layer) prior to the compression test, followed by a strain history similar to the experimental loading sequence. The height of the sample was determined from the zero force point reached during the transition from tension to compression. From the model predictions, the state of the material at the starting point of both compression tests was identified by the values of the inelastic principal stretch ratios of all viscoelastic modes  $i$  in the model.

### 5.2.2 Effect of friction

To obtain a homogeneous state of deformation when testing soft tissue in unconfined compression, it is required that friction between the sample and the plate is negligible. To evaluate the amount and type of friction between the samples and the Teflon-coated plate, shear measurements were performed using the same sample-plate interface conditions. The purpose of these tests was to determine the rate dependent properties of the sample-plate friction when tested with a slip interface. Before these friction measurements, the height of the sample was estimated from a compression measurement (protocol 1) as described before. The friction measurements were performed in an eccentric configuration with Teflon tape attached to the top plate, whereas sand paper was attached to the bottom plate. Consequently, the lowest friction is between the sample and the top plate. After a pre-compression of approximately 10 % was applied, a series of four loading-unloading shearing cycles at a constant velocity per cycle was applied to the samples. The loading up to a relative displacement (displacement/gap between plates) of 1 is applied to the bottom plate within 10, 5, 1, and 0.5 seconds. Between each cycle, the material was left to recover for a period of 2 minutes at zero strain. Afterwards, the third loading/unloading test was repeated with sandpaper attached on the top plate, to compare the results from slip/no-slip boundary conditions. These tests were performed without moist chamber to allow video-images of the deformation of the sample and the interface to be taken. Since the tests were completed within 15 minutes, it is believed, based on experimental experience, that the changes caused by moist reduction were minimal. The friction obtained with a Teflon-coated top plate was measured for 9 samples, whereas friction obtained with sandpaper attached to the top plate (i.e. no-slip) was measured for 5 samples.

### 5.2.3 Model validation

The results from the shear experiments were compared to predictions by the constitutive model presented in Chapter 4. To enable the description of the response of the brain tissue to sufficiently high frequencies, an extra viscoelastic mode has been added to the model based on the experimental data by Shen et al. [64] and data obtained in Chapter 2. The brain tissue was assumed to be homogeneous, isotropic with the material parameters given in Table 5.1. To simulate the compression experiments, a compressible version of the constitutive model has been implemented in the explicit FE code MADYMO, see Appendix A. A 3-D model of a quarter of a sample with similar dimensions (diameter



= 8 mm, height = 2 mm) as the samples used in the experiments was used to predict the compressive response (see Figure 5.2). Symmetry conditions are used for the  $xz$  and  $yz$  planes. The sample was compressed at a strain rate of  $-0.1 \text{ s}^{-1}$  prescribing the  $z$ -displacement of the top nodes while suppressing vertical displacements of the bottom nodes. The responses using two limiting conditions between the sample and the loading plates were compared with the results of the compression experiments: (i) perfect slip conditions and (ii) no-slip conditions obtained by suppressing all in-plane displacements of the top and bottom nodes.

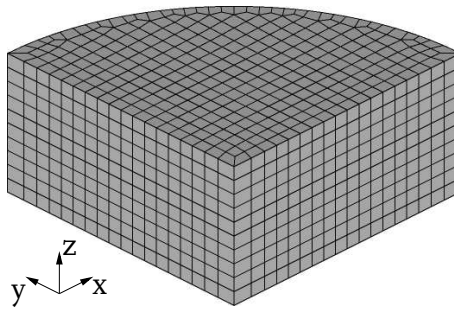


Figure 5.2: Finite Element model of a quarter of a sample.

Table 5.1: Material parameters.

Elastic and viscous parameters	Viscoelastic parameters
$G_e = 182.9 \text{ Pa}$	$G_1 = 9884 \text{ Pa}$ $\lambda_1 = 0.00013 \text{ s}$
$A = 0.73$	$G_2 = 835.5 \text{ Pa}$ $\lambda_2 = 0.012 \text{ s}$
$C = 15.6$	$G_3 = 231.2 \text{ Pa}$ $\lambda_3 = 0.35 \text{ s}$
$n = 1.65$	$G_4 = 67.1 \text{ Pa}$ $\lambda_4 = 4.62 \text{ s}$
$\tau_0 = 9.7 \text{ Pa}$	$G_5 = 3.61 \text{ Pa}$ $\lambda_5 = 12.1 \text{ s}$
$k = 0.39$	$G_6 = 2.79 \text{ Pa}$ $\lambda_6 = 54.3 \text{ s}$
$K = 2.5 \text{ GPa}$	

## 5.3 Results

### 5.3.1 Effect of test conditions

Compression measurement results of protocol 1 and 2 are shown in Figure 5.3. Biological variability and anisotropy are aspects that contributed to the variations in the data. However, the characteristic shapes of the stress-strain responses are consistent for each protocol. Whereas the stress obtained with protocol 1 exhibits a convex shape over the whole strain domain, results of protocol 2 showed an initially concave shape corresponding to a stiffer response for small strains. The stress measured with protocol 2 at a strain

of 0.1% was found to be, in average, 6.6 times larger than the stress measured with protocol 1. The average initial Young's modulus computed from these measurements was found to be 606 Pa and 4017 Pa for protocol 1 and protocol 2, respectively. Model predic-

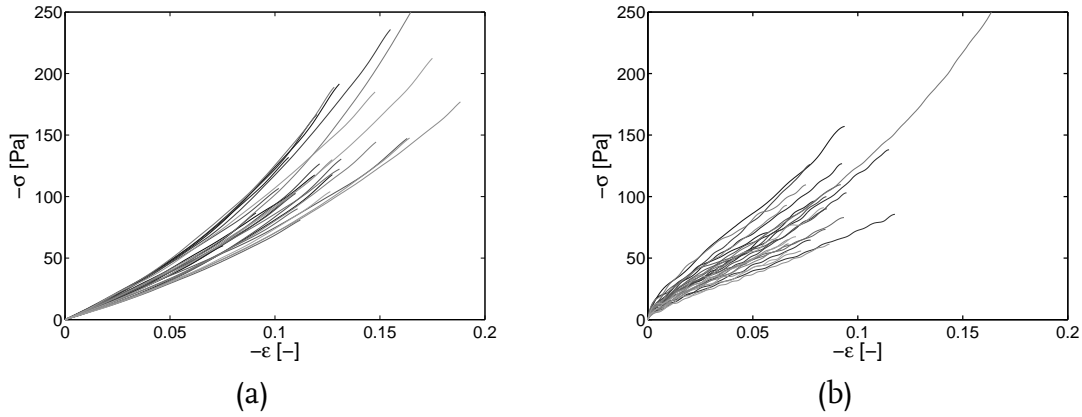


**Figure 5.3:** Compression results of 28 samples (a) without initial contact - protocol 1, (b) with initial contact - protocol 2.

tions of the stress response with both compression protocols are compared in Figure 5.4. A similar difference between protocol 1 and 2 as found experimentally is obtained also from the model predictions. The stress prediction obtained with protocol 2 at a strain of 0.1% was found to be 5.1 times larger than the stress prediction obtained with protocol 1. As can be seen in Figure 5.4, the difference in the response occurs in the beginning of the loading phase. To investigate the state of the viscoelastic modes at the start of the compression test, the values of the axial component of the inelastic right Cauchy-Green deformation tensor,  $C_p$ , for individual viscoelastic modes are compared in Figure 5.5a. Values for protocol 2 are almost the same for each mode, whereas for protocol 1 they deviate from the equilibrium value  $\lambda^2$ , which is the first component of the right Cauchy-Green deformation tensor  $C$ . This difference confirms that the state of the material is being out of equilibrium which explains the differences in the observed mechanical response (Figure 5.5b). Based on these results, protocol 2 is chosen for the model validation. The standard deviation of stress response during the loading phase of protocol 1 is up to 28%, whereas for the protocol 2 it is up to 40%.

### 5.3.2 Effect of friction

The measured shear force  $F_s$  during friction measurements is normalised by the cross-sectional areas  $A$  of each sample. A clear dependence of the resulting shear stress on the velocity normalised by the height of the sample is obtained from the shear measurements with a Teflon-coated plate (Figure 5.6a). Also, the value of the relative displacement where the shear stress reaches a plateau value is linearly increasing with the velocity. Figure 5.6b shows the viscosity-like quantity  $\tau/v_s^*$  [Pa.s/mm] of the fluid layer on the sample versus the scaled velocity  $v_s^* = v_s h_0/h$  [mm/s], where  $\tau$  is the measured shear stress,  $v_s$  is

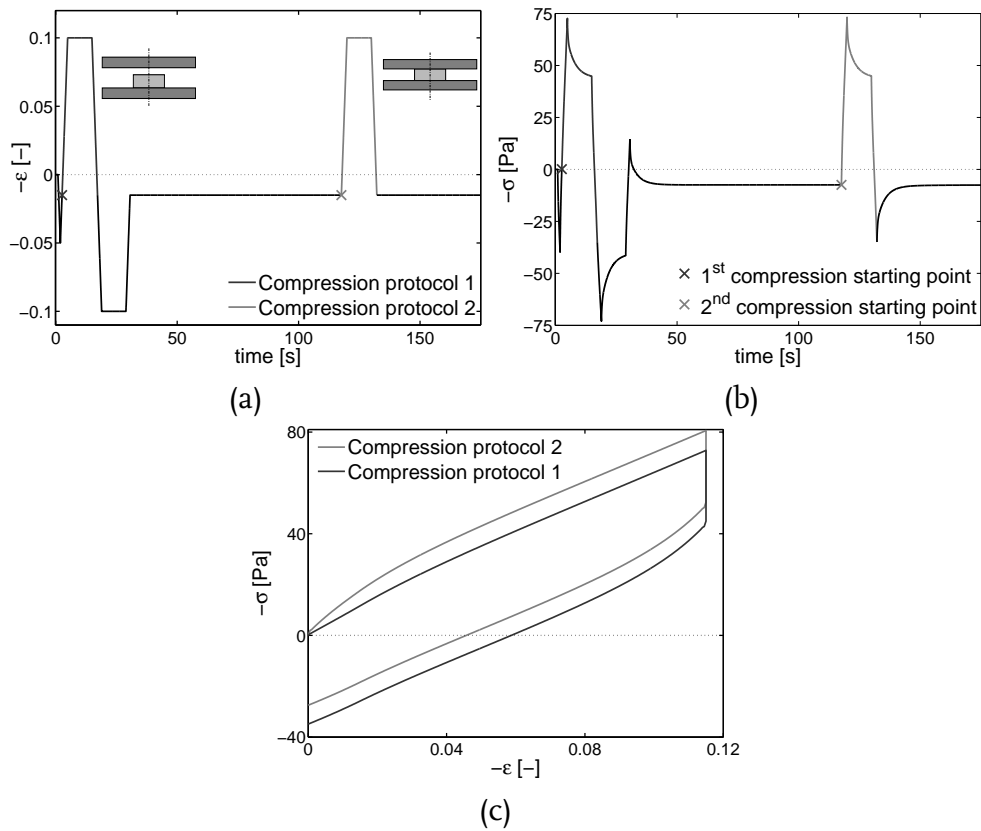


Figure 5.4: Model prediction for the compressive response using the two different protocols.

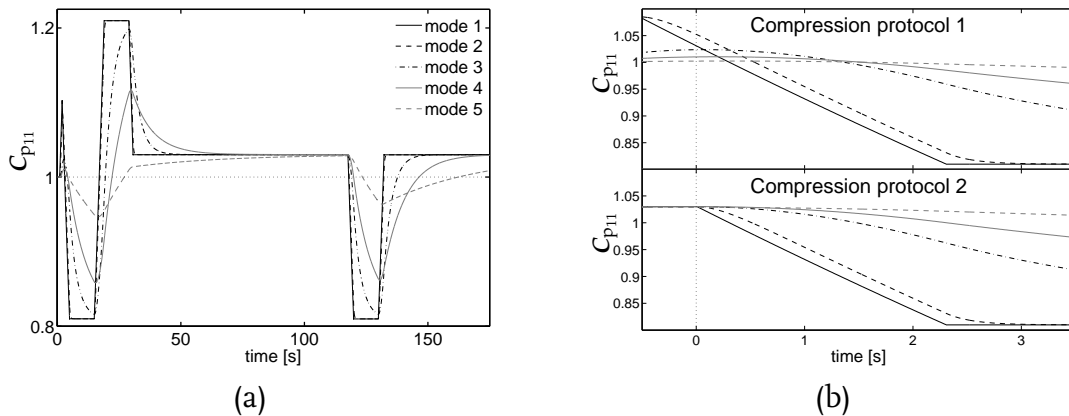
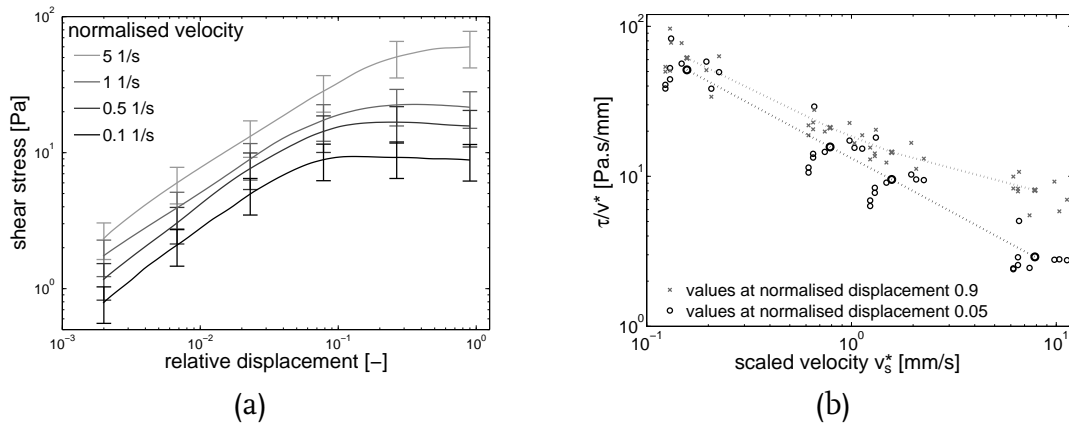


Figure 5.5: (a) The axial inelastic deformation of each viscoelastic mode versus time for the model prediction in Figure 5.4, (b) an enlargement of the response during the two compression tests, where zero time corresponds to the 1<sup>st</sup> and 2<sup>nd</sup> starting point in Figure 5.4a.

the applied velocity and  $h_0$  is the initial sample height. The viscosity-like quantity  $\tau/v_s^*$  is decreasing with increasing apparent shear rate before as well as after the maximum shear stress obtained. The maximum shear stress at  $5 \text{ s}^{-1}$  was found for a relative displacement of 0.9. Therefore, the maximum shear stress for this velocity could also be found at a higher relative displacement. Results of friction measurements on five samples with a



**Figure 5.6:** (a) Evolution of shear stress as a function of relative displacement for different velocities, (b) rate dependence of measured stress response.

Teflon-coated plate and a plate coated with sandpaper (i.e. no-slip) are compared in Figure 5.7, where a relative displacement of 1 was applied within 1 s. Sample five from Figure

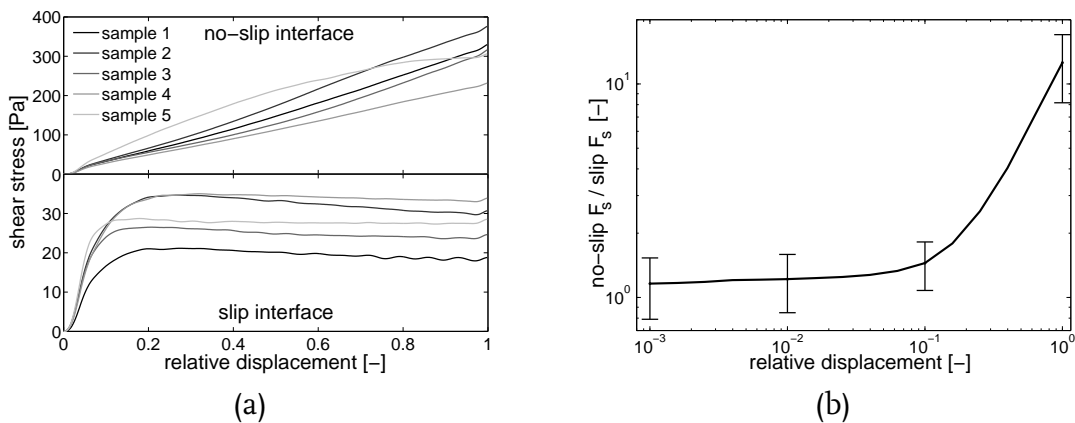


**Figure 5.7:** Difference between shear stress obtained from measurements with no-slip and slip interface for a relative velocity of 1 s<sup>-1</sup>.

5.7a was not accounted for in the mean value and the standard deviation in Figure 5.7b because of the different characteristic shape. In Figure 5.7a it can be seen that whereas the shear force measured from a no-slip interface test continuously increases, the shear force measured from a slip interface test reaches a plateau value after approximately a relative displacement of 0.2. The average value of the maximum friction stress from measurements with a Teflon-coated plate was found to be 27 Pa which corresponds to a shear strain of the sample of 5% in the case of measurements with a plate coated by sandpaper, assuming no-slip conditions for the latter. The differences between these two tests were relatively small in the beginning of the test, when the response is determined by the properties of the sample, whereas after a relative displacement of 0.1 the difference increased linearly (see Figure 5.7b). The standard deviation of the stress response during the loading phase in the shear measurements with a Teflon-coated top plate is 20-30%,

depending on the applied velocity, whereas it is up to 25% for the test with sandpaper attached to the top plate. Notice that the observed rate dependence indicates that this friction behaviour is far more complicated than Coulomb friction.

### 5.3.3 Model validation

Figure 5.8 shows experimental results and model predictions for both shear and compression. The model prediction in shear is in a good agreement with the average experimental results (Figure 5.8a). The initial slope of this curve is determined by the spectrum given in Table 5.1 whereas the characteristic shape of this curve is dominated by the non-linear parameters of the model. The model prediction of the shear stress is up to 10% stiffer and up to 30% more compliant in the loading and the unloading phase, respectively, than the mean of the measured responses. The standard deviation of the response during the loading phase is up to 26%. In Figure 5.8b, the responses of the FE model of a brain sample in compression using different sample-plate interface conditions are compared with experimental results. The effect of the varying loading rates in the compression experiments was found to be small in the model predictions, see Figure 5.8b. The model

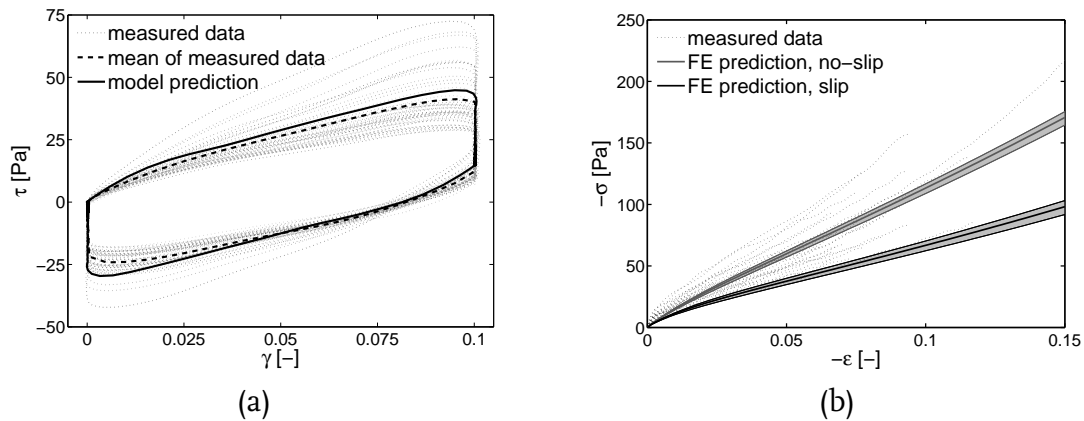


**Figure 5.8:** Comparison of model prediction with measurement results (a) for shear and (b) for compression. The compression model predictions were made using an FE model with a no-slip and slip interface. The shaded areas indicate the range of model predictions for the range of loading rates used in the experiments.

simulation with slip conditions corresponds with the lower range of the experimental results. However, video images of the compression tests have indicated that friction plays a significant role in these tests, even though the plates were Teflon-coated. This is to be expected in view of the friction behaviour shown in the previous section. The response of the simulation with no-slip conditions is found to correspond with the average experimental behaviour in compression. The response of the simulation with a no-slip condition is up to 70% stiffer than the results of the simulation with a slip condition for strains up to 15%. In addition, a comparison of the strain rate dependency of the model with experimental data is given in Appendix 5.A.

## 5.4 Discussion and conclusions

To obtain a reliable prediction of injury from any FE model, constitutive models used for the materials involved have to be chosen carefully. Crucial for head model simulations is the ability of the constitutive model for brain tissue to correctly describe the non-linear behaviour during complex loading histories and large deformations in different deformation modes. In the current study, several aspects of compression experiments have been examined to obtain reliable results for the compressive behaviour of brain tissue. Thereafter, a consistent data set has been obtained by combining measurements performed in shear and compression for the same samples. This way, variation caused by inter-sample differences is reduced. These results were used to validate the predictions of a constitutive model developed in Chapter 4 for both shear and compression.

**Effect of test conditions:** Miller and Chinzei [53] and Shen et al. [64] have highlighted the tendency of a sample to adhere to the top plate of a rheometer, which takes place even before touching the sample. This is caused by the surface tension of a thin fluid layer on top of the sample, and may affect the results. Whereas Miller and Chinzei [53] and Estes and McElhaney [43] have started their compression tests without initial contact between the sample and the top plate, Shen et al. [64] and Cheng and Bilston [39] conducted compression tests with the top plate initially touching the sample. Measurements according to these two methods were used to examine the effect of a fluid layer on the measured response. When starting the compression without initial contact between the sample and the top plate, the initial compressive response of the sample is underestimated up to 6.6 times compared to the response to compression with initial contact. A similar difference between the stress response of these two protocols is obtained from a model prediction as well. It was shown, that the difference was caused by the state of the material being different in the beginning of the loading part of each sequence. Due to the tensile loading before a compression test without initial contact, the material is not in an equilibrated state at the onset of the compression test, which leads to a compliant initial response. Therefore, it was concluded that a compression test should start with the top plate touching the sample, after the sample is fully recovered. The higher standard deviation achieved in the case of compression tests performed according to protocol 2 can be explained by the variation in compression rate which varied from sample to sample according to the sample height.

**Effect of friction:** To obtain a homogeneous state of deformation when testing soft tissue in unconfined compression, it is required that friction between the sample and the plate is negligible. There are a few studies dealing with the effect of friction between the plates and the sample by comparing FE model predictions with pure slip, slip with Coulomb friction and with a no-slip boundary condition. However, little is known about the nature and magnitude of friction in soft tissue compression tests. In the current study, the rate-dependence of friction in the interface between brain tissue and a Teflon-coated plate has been investigated using shear measurements. This friction was non-Coulombic due to its rate-dependence and the absence of a compression force during the shear measurements. The latter is caused by fast stress relaxation due to the viscoelastic behaviour of the brain tissue. The shear stress response and also the relative displacement corresponding to the

maximum shear stress obtained from measurements with a Teflon-coated plate increase with the applied relative velocity. From results of the current study it can be concluded, that the specimen/plate friction significantly affects the results in a compression test by increasing the stress response. This effect should not be ignored when interpreting compression experiments. Miller [84] has proposed a new method (“confined” compression) for measuring the response of soft tissue in compression. The motivation for this was the unknown friction coefficient during unconfined compression, which is usually assumed to be zero. However, the limitation of the proposed method is that it cannot be used for strains higher than 20%. In this work, FE simulations were used to account for the effect of friction during compression measurements.

**Model validation:** Predictions of the shear response of brain tissue with the constitutive model developed in Chapter 4 were found to be in good agreement with experimental results. Notice that the model parameters were obtained from a fit to shear measurements at a temperature of 37°C and the sample was pre-compressed by a force of 10 mN, whereas the experimental data presented in this study were obtained at a temperature of 23°C and the sample was pre-compressed by a force of 5 mN. Results presented in Chapter 2 have showed a stiffening of the stress response of brain tissue with decreasing temperature and an increase of the stress response with increasing pre-compression force. To validate the constitutive model in another deformation mode, a compressible version of this model has been implemented in the explicit FE code MADYMO. A prediction of the compressive deformation of a 3-D model of a quarter of a sample was compared with experimental data. The model prediction with slip conditions at the sample-plate interface corresponds with the lower range of the measured stress response, whereas the response of the simulation with no-slip conditions corresponds with the average experimental behaviour in compression. The response of the simulation with a no-slip condition is up to 70% stiffer than the results of the simulation with a slip condition for strains up to 20%, which is in a good agreement with the variation found by Wu et al. [86] and Miller [84]. Two other studies have presented combined shear and compression measurements and subsequent model predictions but the results for different deformation modes have been obtained from different samples [63,64]. Prange and Margulies [63] have shown a good model prediction of shear stress relaxation, however the compressive response was validated only with the equilibrium stress obtained from compression stress relaxation. On the other hand, Shen et al. [64] have validated a simplified version of a constitutive model developed by Bilston et al. [36] with constant strain rate measurements in compression only up to a strain of 5%, assuming frictionless loading. However, in both of these studies, the model tends to underpredict the tissue response in compression, which is similar to results obtained in the current study using a slip boundary condition.

To be able to obtain accurate stress and strain levels from FE model predictions, the correct description of the constitutive response of brain tissue is required. Only with a well-validated and uniformly accepted constitutive model for brain tissue, numerical head models may be accepted as injury predictors and can be incorporated in safety regulations. The constitutive model used in FE calculations should be based on accurate measurements of the non-linear behaviour of brain tissue during complex loading histories and large deformations in different deformation modes. The ability of a model to

describe the behaviour in tension should be considered as well. Finally, the anisotropic behaviour of brain tissue may be important for FE predictions, even though it was found to be relatively low [85,57,63].

## 5.A Summary of results from compression experiments

In addition to the compression experiments on the ARES II rotational rheometer as described in this chapter, similar compression experiments were conducted on an MTS mechanical testing apparatus. These experiments were performed for a range of strain rates. The results from compression tests on both devices is shown in Figure 5.9. These results are found to agree with collective data from literature which are shown as well. A model prediction assuming frictionless conditions for the tissue-plate interface (i.e. a lower bound prediction) is found to correspond with the lower range of the experimental data. The strain rate dependency of the model is in agreement with the dependency of the experimental data on the strain rate.

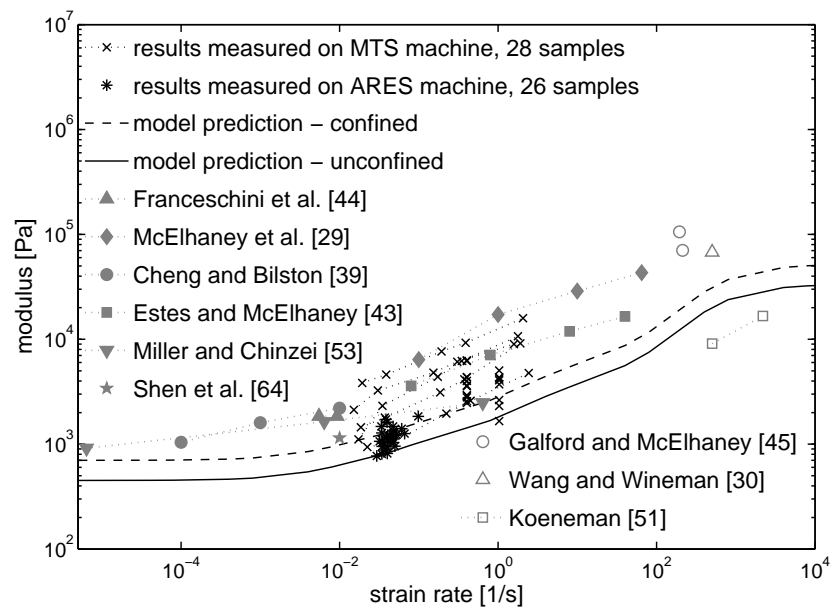


**Figure 5.9:** Summary of compression results obtained in the current study and from literature. Compression moduli from this study were computed from the stress obtained for a strain of 0.04.





# Influence of constitutive modelling in a 3D head model<sup>I</sup>

---

## Abstract

The objective of this work was to investigate the influences of constitutive non-linearities of brain tissue in numerical head model simulations by comparing the performance of a recently developed non-linear constitutive model (see Appendix A) with a simplified version, based on neo-Hookean elastic behaviour, and with a previously developed constitutive model [12]. Numerical simulation results from an existing 3-D head model in the explicit FE code MADYMO were compared. A head model containing a sliding interface between the brain and the skull was used and results were compared with the results obtained with a previously validated version possessing a tied skull-brain interface. For these head models, the effects of different constitutive models were systematically investigated for different loading directions and varying loading amplitudes in both translation and rotation. In the case of the simplified and fully non-linear version of the model, the response predicted with a head model for varying conditions (i.e. severity and type of loading) varies consistently with the constitutive behaviour. Consequently, when used in a finite element head model, the response can be scaled according to the constitutive model used. However, the differences found when using the non-linear model of [82] were dependent on the loading conditions. Hence this model is less suitable for use in a numerical head model.

---

<sup>I</sup> *Reproduced from:* M. Hrapko, J. A. W. van Dommelen, G. W. M. Peters, J. S. H. M. Wismans, (2008). On the consequences of nonlinear constitutive modelling of brain tissue for injury prediction with numerical head models, submitted.

## 6.1 Introduction

More than one third of all injuries are TBI, which also represent one of the major causes of death resulting from traffic accidents [2]. Despite the major advances in prevention and treatment, head injury remains a major health and social problem. TBI can be caused when the head is suddenly struck by an object with or without the object penetrating the skull and the brain. These injuries can be divided into primary injuries, which occur at the moment of impact, and secondary injuries, which develop at a later stage. The majority of brain injuries are caused by DAI characterised by microscopic damage of axons. DAI can occur without any direct impact on the head, as it can be the result of rapid acceleration/deceleration. DAI is thought to be the most common and important pathology in mild, moderate, and severe traumatic brain injury [3]. It may develop over a period of hours or even days after an accident.

To develop protective measures, an accurate assessment of the risk of injury is required. In the early sixties, the currently used Head Injury Criterion was developed [7] based on the Wayne State Tolerance Curve [8]. However, it is based on translational head acceleration only and it does not allow for a distinction between different injury mechanisms. By using a detailed FE model of the head, the behaviour of the brain can be predicted for any loading condition and such models can serve to provide improved injury criteria which can be implemented into safety standards. These FE models often contain a detailed geometrical description of the anatomical components but lack accurate descriptions of the mechanical behaviour of the brain tissue.

A number of constitutive models have been developed to describe the mechanical behaviour of brain tissue. Some authors propose integral models [76,53,56,58,63,68] often in combination with Ogden hyper-elasticity, whereas others propose differential models [36,12,42,49,64] which are more suitable for implementation in numerical codes. Important for the use of these models to predict injury may be the ability to correctly describe the non-linear behaviour for complex loading histories and large deformations in different deformation modes.

To be able to use uniform tissue level injury criteria, i.e. injury criteria that can be transferred between different head models, accurate stress and strain levels should be predicted, for which the correct description of the constitutive response of brain tissue is required. Therefore, the objective of this study is to investigate the consequences of using different constitutive descriptions of the mechanical response of brain tissue in FE head models for injury prediction. For this purpose, a non-linear viscoelastic constitutive model for brain tissue is used, see Chapter 4. This model has shown to provide a good prediction of the response to both shear and compression, see Chapter 5. Numerical simulations using the constitutive model in a 3-D head model were compared with predictions using a simplified version of this model and the constitutive model developed by Brands et al. [12]. These constitutive models are used within a 3D head model with a sliding interface between the brain and the skull. However first, this sliding interface model is also compared to a previously validated 3D head model with a tied interface [87,82]. The effect of the size of a subdural space in FE models, has been investigated by Kleiven and

Von Holst [88], showing an increase in relative motion between the brain and the skull with an increasing size of the subdural space. Kleiven and Hardy [89] have compared predictions of models with tied and sliding interfaces with and without separation and concluded the intracranial pressure of the tied interface model to correlate better with experimental results than models with a sliding interface. On the other hand, Al-Bsharat et al. [90] have compared predictions of models with tied and sliding interfaces and found the results of a sliding interface model to compare better with experimental pressure data of Nahum et al. [91]. However, Bradshaw and Morfey [92] have concluded that varying the shear modulus by an order of magnitude produces little change in pressure response in an FE model of TBI, while the peak maximum principal strain is very sensitive to changes in shear modulus. Therefore, the head model with the sliding interface will be used to assess the consequences of the different constitutive models for brain tissue for equivalent stress and strain predictions.

## 6.2 Methods

An existing 3-D numerical head model with different skull-brain interfaces is used to investigate the consequences of constitutive non-linearities. First, the effect of the different interface conditions will be examined. Thereafter, influences of constitutive non-linearities of brain tissue in numerical head model simulations will be investigated by comparing the performance of different constitutive models. For these simulations the explicit FE code MADYMO, version 6.3.2 is used.

### 6.2.1 Effect of the skull-brain interface conditions

To investigate the consequences of using different skull-brain interfaces in a finite element head model, two head models are compared.

First, a model developed by Claessens et al. [87] and Brands et al. [82] is used. In this model the brain, dura mater and skull are tied, not allowing sliding and separation of each other. This model will be referred to as the **Tied interface model** and was validated [87] using the experimental data of Nahum et al. [91]. All anatomical components are described by solid, reduced integration, eight node brick elements. The skull consists of 3212 elements, the dura mater consists of 3178 elements, and the brain is modelled by 7478 elements. The skull is assumed to be rigid and the dura mater is modelled as a linear elastic material. Material parameters of these components are summarised in Table 6.1.

For a comparison of these models, the brain tissue was assumed to be isotropic, homogeneous and it was modeled with the non-linear viscoelastic model developed in Chapter 4. This model was validated for both shear and compression in Chapter 5. The model, which is summarised in Appendix A, is of a multi-mode Maxwell type and consists of a non-linear elastic mode in combination with a number of viscoelastic modes. These viscoelastic modes consist of an elastic Mooney-Rivlin model and a viscous Ellis model. The

**Table 6.1:** Material parameters of the various anatomical components of the FE head model.

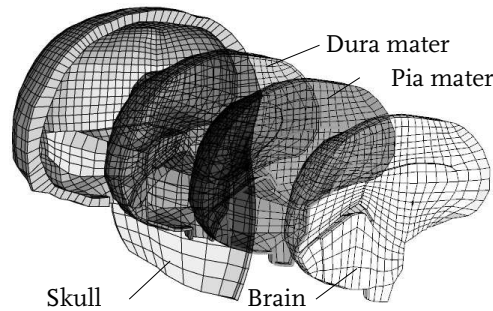
	Young's modulus $E$ [Pa]	Poisson's ratio $\nu$ [-]	Mass density $\rho$ [kg/m <sup>3</sup> ]
Skull	–	–	2070
Dura mater	$3.15 \cdot 10^7$	0.45	1130
Pia mater	$3.15 \cdot 10^7$	0.45	1130

	Elastic and viscous parameters	Viscoelastic parameters	
Brain (NLVE-A)	$G_e = 182.9$ Pa	$G_1 = 9884$ Pa	$\lambda_1 = 0.00013$ s
	$A = 0.73$	$G_2 = 835.5$ Pa	$\lambda_2 = 0.012$ s
	$C = 15.6$	$G_3 = 231.2$ Pa	$\lambda_3 = 0.35$ s
	$n = 1.65$	$G_4 = 67.1$ Pa	$\lambda_4 = 4.62$ s
	$\tau_0 = 9.7$ Pa	$G_5 = 3.61$ Pa	$\lambda_5 = 12.1$ s
	$k = 0.39$	$G_6 = 2.79$ Pa	$\lambda_6 = 54.3$ s
	$K = 2.5$ GPa		

non-linear equilibrium mode is described by a Mooney-Rivlin-type model, modified with a non-linear prefactor. The material parameters of the model see Table (6.1) were determined in Chapter 4 and extended with an extra viscoelastic mode for higher frequencies based on experimental data by Shen et al. [64] and data obtained in Chapter 2.

In addition, a more realistic skull-brain interface is used for which the original model is extended with a sliding interface [93,94] (see Figure 6.1). This model will be referred to as the **Sliding interface model**. The interface between the skull and the brain was modelled by a 0.5 mm gap between the dura mater and the pia mater. The brain is not restrained in the foramen magnum in the current model. This was previously compared with the brain being restrained in the foramen magnum, showing only small differences in strains and stresses [93]. In addition to the previous model, the pia mater is composed of 3210 shell elements with 0.5 mm thickness which completely envelope the brain. Sliding and separation is enabled between the dura mater and pia mater by a frictionless contact condition. The skull is assumed to be rigid, whereas the dura mater and the pia mater are modelled as linear elastic materials, see Table 6.1 for material parameters.

**Figure 6.1:** 3-D FE head model with a sliding interface.

For a comparison of the two head models with different interface conditions, the skull was subjected to sinusoidal acceleration pulses for anterior-posterior (AP) translation and posterior-anterior (PA) rotation with six different acceleration pulse amplitudes, see Figure 6.2. The translational acceleration amplitudes were chosen according to HIC values

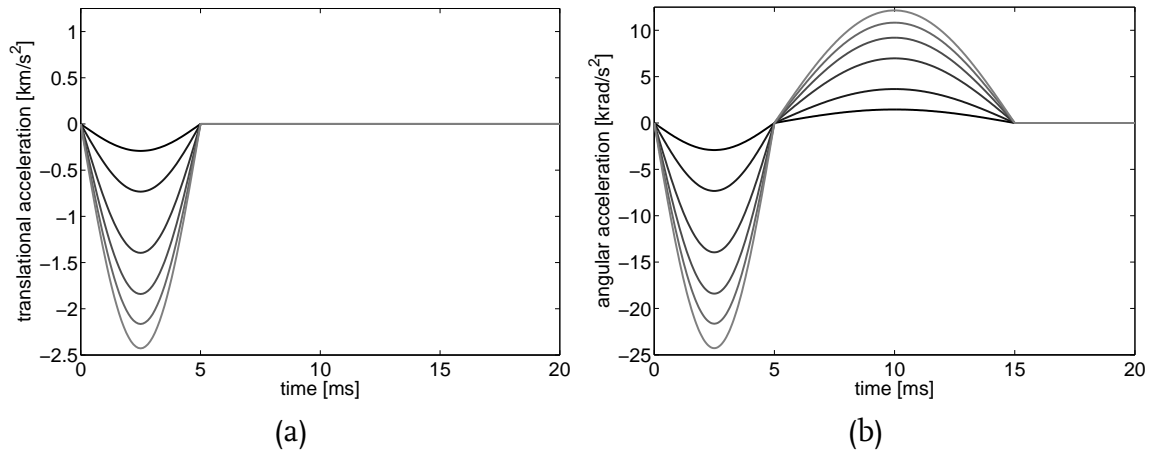


**Figure 6.2:** Sinusoidal acceleration pulses applied to the head, (a) translation, (b) rotation around the anatomical origin.

of 10, 100, 500, 1000, 1500 and 2000. These values are chosen in order to study the model response in a range of loading conditions covering the non-injurious to the injurious regime. For rotational acceleration, the axis of rotation was positioned in the anatomical origin of the model corresponding to the ear hole projected to the sagittal plane, see Figure 6.3. The acceleration amplitudes for rotation were chosen to produce translational acceleration in the upper brain-skull interface approximately corresponding to the previously chosen translational acceleration levels.

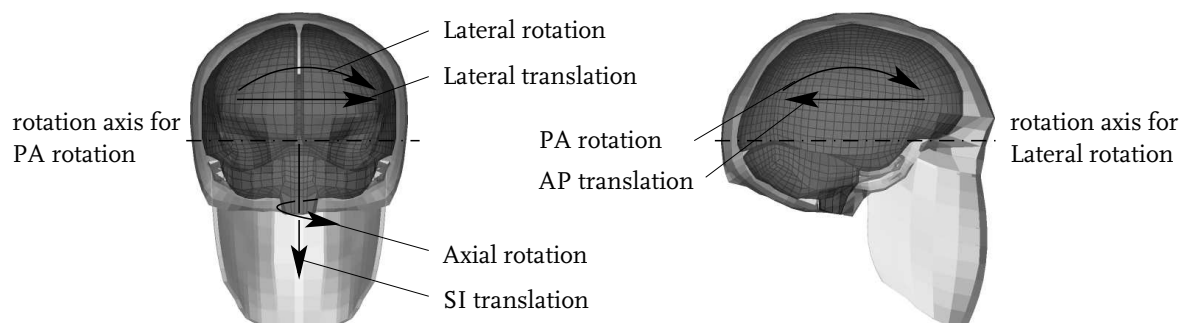


**Figure 6.3:** Loading directions for translational and rotational accelerations applied to the skull. (PA = Posterior-anterior, AP = anterior-posterior, SI = superior-inferior).

## 6.2.2 Effect of different constitutive models

To investigate the consequences of using different constitutive models for brain tissue in an FE head model, the head model developed by Claessens et al. [87] and Brands et al. [82], extended with a sliding interface [94] was used. The brain tissue was assumed to be homogeneous, isotropic and was described by three different constitutive models:

- NHVE - a simplified version of the constitutive model developed in Chapter 4, obtained with  $k = 1$ ,  $A = 1$ . The resulting model is a visco-hyperelastic model in which the elastic behaviour is neo-Hookean. The model is also known as the Upper Convected Maxwell (UCM) model.
- NLVE-A - the non-linear viscoelastic model developed in Chapter 4 which is an extension of the UCM and was described in the previous section. This model is summarised in Appendix A.
- NLVE-B - the non-linear constitutive model developed in Brands et al. [82], using the material parameters obtained from the same study. The model is a non-linear extension of a multi-mode UCM model. The elastic behaviour is modelled by a hyper-elastic, higher order Mooney-Rivlin formulation. The inelastic, time dependent behaviour is modelled using a Newtonian law, acting on the deviatoric part of the stress only.

For each constitutive model, the skull was subjected to translational and rotational accelerations in three directions each, to study the model response in a total of six different loading directions, see Figure 6.3. In addition to the previously described AP translation and PA rotation, translation in lateral and superior-inferior direction and rotation in lateral and axial direction were applied. In all rotational cases, the axis of rotation was chosen to coincide with the anatomical origin of the model, corresponding to the ear hole projected to the sagittal plane. The translational and rotational acceleration pulses are similar as described in the previous section and are depicted in figure 6.2. Results will be presented in terms of equivalent Von Mises stress and strain levels which are defined as:  $\bar{\sigma} = \sqrt{\frac{3}{2} \boldsymbol{\sigma}^d : \boldsymbol{\sigma}^d}$  and  $\bar{\varepsilon} = \sqrt{\frac{3}{2} \boldsymbol{\varepsilon}^d : \boldsymbol{\varepsilon}^d}$ , respectively, with  $\boldsymbol{\sigma}$  the Cauchy stress tensor and  $\boldsymbol{\varepsilon}$  the Left Green-Lagrange strain tensor.

## 6.3 Results

### 6.3.1 Effect of the skull-brain interface conditions

In the case of the tied interface model, the largest deformations were produced mainly in the interior regions of the brain. For the sliding interface model, the highest deformations were exclusively found in the outer regions of the brain. This was mainly caused by the brain being obstructed by the dura mater, the falx cerebri or the tentorium cerebelli. In the sliding interface model, the brain is lagging behind the motion of the skull

during a few initial milliseconds, caused by the gap between the brain and other parts of model. During simulations with AP translation, the tied interface model showed the highest deformations in the anterior part of the corpus callosum at approximately 4 ms, indicated by A in figure 6.4(a). They originated from the brain being obstructed by the

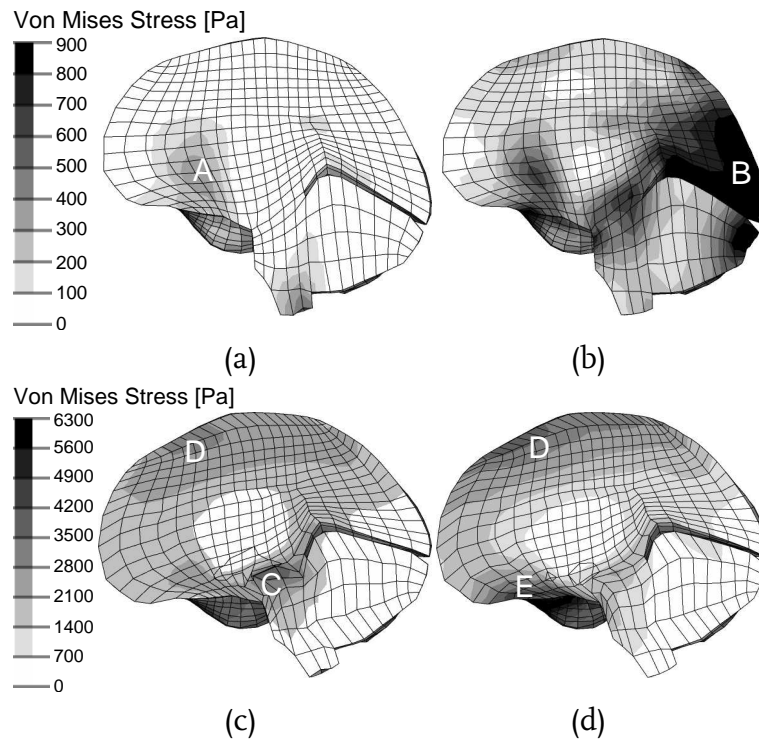


**Figure 6.4:** FE model predictions of Von Mises stress in parasagittal (5 mm off-centre) cross-section for (a)–(b) AP translation at 4.5 ms, (c) PA rotation at 9 ms, and (d) PA rotation at 12.5 ms. (a), (c) tied interface model, (b), (d) sliding interface model.

anterior part of falx cerebri. The sliding interface model showed the maximum deformations in the posterior and inferior side of the region corresponding to the occipital lobe of the brain at approximately 5 ms, indicated by B in figure 6.4(b). During simulations with PA rotation, the tied interface model showed the maximum deformations in the centre of the thalamus and midbrain regions at 12.5 ms, indicated by C in figure 6.4(c). The second major deformation area was observed to be in the superior side of the regions corresponding to the frontal and parietal lobe at 5.5 ms, indicated by D in figure 6.4(c). The sliding interface model showed the highest deformations in the anterior and superior side of the region corresponding to the frontal lobe and anterior side of the region corresponding to the temporal lobe of the brain at approximately 9 ms, indicated by D and E in figure 6.4(d).

For the two head models with different interface conditions, the Von Mises stress or Von Mises strain levels that are exceeded by a certain percentage of elements, are displayed in Figure 6.5. In the case of the tied interface model, the predictions of Von Mises stress and strain are linearly increasing with increasing translational acceleration levels, while



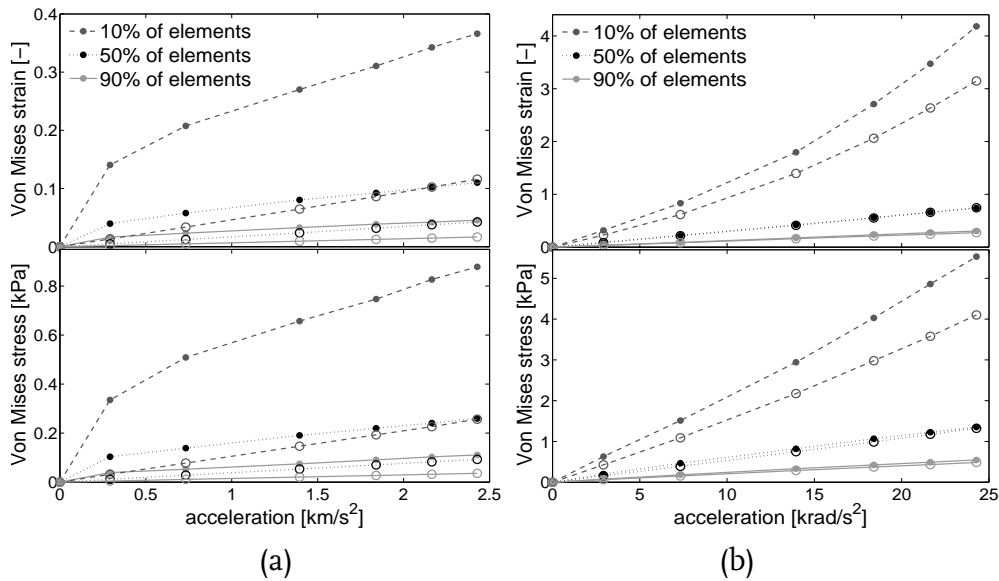


**Figure 6.5:** FE model predictions of Von Mises strain levels and Von Mises stress levels that are exceeded by different percentages of elements for (a) AP translation and (b) PA rotation, obtained with (●) the sliding interface model and (○) tied interface model.

they are increasing non-linearly for the sliding interface model. The predictions of the Von Mises stress during rotational acceleration are increasing non-linearly for both models, while the predictions of Von Mises strains are increasing almost linearly. The relative differences between the Von Mises stress and strain predictions of the tied and sliding interface models are non-linearly decreasing with applied translational acceleration from approximately 9 in the case of  $290 \text{ m/s}^2$  to 3 in the case of  $2400 \text{ m/s}^2$ , see Figure 6.6. The differences between the Von Mises stress and strain predictions of the tied and sliding interface models are mostly constant (approximately 1.15) with the level of applied rotational acceleration in all cases.

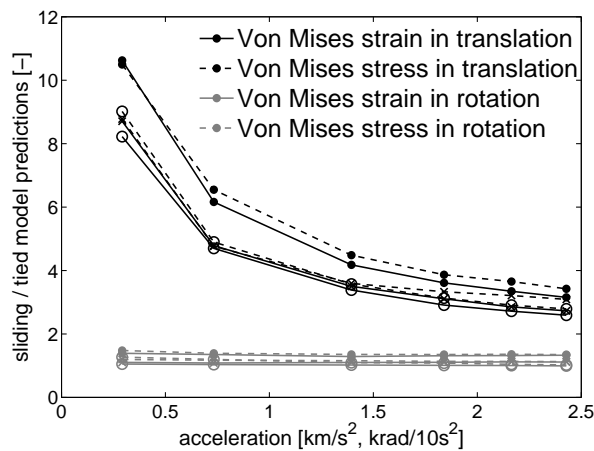


**Figure 6.6:** Difference in the Von Mises strain and Von Mises stress levels that are exceeded by ● - 10%, ○ - 50% and × - 90% of elements for the results plotted in Figure 6.5.

### 6.3.2 Effect of different constitutive models

The patterns of Von Mises stress and Von Mises strain predictions with the FE head model using different constitutive models for brain tissue are compared in figure 6.7. Stress and strain predictions obtained with the different constitutive models show similar patterns. However, the magnitudes of stress and strain concentrations differ. During simulations with translational acceleration, the highest deformations were in all cases caused by the brain being obstructed by relatively stiff parts of the dura mater, the falx cerebri or the tentorium cerebelli. For all models during AP translation, the maximum deformations were observed in the posterior and inferior side of the region corresponding to the occipital lobe of the brain at approximately 5 ms, indicated by A in figure 6.7. In

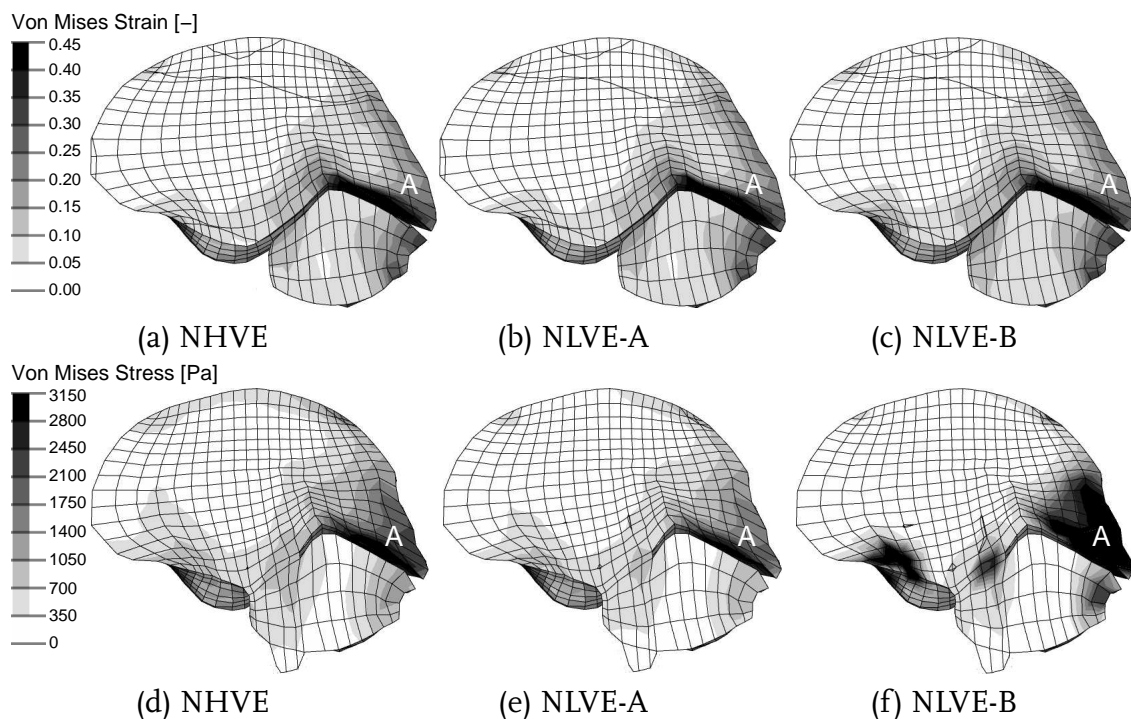


**Figure 6.7:** FE model predictions of (a)–(c) Von Mises strain in a parasagittal cross-section (17.5 mm off-centre) during AP translation with an acceleration of  $730 \text{ m/s}^2$  and (d)–(f) Von Mises stress in a parasagittal cross-section (10 mm off-centre) during AP translational with an acceleration of  $2400 \text{ m/s}^2$  at 5 ms. (a), (d) NHVE model, (b), (e) NLVE-A model, (c), (f) NLVE-B model.

the case of lateral translation, the maximum deformations were observed in the lateral side of the region corresponding to the occipital lobe and the cerebellum of the brain at approximately 5 ms for the NHVE and NLVE-A models and at approximately 8 ms for the NLVE-B model. For SI translation, the maximum deformations were observed in the anterior and posterior side of the thalamus and midbrain regions of the brain at approximately 10 ms for the NHVE and NLVE-A models and at approximately 5 ms for the NLVE-B model.

For all models during PA rotation, the maximum deformations were observed in the anterior, superior and inferior side of the region corresponding to the frontal lobe and anterior side of the region corresponding to the temporal lobe of the brain at approximately 9 ms. A comparison of the strain fields obtained with the different constitutive models for lateral rotation is shown in figure 6.8. The maximum deformations were observed in the posterior side of the corpus callosum of the brain which is caused by the falx cerebri at 10-13 ms, indicated by A in figure 6.8(a)–(c). The second major deformation area was found to be the inferior side of the region corresponding to the frontal lobe at the same time, indicated by B in figure 6.8(d)–(f). For axial rotation, the maximum deformations

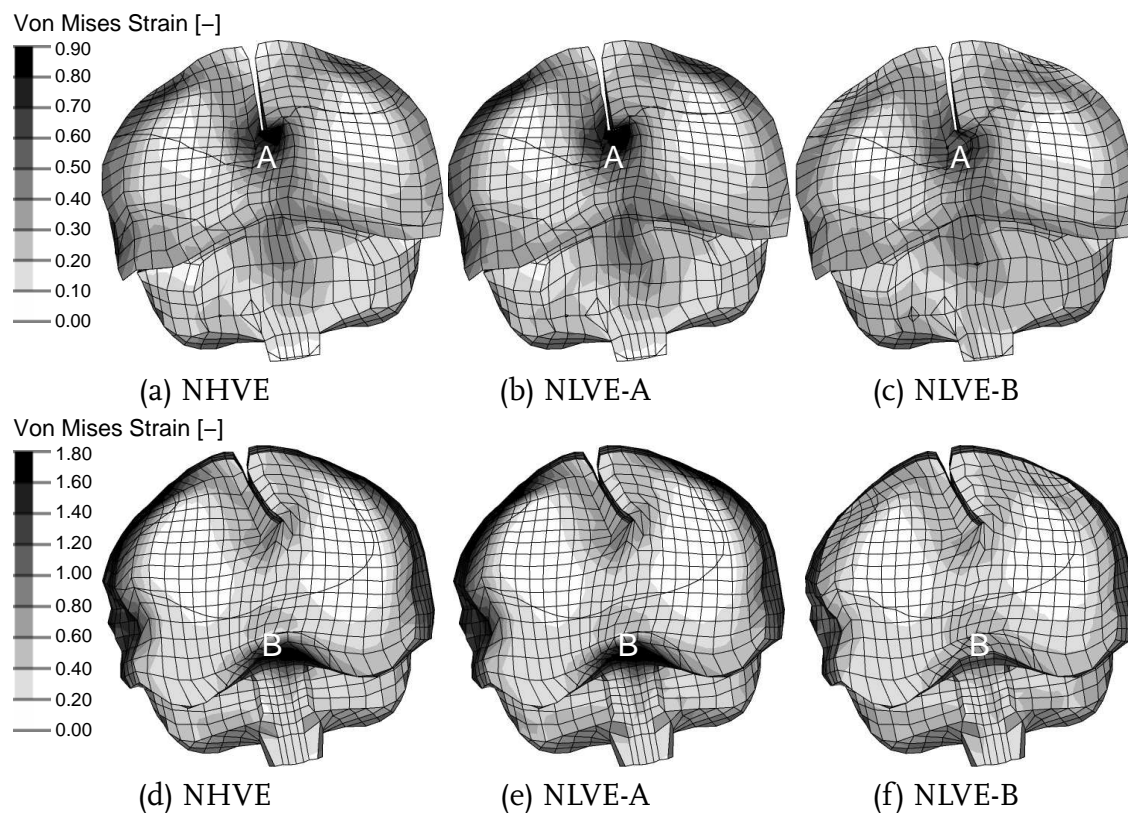


**Figure 6.8:** FE model predictions of Von Mises strain during lateral rotation in (a)–(c) a coronal cross-section (24 mm off-centre) with an acceleration of 7.3 krad/s<sup>2</sup> and (d)–(f) a coronal cross-section (-14 mm off-centre) with an acceleration of 14 krad/s<sup>2</sup> at 9 ms. (a), (d) NHVE model, (b), (e) NLVE-A model, (c), (f) NLVE-B model.

were observed in the anterior side of the region corresponding to the frontal lobe and the corpus callosum of the brain at approximately 8 ms for all constitutive models. The second major deformation areas were observed in the anterior and the posterior side of the corpus callosum at the same time.

Von Mises stress and Von Mises strain values that are exceeded by various amounts of elements in the predictions with the sliding interface model, using different constitutive models for brain tissue are shown in Figure 6.9 and Figure 6.10. For simplicity, only

maximum values obtained during the first 15 ms of the simulation are shown in these figures. The entire time dependent response can be found in Figure 6.13 and 6.14 of Appendix 6.B.

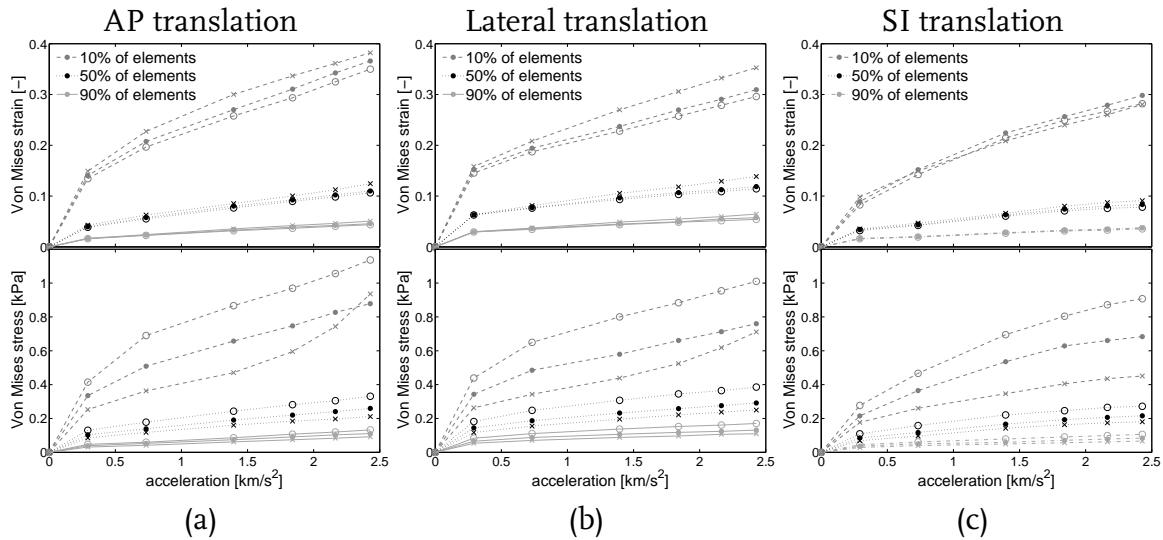


**Figure 6.9:** FE model predictions of Von Mises strains and Von Mises stress in (a) anterior-posterior translation, (b) lateral translation, and in (c) superior-inferior translation.  $\circ$  - NHVE,  $\bullet$  - NLVE-A,  $\times$  - NLVE-B.

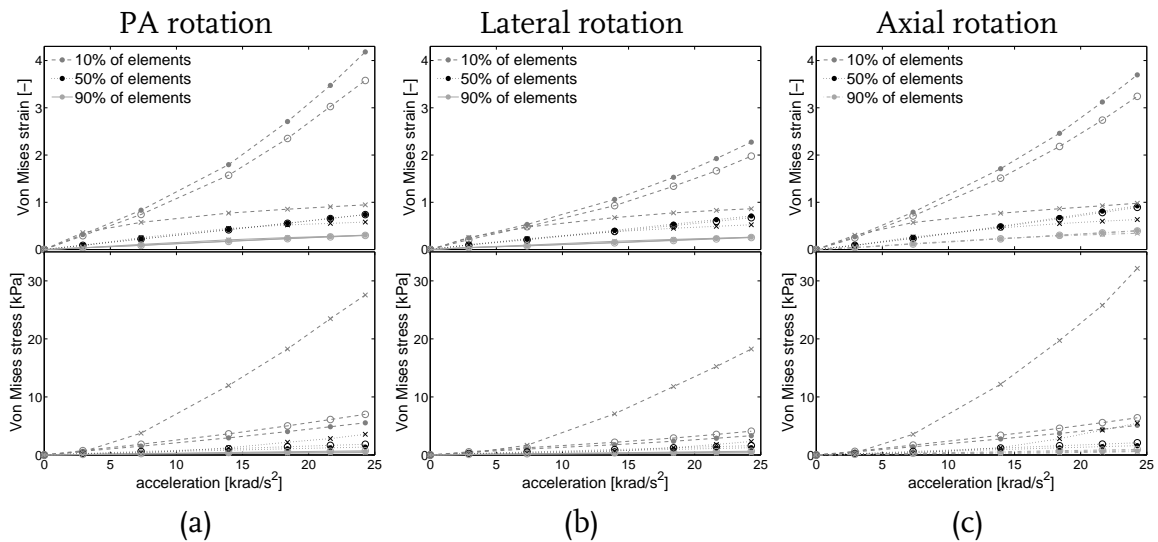


**Figure 6.10:** FE model predictions of Von Mises strains and Von Mises stress in (a) posterior-anterior rotation, in (b) lateral rotation, and in (c) axial rotation.  $\circ$  - NHVE,  $\bullet$  - NLVE-A,  $\times$  - NLVE-B.

The differences found between the NLVE-A and NHVE models are slightly dependent on the applied acceleration amplitude in both translation and rotation. Also the differ-

ences found between predictions with the NLVE-A and NLVE-B model for translation are slightly dependent on the applied acceleration amplitude. However, the differences found between the NLVE-A and NLVE-B model predictions in rotation are strongly depending on the applied acceleration amplitude. In the case of translational acceleration, the relative differences between predictions with different constitutive models are up to 55%. When assuming the NLVE-A model to be the reference model, the NHVE constitutive model predicts up to 10% smaller strains and up to 40% larger stresses, depending on the acceleration amplitude. The strain predictions from the NLVE-B constitutive model were found to be up to 15% larger than the strains obtained with the NLVE-A constitutive model, and the stresses predicted were found to be up to 55% smaller than the stresses predicted when using the NLVE-A constitutive model. In the case of rotational acceleration, the relative differences between predictions of different constitutive models are found to be up to 630% in the case of  $24 \text{ krad/s}^2$ . The NHVE constitutive model predicts up to 17% smaller strains and up to 27% larger stresses than the NLVE-A model. The strain predictions from the NLVE-B constitutive model were found to be up to 450% smaller than the stress obtained with the NLVE-A constitutive model, and the strain predictions were found to be up to 630% larger than the strains predicted when using the NLVE-A constitutive model.

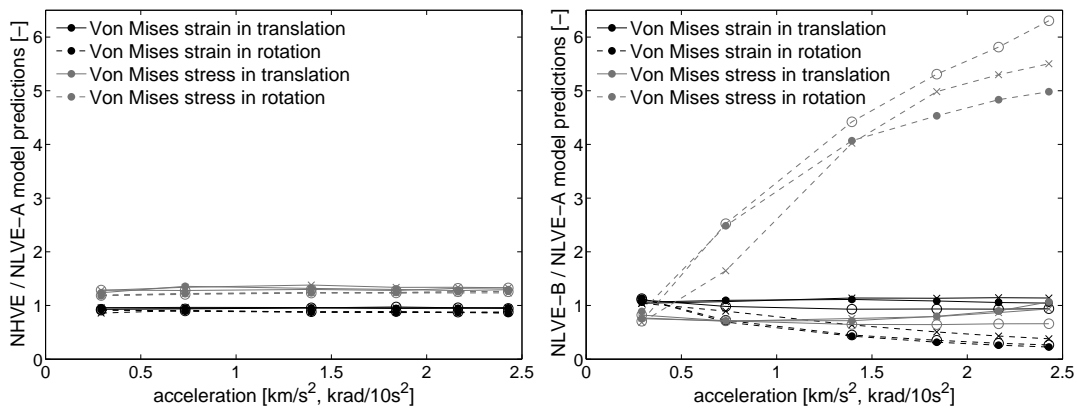


**Figure 6.11:** Difference in the Von Mises strain and Von Mises stress levels that are exceeded by 10% of elements of results plotted in Figure 6.9 and 6.10. ● - PA rotation, AP translation, × - lateral rotation, translation, ○ - axial rotation, SI translation.

## 6.4 Discussion and conclusions

To obtain a reliable prediction of a mechanical response from any FE model, the constitutive models used for the materials involved have to be chosen carefully. The aim of the current study was to analyse the consequences of using different material models for brain tissue in 3D FE head models for injury prediction. For this purpose, a non-linear viscoelastic constitutive model for brain tissue developed in Chapter 4, a simplified ver-

sion of this model, and a previously developed non-linear model [12] were compared.

Before analysing the consequences of different constitutive models, two 3D head models with different skull-brain interface conditions were compared. A more realistic, sliding interface model showed higher deformations for both translational and rotational acceleration than the model containing a tied interface. The differences were most pronounced in the case of translational acceleration and they were dependent on the applied acceleration level. For rotational acceleration the differences were not dependent on the applied acceleration level and were approximately 15%. For the sliding interface model, the higher relative motion is causing the brain to be obstructed by the relatively stiff dura mater, falx cerebri or tentorium cerebelli, therefore the higher deformations are found in the outer regions of the brain. Kleiven and Von Holst [88] showed that by increasing the thickness of the subdural space (1 - 7.3 mm), the relative motion between the brain and the skull is also increasing. Al-Bsharat et al. [90] have found a relative motion of about 5 mm during impact studies on animal and human cadaver heads. They have also compared FE head models with a tied and sliding interface with experimental pressure data of Nahum et al. [91] and concluded the sliding interface to be more realistic. Both of these studies have used solid elements with a low shear modulus representing the CSF layer instead of a frictionless contact between the dura mater and the pia mater, and found similar results. Based on these findings, the head model with a sliding interface was chosen for studying the influences of constitutive non-linearities of brain tissue in FE simulations.

Simulations using a non-linear constitutive model developed in Chapter 4 in a 3-D head model extended with a sliding interface for the skull-brain interaction were compared with predictions obtained from its simplified viscoelastic version and the constitutive model developed by Brands et al. [12]. Different constitutive models show similar patterns for the stress and strain predictions, however, the magnitudes differ. Regions exhibiting maximum deformations were similar for different constitutive models. Comparing predictions of the two non-linear constitutive models, relative differences of 4.5 for Von Mises strain and 6.3 for Von Mises stress levels that are exceeded by 10% of elements were found in the case of rotational acceleration with the highest amplitude. Differences found in translational acceleration were more than a decade smaller. An important observation is that these differences were non-linearly increasing with an increasing amplitude of the acceleration applied. This is due to the non-linearity of the stress response of the NLVE-B constitutive model above shear strains of 0.25, see Appendix 6.A. This non-linearity is considered to be non-physical. Contrary, the variation in the Von Mises stress and Von Mises strain response between the simplified and the non-linear version of the constitutive model developed in Chapter 4 which was found to accurately describe the non-linear response of brain tissue in both shear and compression, was found to be only up to 17% and 40%, respectively. These differences were not dependent on the applied acceleration level in both translation and rotation. Therefore, the simplified version of the recently developed model could be used instead of the non-linear model to obtain reliable injury predictions with FE simulations, since the response can easily be scaled according to the constitutive model used.

In the current study it was shown that choosing a different constitutive model for brain

tissue to be used in a FE model can have large consequences, depending on the presence of non-linearities in the model. However, in the case of a simplified and non-linear version of a model that has been shown to match the non-linear response of brain tissue, the response predicted with a numerical head model for different conditions (i.e. severity and type of loading) varies consistently with the constitutive behaviour used. Therefore, still a reliable assessment of injury can be made with the less accurate simplified constitutive model by using a model-specific injury criterion that then is not a true threshold for injury of brain tissue.

## 6.A Model performances

Figure 6.12 shows the response of the NHVE, NLVE-A, and NLVE-B models for pure shear deformation with  $\dot{\gamma} = 1 \text{ s}^{-1}$  and unconfined compression with  $\dot{\epsilon} = 0.05 \text{ s}^{-1}$ , where the compressive strain is defined as  $\epsilon = \lambda - 1$  and  $\lambda$  is the stretch ratio.

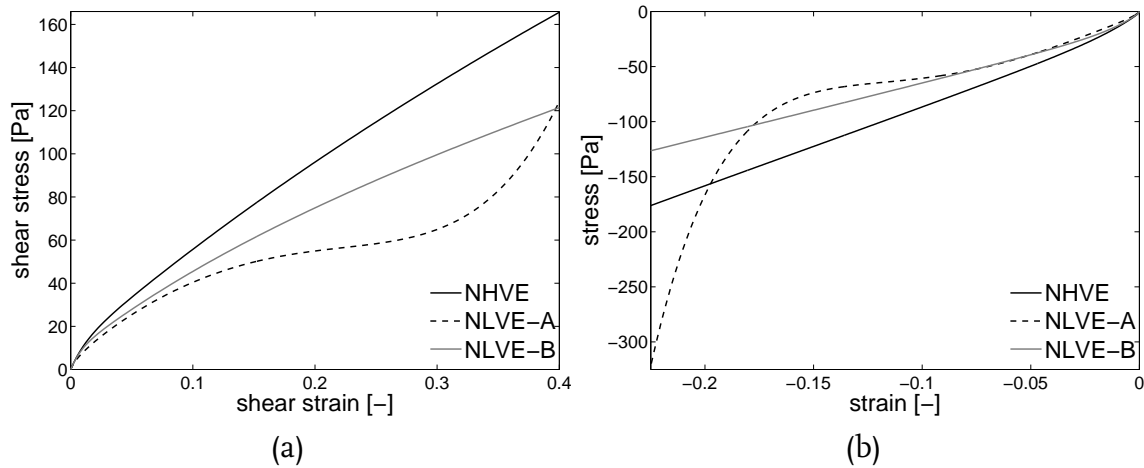


**Figure 6.12:** Comparison of the response of different constitutive models. (a) Shear, (b) compression.

## 6.B Influence of constitutive models for varying loading conditions

The Von Mises stress and Von Mises strain levels that are exceeded by a certain percentage of elements, obtained with FE simulations with different constitutive models are shown in figures 6.13 and 6.14.

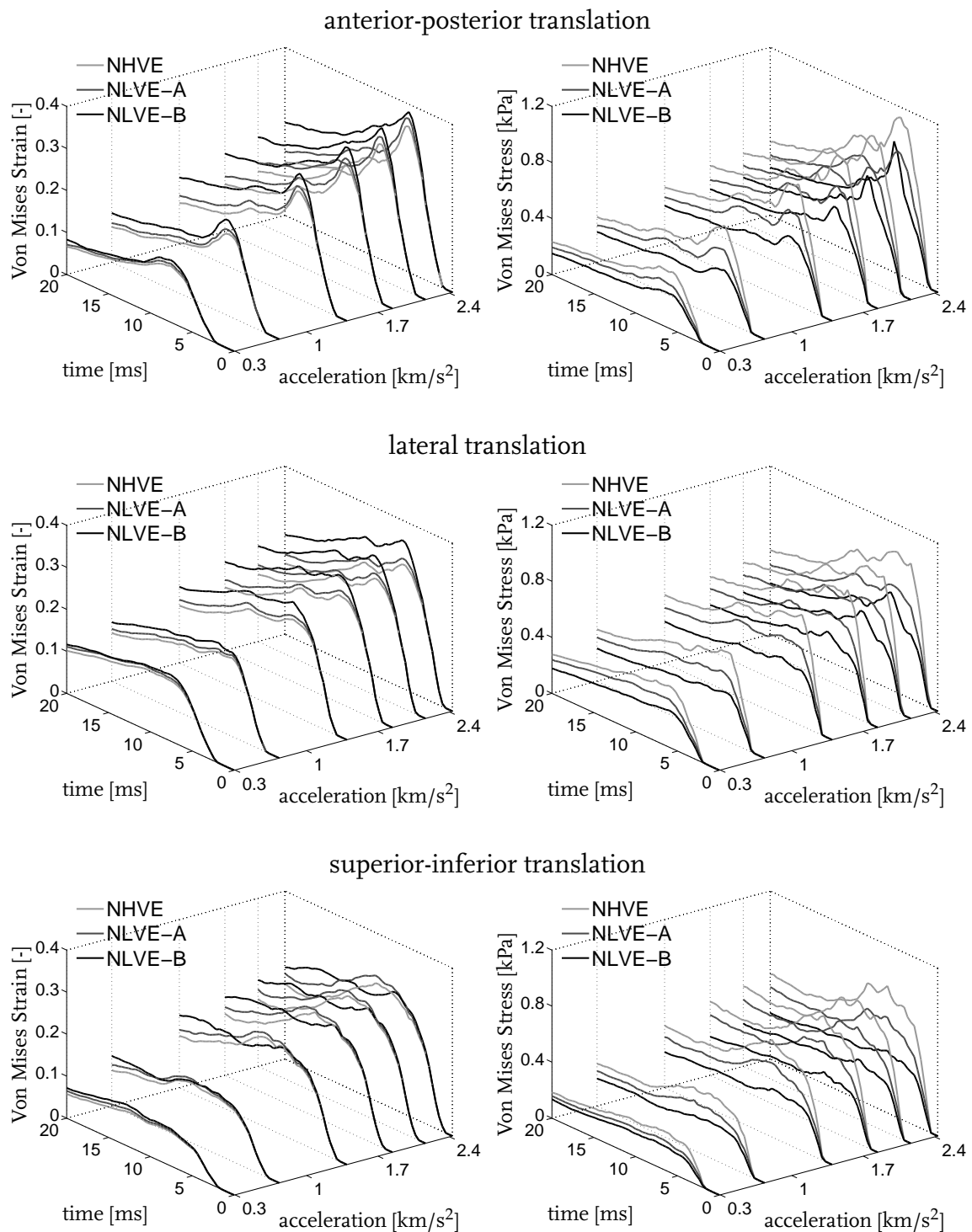


**Figure 6.13:** FE model predictions of the Von Mises stress or Von Mises strain levels that are exceeded by 10% of elements for translation in different directions.



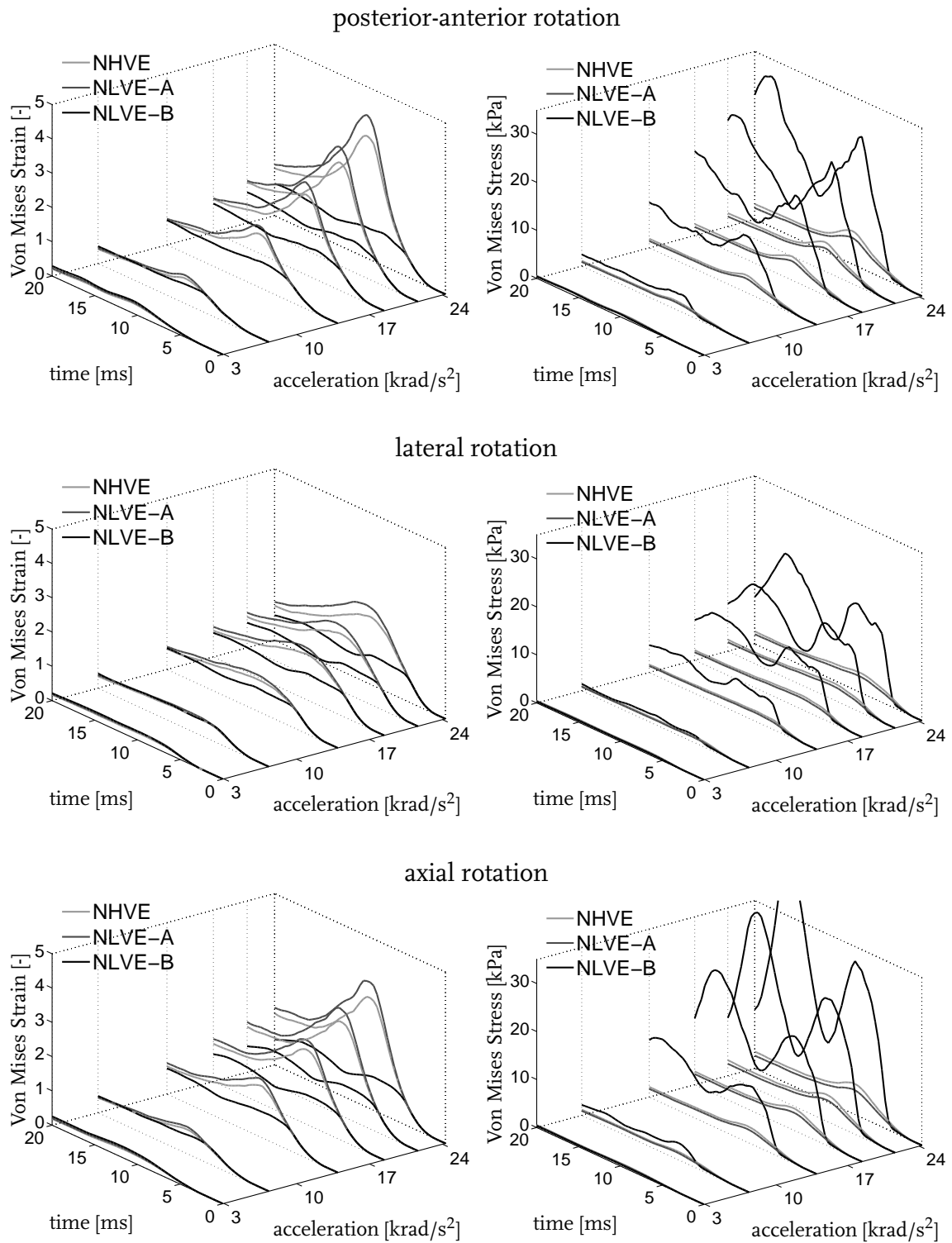


**Figure 6.14:** FE model predictions of the Von Mises stress or Von Mises strain levels that are exceeded by 10% of elements for rotation in different directions.

# Effect of brain heterogeneity<sup>I</sup>

---

### Abstract

The aim of this study was to measure high-resolution strain fields in planar sections of brain tissue during translational acceleration to examine the effect of the geometrical heterogeneities on the mechanical response. Slices were made from fresh, porcine brain tissue, and contained both grey and white matter as well as the complex folding structure of the cortex. The brain slices were immersed in artificial cerebrospinal fluid (aCSF) and were encapsulated in a rigid cavity representing the actual shape of the skull. The rigid cavity sustained an acceleration of about  $900 \text{ m/s}^2$  to a velocity of  $4 \text{ m/s}$  followed by a deceleration of more than  $2000 \text{ m/s}^2$ . During the experiment, images were taken using a high-speed video camera and Von Mises strains were calculated using a digital image correlation technique. The acceleration of the sampleholder was determined using the same digital image correlation technique. A rotational motion of the brain slice relative to the sampleholder was observed, which may have been caused by a thicker posterior part of the slice. Local variations in the displacement field were found, which were related to the sulci and the grey and white matter composition of the slice. Furthermore, higher Von Mises strains were seen in the areas around the sulci.



---

<sup>I</sup> *Reproduced from:* C. Lauret, M. Hrapko, J. A. W. van Dommelen, G. W. M. Peters, J. S. H. M. Wismans, (2008). Optical characterization of acceleration-induced strain fields in inhomogeneous brain slices, submitted.

## 7.1 Introduction

Annually 1.4 million people sustain a TBI in the United States, of which 20% is caused by vehicle traffic accidents [2]. Although vehicles are already equipped with belts and airbags, even more sophisticated preventive measures are needed to further reduce this number of injuries. The development of these measures can be based on injury predictions with numerical head models, by simulating crash situations.

Many numerical head models have been developed [87,82,12,95–97], differing in the constitutive models used and the level of detail in the modelled geometries of the brain and the skull. Constitutive models describe the mechanical behaviour of tissue, which is nonlinear and visco-elastic in the case of brain tissue [49]. Moreover, brain tissue may be anisotropic and show inter-regional variations. The quality of numerical head model simulations depends partly on the ability of the constitutive model to describe this complex mechanical behaviour, and partly on the modelled geometry. Therefore, the constitutive model and the head model need to be validated in order to give reliable and representative injury predictions. However, only limited experimental data exist because of the inaccessibility of the cranium.

Pudenz and Shelden [98] measured the deformation in a macaque brain through a cranial window. Although this was one of the first successful strain measurements of the brain during acceleration, only the deformation of the surface could be observed. Furthermore, in the past two decades the use of living animals is being restricted due to legislations.

To validate model predictions, Brands et al. [82] used both open and closed cylindrical cups filled with silicon gel, which were subjected to transient rotational acceleration. In both setups, the gel response was measured using optical markers and a high-speed video camera. Ivarsson et al. [99,100] studied the natural protection of the brain, also using gel and high-speed tracing of markers. More specifically, lateral ventricle substitutes were included in this physical model to investigate if these structures give strain relief during head impact. Margulies et al. [101] and Meaney et al. [102] recorded the motion of grid patterns painted on gel inside animal and human skulls during angular acceleration. The overall deformation pattern as a result of rotation was compared to the pathological portrait of diffuse brain injury, as determined from animal studies and autopsy reports. Although gel-based setups can provide insight in the global mechanical behaviour, they are unable to mimic the local brain structures like grey and white matter boundaries and the folding structure of the cortex.

Hardy and colleagues used neutral density accelerometers [103] and targets [104] to measure brain motion in human cadavers via high-speed X-ray imaging during angular acceleration. The spatial resolution of these measurements was too low to estimate local strain fields.

Bayly et al. [105] used MRI to measure the deformation of brain tissue induced by mild acceleration in human volunteers. Strains of 0.02 – 0.05 were typical during the occipital deceleration, and compression in anterior regions and stretching in posterior regions were observed. Moreover, the motion of the brain appeared to be constrained by struc-

tures at the frontal base of the skull. A drawback of volunteer tests is that they can only be performed at a level well below the injury threshold. The same method was used to obtain strain fields in the brain of a perinatal rat [106,107]. In these experiments the brain was not accelerated, but the flexible skull was indented by 2 mm and during 21 ms. Lagrangian strains of more than 0.20 at strain rates exceeding  $40 \text{ s}^{-1}$  were observed.

The main objective of this study was to develop an experiment in which a realistic crash situation was mimicked and that can be used to validate numerical head models. Therefore, high-resolution strain-fields were measured in inhomogeneous, planar sections of fresh porcine brain tissue with a complex and detailed geometry, during translational acceleration normally occurring in crash situations. The planar brain samples contained both grey and white matter as well as the complex folding structure of the cortex. It was hypothesized that these inhomogeneities influence the acceleration-induced strain pattern. Since fresh porcine tissue was used, the experiment was conducted within 6 hours post-mortem in order to prevent any time-related changes of the mechanical behaviour of the tissue [46].

During translational acceleration, the samples were immersed in aCSF to prevent dehydration of the tissue. Furthermore, in order to obtain a representative model of the relative motion of the brain inside the skull during acceleration, the sample together with the aCSF layer was encapsulated in an almost rigid cavity with the shape of the actual brain slice. The motion was recorded by a high-speed video camera and displacements and strain fields were obtained using digital image correlation. The strain patterns obtained were qualitatively compared with the grey and white matter composition of the slice and the positions of the sulci.

## 7.2 Materials and methods

Planar brain slices were prepared from female pig brains (Dutch landrace hybrid) of 4–6 months old, obtained at a local slaughterhouse. During transport and preparation, the brains were cooled and stored in porcine based aCSF [108] to prevent dehydration and to slow down the degradation and swelling process of the tissue. Sagittal slices of 4 mm in thickness were made using a standard slicing machine (Bizerba) from the region about 2 cm outwards from the mid-sagittal plane, see Figure 7.1. The medial and lateral sides of the slices differed in grey and white matter distribution and in the geometry of the sulci. However, when comparing corresponding sides of different brain slices, the geometries and distributions of matter were qualitatively similar. The experimental procedure was carried out for two different para-sagittal brain slices and multiple acceleration measurements were conducted on each side of the slice with at least one minute duration between subsequent measurements. Repetitive mechanical loading of brain tissue was found not to affect its constitutive response in a previous study [49]. All the measurements were carried out at room temperature and were completed within 6 hours post-mortem.

In order to use a digital image correlation technique [110–112], a fine, random speckled pattern was applied on the surfaces of the slice, using matte black Enamel (Alkyd resin,



**Figure 7.1:** Lateral (a) and top (b) view of a brain, with indicated sample region [109].

Airbrush email color, Revell GmbH) and an airbrush (Aztek, A4305, The Testor Corporation, USA), see Figure 7.2a. The average dot diameter of the pattern was about 0.5 mm.

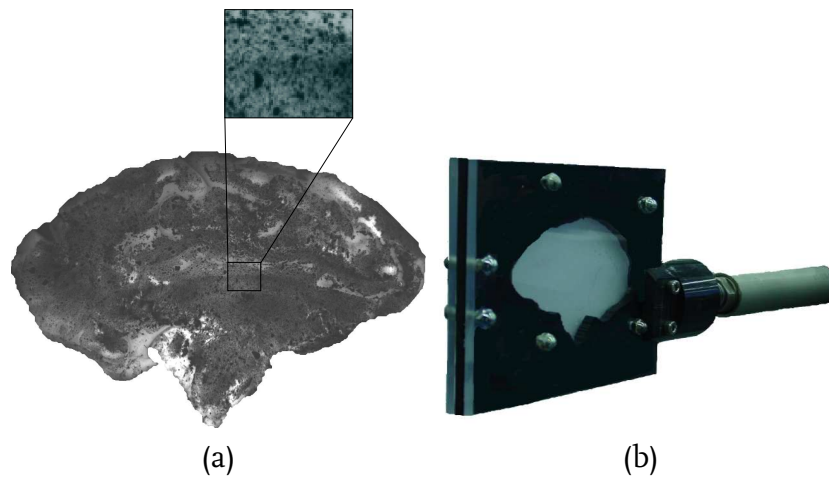


**Figure 7.2:** (a) A brain slice with the applied speckled pattern and a magnification of this pattern, (b) the sampleholder with a milled out sample cavity.

The sample holder (Figure 7.2b) consisted of three plates (125 x 100 mm); two outer plates of transparent polycarbonate and a the middle plate of black polyvinylchloride (PVC), each with a thickness of 5 mm. A cavity with the actual shape of the slice was created in the middle plate by CNC (Computer Numerical Control) milling, but with an additional space of 2 mm around the brain slice for a surrounding aCSF layer. Moreover, the thickness of the middle plate was 1 mm larger than the thickness of the slice, allowing for natural aCSF layers. For the CNC milling, a numerical description of the sample contour was obtained from a digital image of the slice. To prevent the brain tissue from adhering to the inner surface of the plates, they were coated with a Teflon spray. Because of gravity, the slice rested on the bottom of the cavity.

The experimental setup is schematically shown in Figure 7.3 and consisted of an air spring (Amotek, type Deamv) connected to the sampleholder. The sampleholder sustained an acceleration of about  $900 \text{ m/s}^2$  to a velocity of 4 m/s followed by a deceleration

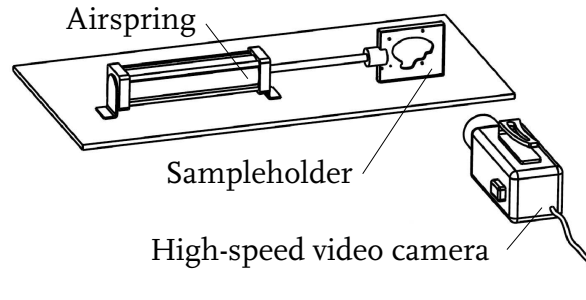


**Figure 7.3:** Schematic illustration of the experimental setup, with an airspring, sampleholder and high-speed video camera.

of more than  $2000 \text{ m/s}^2$ . The acceleration of the sampleholder was measured using digital image correlation of a patch on the surface of the sampleholder. The sampleholder was initially moved in the posterior-anterior direction. Digital images were collected with a high-speed video camera (Phantom v9.0, Vision Research Inc., New Jersey) at a frame rate of  $1600 \text{ Hz}$ . The 8-bit grey-scale images ( $1440 \times 952$  pixels) were cross-correlated (Aramis software, v5.4.1-5, GOM Optical Measuring Techniques GmbH) with an optimised facet size of  $15 \times 15$  pixels.

After the images were cross-correlated, the rigid body movement of the cavity was eliminated from the displacement field by minimising the sum of the displacements of the speckled pattern of the patch, between the reference and the deformed [113]. The resulting displacement field shows the relative movement of the tissue with respect to the sampleholder. Because of this larger relative motion, smaller, local displacement variations were not visible. Therefore this relative (mostly rotational) displacement field of the tissue was eliminated in the same way as the rigid body motion of the cavity, but now the speckled pattern of the tissue was used. The local displacement field shows the internal displacements of the tissue with respect to the rest of the slice. Finally, an equivalent Von Mises strain field was calculated, for which the out-of-plane strains were computed assuming incompressibility of the tissue. This equivalent strain measure is defined as:

$$\bar{\epsilon} = \sqrt{\frac{3}{2} \boldsymbol{\epsilon}^d : \boldsymbol{\epsilon}^d}, \quad (7.1)$$

with  $\boldsymbol{\epsilon}$  the logarithmic strain tensor and the superscript “d” denoting the deviatoric part.

## 7.3 Results

### 7.3.1 Strain fields

Two brain slices, obtained from different brains, were used and 17 measurements were conducted in total. Field information was obtained from either the lateral or the medial side of the slice. The results are shown from both the lateral and medial sides of one

slice, at the most pronounced moments in time. The displacements are presented as vector fields, plotted on an image of the corresponding brain slice, taken before spraying a pattern on the surface. The vectors were scaled corresponding to the largest displacement value present in each stage. Vectors are only shown for locations where a successful image correlation was obtained.

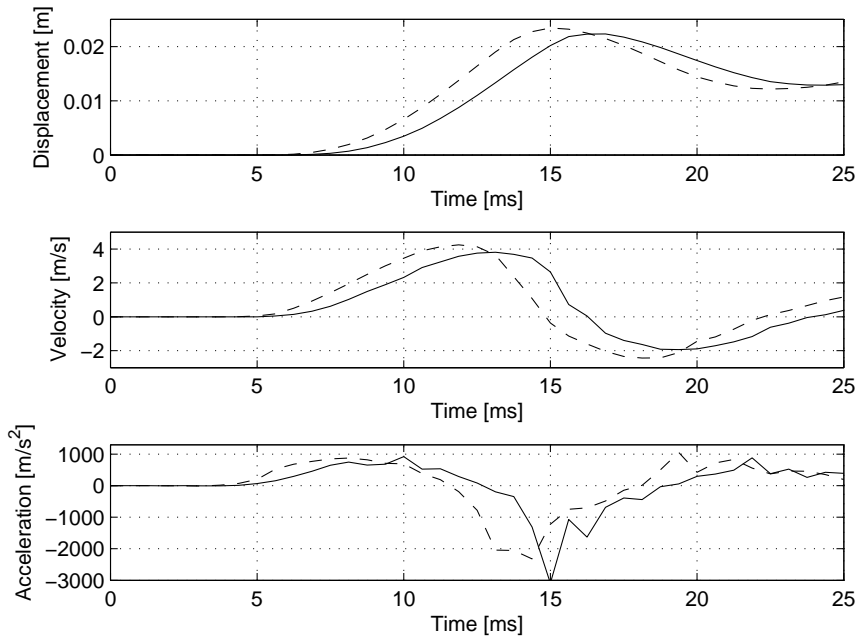
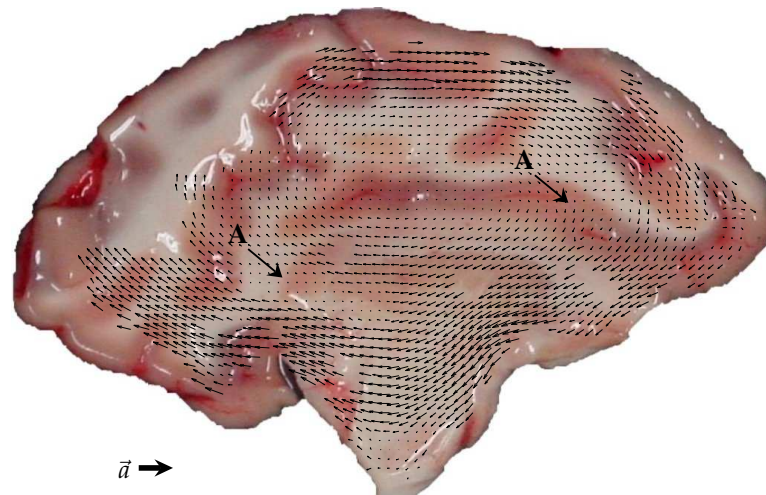
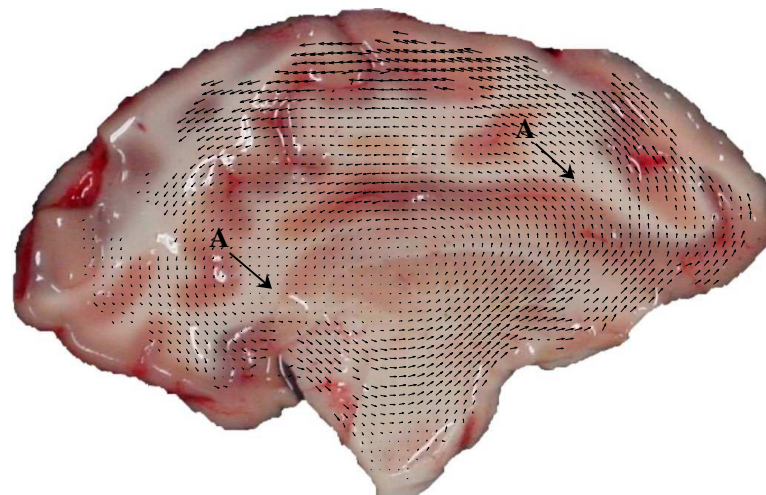


**Figure 7.4:** Displacement, velocity and acceleration of the sampleholder during two experiments in which images from the lateral side (dashed line) and medial side (solid line) of the same sample are obtained.

The dashed line in Figure 7.4 shows the displacement, velocity and acceleration of the sampleholder of which the corresponding global, rotational motion of the lateral side of the brain tissue relative to the sampleholder can be seen in Figure 7.5. The clockwise relative motion in Figure 7.5a corresponds to the maximum velocity of the sampleholder to the right (12 ms), whereas the counter-clockwise relative motion in Figure 7.5b corresponds to a second positive acceleration after the backward motion has halted (23 ms). Because the centre of rotation is in the middle of the slice, these relative displacements are gradually increasing towards the edge. However, two regions can be observed with almost no displacement relative to the sampleholder, indicated by A. In Figure 7.6, the local displacement patterns are visualised after eliminating the tissue rotation relative to the sampleholder, from the displacement field. A local displacement pattern parallel to the sulcus can be observed, indicated by B. Just below the horizontal sulcus on the border of grey and white tissue, the displacement field changes sign over a relatively small distance, indicated by C. However, this last pattern cannot be found in Figure 7.6, as here a more local centre of rotation can be seen at that position. The vertical sulcus on the pos-



(a) Situation at 12 ms

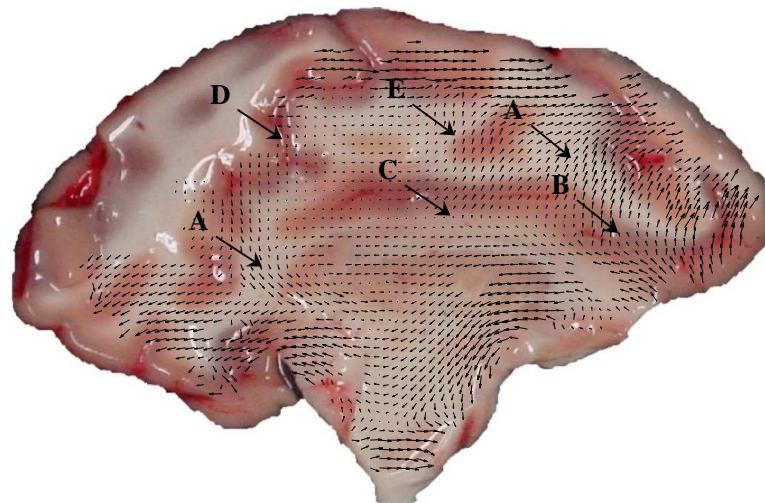


(b) Situation at 23 ms

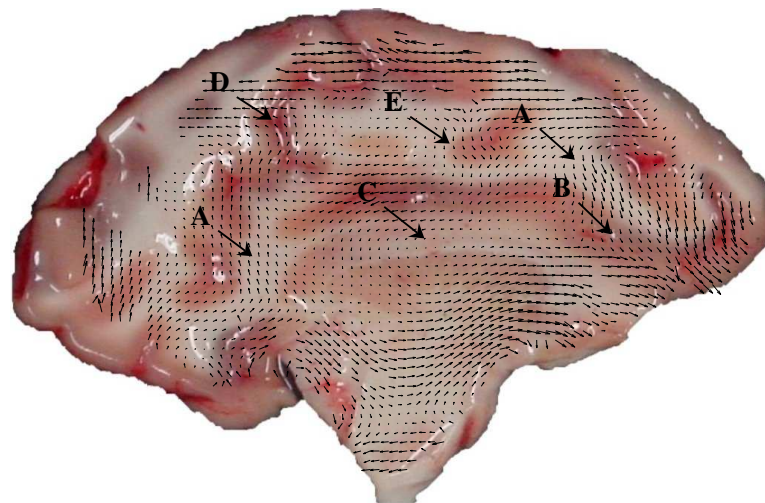
**Figure 7.5:** Relative displacements of the lateral side of the brain slice with respect to the sample-holder, with an initial posterior-anterior acceleration, indicated by  $\vec{a}$ , with a displacement vector magnification factor of 2.2. Areas indicated by A show almost no relative displacement.

terior side and the small sulcus above the midline both influence the displacement field locally, indicated by D and E, respectively. From the displacement field, the logarithmic strain field with respect to the initial configuration has been calculated. In Figure 7.7, the equivalent Von Mises strain is shown, where strains of 11% can be seen in the regions around the vertical sulci, indicated by F. In addition, Figure 7.7a shows Von Mises strains between 0 and 2% in the region around the horizontal sulcus, indicated by G. However, this pattern is less pronounced in Figure 7.7b.





(a) Situation at 12 ms.



(b) Situation at 23 ms.

**Figure 7.6:** Local displacement fields of the lateral side of the brain slice with an initial posterior-anterior acceleration, and with a vector magnification factor of 3.1. (a) Obtained after correction for a rigid body rotation of the results in Figure 7.5a by  $1.5^\circ$  (counter-clockwise) and (b) obtained after correction for a rigid body rotation of the results in Figure 7.5b by  $0.6^\circ$  (clockwise). The areas indicated by A show the opposite local displacement of the tissue, areas indicated by B, C, D and E show the influences of the inhomogeneities on the local displacement field.

The solid line in Figure 7.4 shows the displacement, velocity and acceleration of the sampleholder of which the corresponding motion relative to the sampleholder and the local displacement fields of the medial side of the same slice discussed previously, can be seen in Figure 7.8. These results correspond to a maximum velocity of the sampleholder to

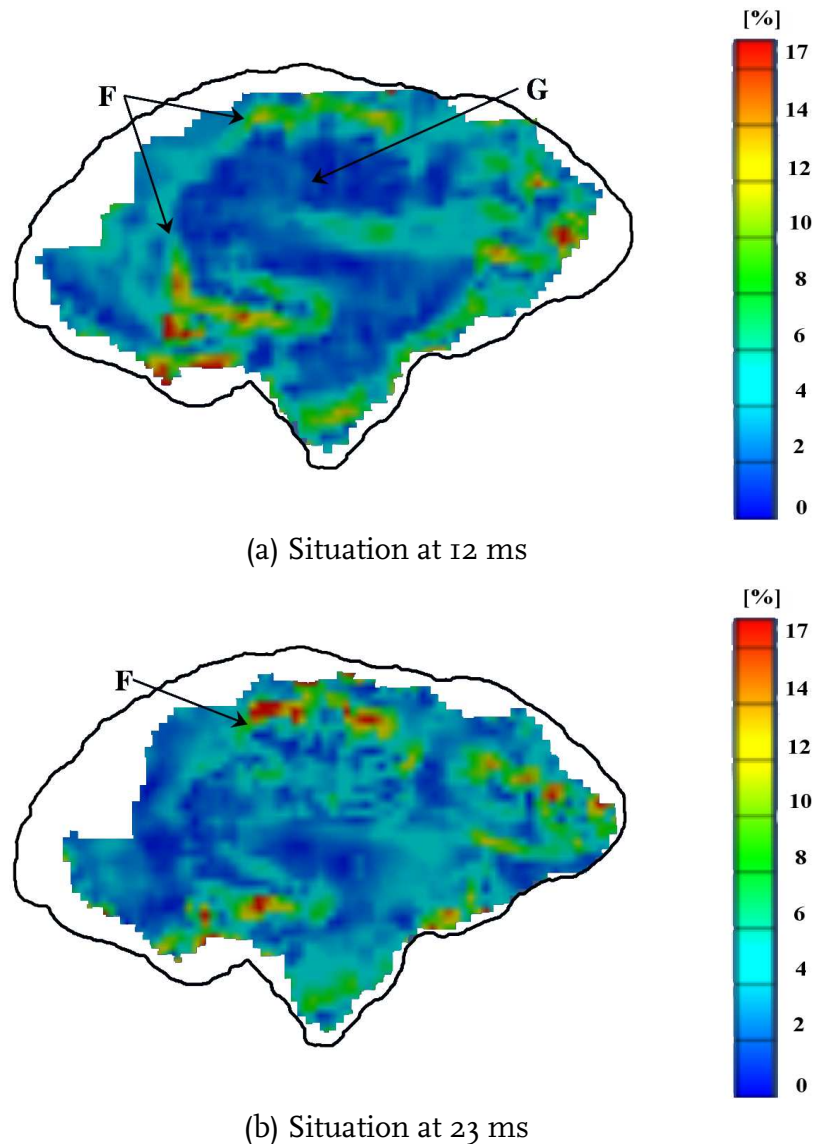


**Figure 7.7:** Equivalent Von Mises strains of the lateral side of the brain slice, with F indicating Von Mises strains of 11% around the vertical sulcus on the posterior side, and G the Von Mises strains of 0.2% in the area around the horizontal sulcus. Only for coloured regions, digital image correlation results were obtained.

the left (at 12.5 ms). In Figure 7.8a, a rotational motion of the brain tissue with respect to the sampleholder can be seen, with three areas with almost no displacement, indicated by H.

The centre of rotation was not located in the middle region of the sample, as it was for the lateral side. In the top part of the cavity a small air bubble was present, influencing the relative, rotational motion, as well as the local displacements. Although the medial side had less pronounced inhomogeneities compared with the lateral side, still influences of the substructure could be observed. For example, arrows I and J indicate two areas where

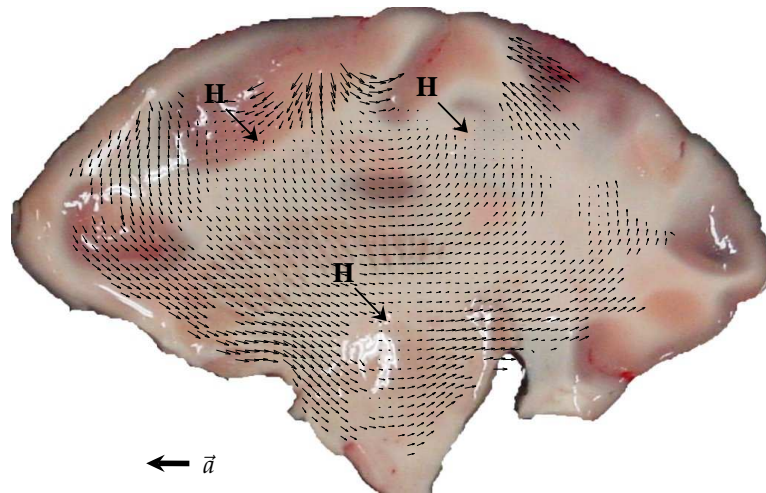
local changes in the direction of the vector field occur. Figure 7.9 shows the equivalent Von Mises strains of the medial side of the brain slice. In the central region of the slice, Von Mises strains of 0–2% can be seen, indicated by K. L indicates areas with Von Mises strains of up to 14% in the grey matter areas. These areas correspond with grey matter regions, see Figure 7.8. M indicates the area where the air bubble was present, which induced apparent Von Mises strains of up to 17%. Finally, the area indicated by N also shows Von Mises strains up to 17% as well.

### 7.3.2 Reproducibility

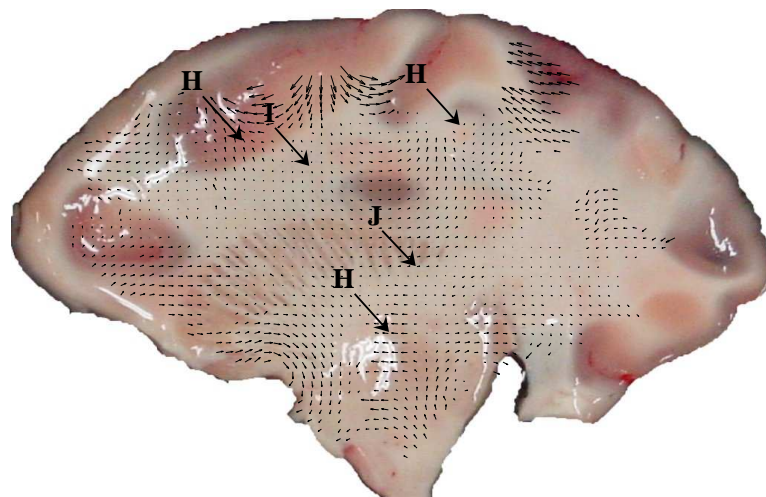
The data of 17 measurements were used in order to investigate the reproducibility of the setup and the influence of the severity of the acceleration pulse on the strain levels obtained. For this, two different samples were used, and a distinction was made between the medial and lateral side of the samples. Figure 7.10a presents the displacement, velocity and acceleration histories of sample 1, and shows the repeatability of the actuation of the experimental setup. The relative number of correlated facets that exceed a certain Von Mises strain level at the time of maximum velocity is displayed in Figure 7.10b. This excludes peak Von Mises strains calculated for a small percentage of facets, possibly caused by incorrect image correlation. Figure 7.11a represents the progression of the Von Mises strain in time averaged for all the experiments done on sample 1 (except for the experiment with lower acceleration magnitude) and corresponding to a fixed percentage of facets. After the first acceleration peak has been reached, the Von Mises strain obtained for 10% of the facets remains in the range of 0.08–0.1. Figure 7.11b shows the sustained Von Mises strain at the moment of maximum velocity corresponding to a fixed percentage of facets versus the maximum velocity applied. One measurement was done with a significantly lower acceleration level. Figures 7.10b and 7.11b show that the tissue in this measurement sustained lower Von Mises strains compared to the other measurements.

## 7.4 Discussion and conclusions

Strain fields were measured in porcine brain tissue slices, during translational acceleration. Although the sampleholder was accelerated translationally, a rotation of brain tissue relative to it was found. This may have been induced by a small rotation of the sampleholder during the onset of the acceleration pulse. However, this rotation was limited to about 2°, compared to a maximum translation of about 23 mm. Instead, the rotational displacement field could also be due to variations in slice thickness. Unpublished finite element simulations have shown a rotational displacement field to appear due to relatively small thickness variations (order of magnitude 1%). Moreover, this mechanism was found to be independent of the sample geometry. Thickness variations may have been caused by the slicing procedure. Furthermore, during the experiment the lower part of the sample was resting on the sampleholder, which could have influenced the relative motion of the tissue.



(a) Situation at 12.5 ms



(b) Situation at 12.5 ms

**Figure 7.8:** (a) Relative displacement field of the medial side of the brain slice with respect to the sampleholder and with a vector magnification factor of 1.8. Initial posterior-anterior acceleration indicated by vector  $\vec{a}$ . Areas indicated by H show almost no relative displacement. (b) Local displacement field of the medial side of the brain slice and with a vector magnification factor of 2.7, obtained after correction for a rigid body rotation of the results in Figure 7.8a by  $1.8^\circ$  (clockwise). Areas indicated by H show the opposite internal displacement; areas I and J show the influences of the inhomogeneities on the local displacement field.

The internal displacement patterns showed an influence of geometrical heterogeneities such as sulci and constitutive variations between the surrounding grey and white matter on the local displacement field. Sulci are geometrical boundaries and the opposite

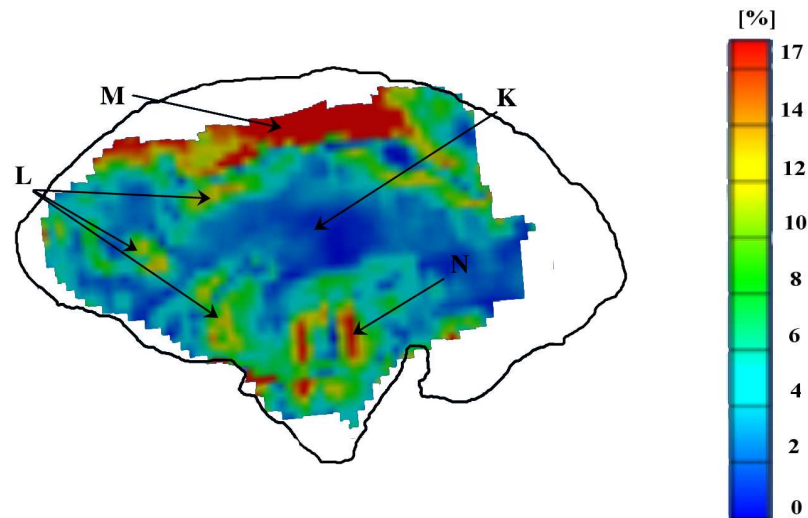


**Figure 7.9:** Equivalent Von Mises strains of the medial side of the brain slice, with K indicating Von Mises strains of 0–2%, L indicating strains of up to 14% in the grey matter areas, M indicating the area with Von Mises strains of more than 17% in the area of the airbubble and N also showing higher Von Mises strains, around a thicker part of the brain slice. Only for coloured regions, digital image correlation results were obtained.

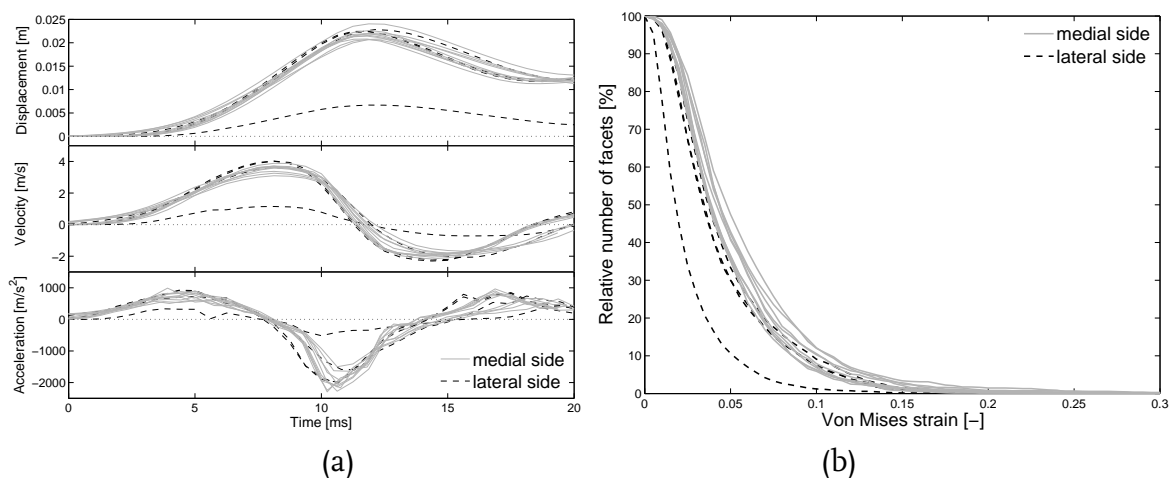


**Figure 7.10:** (a) Displacement, velocity and acceleration of the sampleholder and (b) relative number of facets exceeding a certain Von Mises strain at the time of maximum velocity, for 14 measurements conducted on sample 1 for the lateral (black) and medial (grey) side.

surfaces may slide relative to each other. In addition, sulci are always surrounded by grey matter which differs in mechanical properties from its neighbouring white matter. Cloots et al. [114] have shown the potential importance of geometrical heterogeneities for the stress or strain levels that occur in brain tissue during severe inertial loading with numerical simulations. Bayly et al. [105] presented MRI data with indications that there were strain concentrations at the interface of grey and white matter, but could not unambigu-

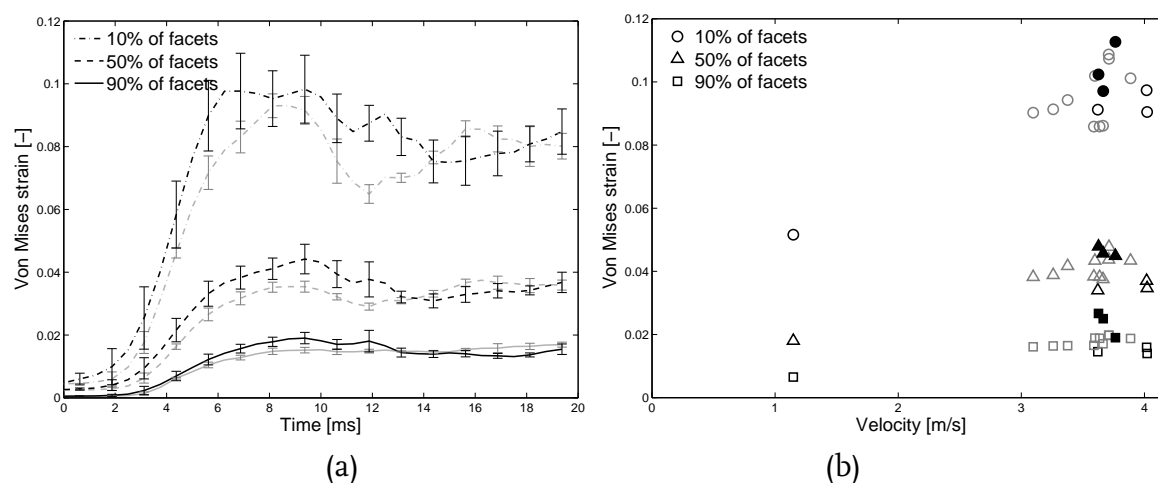


**Figure 7.11:** (a) Evolution of Von Mises strain in time, averaged for all measurements of each side of sample 1 and (b) Von Mises strain for sample 1 (open symbols) and sample 2 (closed symbols) at the maximum velocity corresponding to a certain fraction of facets versus the velocity of the sampleholder. The medial side is indicated in black and the lateral side is grey.

ously identify these effects. Moreover, Graham et al. [115] supported these indications by observations of more severe local injury near these boundaries. The highest strains experienced by 10% of the correlated surface area of the sample was found to be in the range of 0.08–0.1 for the typical acceleration level applied in these experiments. Furthermore, this strain level was found to depend on the severity of the acceleration pulse.

Enamel was used for the application of a speckled pattern because of its relatively good adherence to the wet surface of the tissue. Narmoneva et al. [116], used Enamel to apply a speckled pattern on cartilage. A microscopic examination of the cartilage sample surface showed that the water-resistant Enamel was attached well to the surface. Moreover, the paint was found not to penetrate into the sample, and the dot size and shape were preserved during the experiment. Although the digital image correlation software can correlate the pattern present on the brain slices, the pattern is less fine than in a standard experiment where the specimen does not need to be hydrated and for which an accuracy of 0.1% can be achieved [113]. Therefore, the accuracy of the correlated regions was investigated for this specific experimental situation. For this purpose, two experiments were done in which a known rigid body translation was applied to the sampleholder containing a tissue slice similar to the samples used in the actual experiment. The displacement obtained with the correlation technique was found to be 4.8% smaller than the applied displacement. This deviation is believed to be due to inaccuracy in scaling to actual coordinates, in combination with reflections of the wet surface and the motion of the sample relative to the lights. Moreover, the pattern density on the grey matter was lower than on the white matter because of a difference in adherence capacity of the two tissues with Enamel. The maximum Von Mises strain of the surface obtained for this rigid body translation was found to be 0.4%.

The medial and lateral sides of the slices differed considerably in grey and white matter

distribution and geometry of sulci. Both sides were measured, however, this could not be done in the same experiment. However, strain levels obtained in repeated experiments were found to be well reproducible. In future studies, the setup could be extended to a system that is able to obtain field information from both sides of the slice simultaneously. Furthermore, the setup could be modified to apply rotational accelerations as well.

# Discussion, conclusions and recommendations

---

## 8.1 Discussion and conclusions

The brain is a part of the central nervous system which controls and regulates all body activity. This makes the brain one of the most important parts of the body. Even though it is enclosed in a relatively stiff skull, it is very sensitive to either very fast or very high loads, which often originate from falls, traffic accidents, assaults, etc.

Mechanical properties of brain tissue have been studied for almost half a century. During this period, several properties were solidly settled in the research community. Brain tissue is now clearly defined as a heterogeneous, viscoelastic solid that exhibits a relatively high bulk modulus compared to the shear modulus [117] and consists for up to 80% of water [118]. However, for another group of properties no consensus has been found, among which the linear viscoelastic moduli of brain tissue. An overview of studies on the mechanical properties of brain tissue was given in Chapter 2, focusing on testing methods. The influence of important test conditions such as temperature, anisotropy, pre-compression, the sample preparation procedure, different loading histories and post-mortem time on the mechanical response of porcine brain tissue for shear deformation was experimentally determined in Chapter 2 and 3, mostly in the linear viscoelastic regime. Results measured at room temperature show a stiffer response than those measured at body temperature with a horizontal shift factor of up to 11. The variation caused by anisotropy between planes and within the same plane of individual samples was found to be up to 30% and 60%, respectively. The effect of pre-compression on shear results was investigated and was found to stiffen the sample response. The stress response showed a clear dependency on post-mortem time, becoming more stiff with increasing time. In addition, the effects of some conditions for compression measurements were studied in Chapter 5. Combinations of these and other factors can lead to large differences among different studies, depending on the different test conditions. Therefore, the experimen-



tal conditions during characterisation tests of brain tissue should be carefully controlled and reported. In addition it should be noted that the variations due to varying test conditions found can not completely explain the differences found between different studies in literature.

Two important aspects of testing biological material, were not investigated in the current study. One aspect which always affects in vitro biological material tests is the difference between the in vitro and the in vivo state. The post-mortem time causes the tissue to degenerate depending on the surrounding temperature due to various reasons (e.g. autolytic processes, completion of rigor mortis, osmotic swelling, etc.). In addition to this effect, properties obtained in in vitro measurements may deviate from the original properties of the in vivo state. Although in the current study, the effects caused by increasing post-mortem time were minimised by limiting the post-mortem time to about 6 hours, the properties obtained may differ from the in vivo properties. In an earlier study, Metz et al. [52] have reported an up to 70% decrease of the tissue stiffness within 1 hour post-mortem. In a more recent study of Gefen and Margulies [48] the force response of indentation measurements was found to decrease by 10 to 50% from the in vivo to the in situ situation. The difference seemed to be increasing with decreasing rate of indentation. Another important aspect of the experiments is the donor type. Some studies have been performed on human brains obtained from autopsies or lobotomies on epileptic patients, however most studies were performed on animal brains. Sherwood et al. [119] have investigated whether the glial-neuron ratio differ between 18 species of anthropoids in the frontal cortex region of the brain. The human glial-neuron ratio was found to be higher than in other primates, however this ratio did not differ significantly when scaled by brain size. Even though structural differences are present between human and animal brains, based on ethical reasons large domesticated animals and small rodents are preferred over other primates. Porcine brain resembles the human brain more in anatomy, growth and development than small laboratory animals and therefore are preferred as a substitute for human brains in neuroscience [120]. Furthermore, the differences between the measured mechanical response of tissue from human and animal brains are often considered relatively small, 30–40%, which enables animal brains to be used as a substitute for human brains [63,68] in mechanical testing. In the current study, all experiments were conducted on porcine brain tissue. Eventually, a scaling of results to in vivo human brain tissue may be needed. However, since these differences (in vivo vs. in vitro, human vs. porcine) may depend on the rate of deformation and on other still unknown factors, no scaling of the constitutive behaviour was applied in the current study.

After establishing the effect of test conditions in the linear viscoelastic regime, the mechanical behaviour of brain tissue was determined for large shear deformations with strains up to 0.5 and strain rates from 0.01 to 1 s<sup>-1</sup>, see Chapter 4. A technique producing an approximately homogeneous strain field and leading to an enhanced accuracy was used during rotational shear experiments. No significant immediate mechanical damage was observed for these shear deformations up to strains of 0.45. A new differential viscoelastic model has been developed based on the large strain response to shear deformation of a representative sample. A sample was chosen for which the response was close to the mean response of a total of 21 samples. This way, the non-linearity of

the tissue behaviour was preserved while still keeping a statistically relevant response. The behaviour of this representative material was then compared to more shear results and was also validated for compression measurements in Chapter 5. Results for these two deformation modes were obtained from the same 28 samples. It should be mentioned that these measurements were performed at a different temperature. However also pre-compression applied prior to shear measurements was altered. These effects were previously studied and proved to compensate each other. Therefore the model fit based on the previous set of data was found to be applicable. Since techniques for testing soft tissue in compression are not well established, different measurement protocols and testing conditions affecting the results of compression measurements were examined beforehand. The initial conditions of a compression test were found to be highly important and were defined such that the material was in an equilibrated state.

Several constitutive models for brain tissue have been presented in literature so far. The material model presented here was developed based on the material response obtained from stress relaxation measurements. In this model, an elastic mode was added to a number of viscoelastic modes. This elastic mode is described by a Mooney-Rivlin-type model, modified with a non-linear prefactor. The shape of this non-linear prefactor was obtained from the equilibrated response of the stress relaxation experiments at different strain levels. Currently this model seems to accurately describe the response of brain tissue to dynamic loading, constant strain rate loading and stress relaxation in shear deformation. The unloading and recovery parts after stress relaxation are less well described. To enable the description of the response of the brain tissue for impact conditions, the constitutive model was extended with an extra viscoelastic mode for high frequencies, based on experimental data. In addition to shear deformation, the model was validated for constant strain rate loading in compression. This was done by comparing the results of a 3-D model of a quarter of a sample with frictionless and no-slip sample-plate interface conditions in the FE code MADYMO. While the model prediction with frictionless conditions at the sample-plate interface corresponds with the lower range of the measured stress response, the response of the simulation with no-slip conditions corresponds with the average experimental behaviour in compression. The Mooney-Rivlin parameters were set to  $a = b = 1$ , allowing for a simplification of the model. So far, only two other studies have shown a material model for brain tissue to describe both shear and compression deformation modes. Prange and Margulies [63] used an integral model in combination with Ogden hyper-elasticity to predict shear stress relaxation, however the behaviour during constant strain rate loading was not considered. The compressive response was validated only with the equilibrium stress obtained from compression stress relaxation. Furthermore, the model with the parameters as determined in that study can not predict the response for frequencies as high as the model presented in current study, which is a very important aspect for application in a FE head model for assessment of injury levels. Shen et al. [64] have validated a simplified version of a constitutive model developed by Bilston et al. [36] with constant strain rate measurements in compression only up to a strain of 5%, assuming frictionless loading. Similar to results obtained in the current study when using a slip boundary condition, the models presented in these studies tend to underpredict the tissue response in compression.

A compressible version of the newly developed non-linear viscoelastic model was implemented in the explicit FE code MADYMO see Appendix A. The performance of a 3-D head model with a sliding skull-brain interface was compared with a previously developed and more extensively validated head model with a tied skull-brain interface, see Chapter 6. For an assessment of consequences of constitutive non-linearities in a numerical head model, a sliding interface model was preferred over a tied interface model, based on results of the current study and those presented in literature. Although, the sliding interface model is considered to be a more realistic one, the thickness of the gap of approximately 0.5 mm in the current configuration can have an influence on the relative motion between the brain and the skull. Similar to a previous study in literature, this may affect the deformations observed in the FE simulation. The influences of constitutive nonlinearities of brain tissue in numerical head model simulations are investigated by comparing the performance of the new constitutive model with its simplified version and with a previously developed constitutive model. FE simulation predictions of the simplified and the fully non-linear version of the model varied consistently with the constitutive behaviour. Therefore, the simplified version of the newly developed model could be used for reliable injury predictions with FE simulations instead of the non-linear model, since the results can be easily scaled for the constitutive model used. The other constitutive model considered [82] contains non-physical non-linearities causing differences of the head model response that vary with the loading conditions. Hence, no reliable assessment of injury can be made with that constitutive model for brain tissue.

A digital image correlation technique was used to obtain high-resolution strain field information in planar sections of the brain. The brain slices containing the complex folding structure are encapsulated in a cavity filled with artificial cerebrospinal fluid and subjected to translational acceleration of 800 - 1000 m/s<sup>2</sup>. Geometrical heterogeneities such as sulci and constitutive variations between the surrounding grey and white matter were experimentally found to have an influence on the local strain field in brain slices subjected to transient translational acceleration. However this study has some limitations such as some uncertainty about possible friction between the tissue and the covering plate and geometrical variations through the thickness although the thickness was limited to 4 mm. Nevertheless, the experimental results demonstrate the potential importance of these geometrical heterogeneities for the next generation of injury assessment tools. However this would require a large number of elements, which would result in an enormous increase of computational time. This seems feasible in coming years considering the rapid advances in computer hardware.

## 8.2 Recommendations

The aim of this thesis was to develop a constitutive model for brain tissue based on reliable measurements. Because of variation in measurement results found in literature, a new data set covering two deformation modes was obtained. Samples of porcine brain tissue were mechanically loaded in shear and compression. The properties were obtained at the level of homogeneous brain tissue and a constitutive description of these properties

was given. Some recommendations are given for future studies:

- The experimental conditions during characterisation tests of brain tissue should be carefully controlled and reported. They were found to affect measured properties.
- Other techniques like ultrasound [27] or magnetic resonance elastography [121] have already been used to obtain material properties of brain tissue and maybe used in future studies to investigate inter-regional variations and in vivo behaviour.
- The methodology developed and used in the current study can possibly be applied to study the mechanical properties of human brain tissue.
- For compression experiments, better defined boundary conditions may be obtained if slip between the tissue and the loading plate is prevented rather than promoted.
- In addition to the current deformation modes, tensile experiments can be used to validate the model.
- The constitutive model developed in this work could be further improved to provide a better description of recovery after unloading of a stress relaxation test in shear deformation.
- With improvement of micro and nano measurement techniques, the mechanical response of single nerve cells or the axons connecting them could also be studied in support of micromechanics-based studies on brain injury.
- Similar to the miniaturisation of measurements mentioned before, new constitutive models can be developed based on a micro-macro modeling approach. This may provide deeper insight into the origin and magnitude of anisotropy and inter-regional variations.

The final test for a constitutive model is the validation with experiments on a real head or with an alternative experiment that has all important features of the brain-skull contribution, i.e. inhomogeneous material behaviour, geometrical details, and complex boundary conditions. Such an experiment is preferred since it can be designed to be accessible for strain measurements at impact conditions. For this purpose the following recommendations are made:

- The technique for measuring a strain field in planar sections of brain tissue presented in Chapter 7 could be used in the future for validation of constitutive models in a finite element context.
- Displacement fields from both side could be used to account for through-thickness variations.
- Further development of the technique is necessary with more focus on the effect of boundary conditions. The size of the cavity which encloses the brain slice could be increased. This would deviate from reality but would be preferred for constitutive model validation.

- The acceleration pulse could be better controlled.
- 3D experiments for further numerical model or constitutive model validation can be developed based on e.g. magnetic resonance imaging.
- The experimental results presented in Chapter 7 and numerical results of Cloots et al. [114] showed the geometrical heterogeneities to influence the mechanical response of brain tissue resulting from inertial loading. Therefore, 3-D head models may need to account for the consequences of these details.
- The mechanical behaviour of the pia mater and other meninges have not been defined yet, and could have an influence on FE predictions.
- Further refinement of the 3-D head model used in the current study is required. The size of elements of the mesh used in the FE head model has been previously criticised and it was suggested to decrease this element size [93,94].
- The effect of the size of the gap representing the CSF should be investigated, since it is suggested to have an influence on the relative motion between the brain and the skull.

3D FE head models can be used to assess injury based on predictions of the mechanical response of the contents of the head during impact. To successfully use numerical head models as an injury criterion, the following recommendations are made:

- World-wide agreement on the mechanical properties of brain tissue is required.
- Similarly, agreement on other aspects of numerical head models is required.
- To accurately obtain true tissue level deformations and stresses would require to incorporate the influence of details such as heterogeneities, grey and white matter, etc.

# Finite element implementation

---

### Abstract

A constitutive description capturing the material behaviour of porcine brain tissue, observed in the experiments is extended with compressibility. The model is based on a multi-mode Maxwell model and consists of a non-linear elastic mode in combination with a number of viscoelastic modes. These viscoelastic modes consist of an elastic Mooney-Rivlin model and a viscous Ellis model.

The constitutive model is implemented in the explicit FE code MADYMO. For time integration, an improved Euler integration method (Heun's predictor-corrector) was applied to obtain sufficient accuracy for time steps commonly used in explicit head impact simulations.



## A.1 Compressible viscoelastic model for brain tissue

The constitutive model consists of an elastic part, denoted by the subscript “e” and a (deviatoric) viscoelastic part, denoted by the subscript “ve”, with  $N$  viscoelastic modes. In analogy to Equation (4.2), the total Cauchy stress is written as:

$$\boldsymbol{\sigma} = \boldsymbol{\sigma}_e + \sum_{i=1}^N \boldsymbol{\sigma}_{ve_i}^d, \quad (\text{A.1})$$

in which the superscript “d” indicates a deviatoric tensor. The viscoelastic model is schematically represented in Figure A.1. It shows the elastic mode ( $\boldsymbol{\sigma}_e$ ) and the viscoelastic modes ( $\boldsymbol{\sigma}_{ve_i}^d$  with  $i = 1, \dots, N$ ). In Chapter 4, the elastic stress was derived

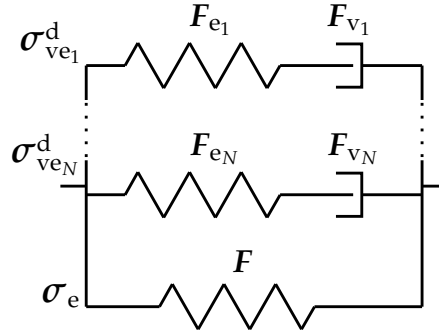


**Figure A.1:** Schematic illustration of the viscoelastic model. The viscoelastic modes ( $\boldsymbol{\sigma}_{ve_i}^d$ ) are represented by elastic springs ( $F_{e_i}$ ) and dashpots ( $F_{v_i}$ ) and a non-linear elastic model ( $\boldsymbol{\sigma}_e$ ) is represented by an elastic spring.

from the strain energy function  $W_e(I_1, I_2)$  which was given by Equations (4.10) and (4.11) and where  $I_i$  denotes the  $i$ th invariant of the Finger tensor  $\mathbf{B}$ . Here, a generalised compressible extension of this strain energy function is used:

$$W_e = \tilde{W}_e(\tilde{I}_1, \tilde{I}_2) + W^h(I_3), \quad (\text{A.2})$$

where  $\tilde{I}_1 = I_3^{-\frac{1}{3}} I_1$ ,  $\tilde{I}_2 = I_3^{-\frac{2}{3}} I_2$  are the invariants of the isochoric Finger tensor  $\tilde{\mathbf{B}} = I_3^{-\frac{1}{3}} \mathbf{B}$  and where for the function  $\tilde{W}_e(\tilde{I}_1, \tilde{I}_2)$  the same function as the original function  $W_e(I_1, I_2)$  is used. The stress in the elastic mode can then be written as:

$$\boldsymbol{\sigma}_e = \boldsymbol{\sigma}_e^d + \boldsymbol{\sigma}_e^h, \quad (\text{A.3})$$

where “h” indicates the hydrostatic part. The deviatoric part of the elastic stress is obtained as:

$$\boldsymbol{\sigma}_e^d = \frac{2}{\sqrt{I_3}} \left[ \frac{\partial \tilde{W}}{\partial \tilde{I}_1} \tilde{\mathbf{B}}^d - \frac{\partial \tilde{W}}{\partial \tilde{I}_2} (\tilde{\mathbf{B}}^{-1})^d \right] \quad (\text{A.4})$$

$$= \frac{G_\infty}{\sqrt{I_3}} \left[ (1-A) \exp \left( -C \sqrt{b\check{I}_1 + (1-b)\check{I}_2 - 3} \right) + A \right] \left[ b\check{\mathbf{B}}^d - (1-b)(\check{\mathbf{B}}^{-1})^d \right], \quad (\text{A.5})$$

with  $G_\infty$  the elastic shear modulus and  $A$ ,  $C$ , and  $b$  elastic fitting parameters.

For the hydrostatic part, the following strain energy function is assumed:

$$W^h = \frac{1}{2} K (\sqrt{I_3} - 1)^2, \quad (\text{A.6})$$

with  $K$  the bulk modulus and  $\sqrt{I_3} = \det(\mathbf{F})$  the volume ratio. Then, the hydrostatic part of the elastic stress is given by:

$$\boldsymbol{\sigma}^h = 2\sqrt{I_3} \frac{\partial W^h}{\partial I_3} \mathbf{I} \quad (\text{A.7})$$

$$= K(J-1)\mathbf{I} \quad \text{with} \quad J = \sqrt{I_3}. \quad (\text{A.8})$$

The second term on the right hand side of Equation (A.1) consists of the summation of the viscoelastic modes. For these modes, the deformation gradient tensor  $\mathbf{F}$  is partitioned into an elastic deformation gradient tensor  $\mathbf{F}_{e_i}$  and a viscous deformation gradient tensor  $\mathbf{F}_{v_i}$  [79]. The partitioning of the viscoelastic deformations is depicted in Figure A.2. For

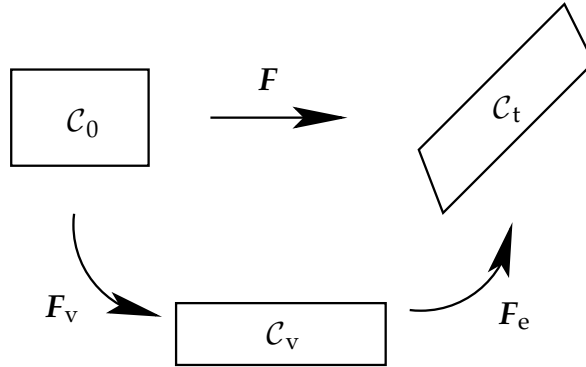


**Figure A.2:** Partitioning of the deformation gradient tensor  $\mathbf{F}$  into an elastic deformation gradient tensor  $\mathbf{F}_e$  and a viscous deformation gradient tensor  $\mathbf{F}_v$  in order to obtain a fictitious stress-free state  $C_v$  between the initial configuration  $C_0$  and the current configuration  $C_t$ .

simplicity, the subscript  $i$  indicating the viscoelastic mode  $i$  is omitted throughout the remaining part of this section. A multiplicative decomposition of the deformation gradient tensor  $\mathbf{F}$  is assumed:

$$\mathbf{F} = \mathbf{F}_e \cdot \mathbf{F}_v. \quad (\text{A.9})$$



The decomposition involves a fictitious intermediate state, which could exist after application of merely the viscous deformation gradient tensor  $F_v$ . After application of the elastic deformation tensor  $F_e$ , this stress-free state transforms into the final state.

By using Equation (A.9) with the definition of the velocity gradient tensor  $L = \dot{F} \cdot F^{-1}$ , it follows that

$$L = L_e + L_v \quad \text{with} \quad L_e = \dot{F}_e \cdot F_e^{-1} \quad \text{and} \quad L_v = F_e \cdot \dot{F}_v \cdot F_v^{-1} \cdot F_e^{-1}. \quad (\text{A.10})$$

The velocity gradient tensor  $L$  can also be decomposed as

$$L = D + \Omega \quad \text{and} \quad L_e = D_e + \Omega_e \quad \text{and} \quad L_v = D_v + \Omega_v. \quad (\text{A.11})$$

in which  $D = \frac{1}{2}(L + L^T)$  is the symmetric rate of deformation tensor and  $\Omega = \frac{1}{2}(L - L^T)$  is the skew-symmetric spin tensor. To obtain a unique intermediate state, the viscous deformations are chosen to be spin-free, so that  $\Omega_v = O$ .

Furthermore, the viscous right Cauchy-Green deformation tensor is defined as

$$C_v = F_v^T \cdot F_v. \quad (\text{A.12})$$

In order to update the tensor  $C_v$  in the time integration scheme (see section A.2), use is made of its time derivative, which can be written as:

$$\dot{C}_v = F^T \cdot B_e^{-1} \cdot [(L - L_e) \cdot B_e + B_e \cdot (L^T - L_e^T)] \cdot B_e^{-1} \cdot F. \quad (\text{A.13})$$

Using the assumption of a spin-free viscous deformation, the time derivative of the viscous right Cauchy-Green deformation tensor for a unique intermediate state yields

$$\dot{C}_v = 2 \cdot F^T \cdot B_e^{-1} \cdot D_v \cdot F, \quad (\text{A.14})$$

where the elastic Finger tensor is calculated by

$$B_e = F \cdot C_v^{-1} \cdot F^T. \quad (\text{A.15})$$

For the response of the viscoelastic modes, in analogy to the elastic mode, the elastic strain energy is assumed to be given by

$$W_{ve} = \frac{1}{2}G [a\tilde{I}_{e1} + (1-a)\tilde{I}_{e2} - 3], \quad (\text{A.16})$$

with  $G$  the shear modulus,  $\tilde{I}_{e_i}$  the invariants of the isochoric elastic Finger tensor  $\tilde{B}_e$ , and  $a$  a fitting parameter. As a result, the viscoelastic stress is given by:

$$\sigma_{ve}^d = \frac{G}{\sqrt{I_3}} \left[ a\tilde{B}_e^d - (1-a)(\tilde{B}_e^{-1})^d \right]. \quad (\text{A.17})$$

The viscous deformation  $F_v$  is assumed to be volume-invariant, so that  $\det(F_v) = 1$  and  $\det(F_e) = \det(F)$ . This justifies the use of the third invariant of  $B$  instead of  $B_e$  in Equation (A.17).

The viscous rate of deformation tensor is calculated from the following flow rule, assuming viscous incompressibility:

$$D_v = \frac{\sigma_{ve}^d}{2\eta(\tau)} \quad (\text{A.18})$$

where the dynamic viscosity  $\eta$  is a function of the scalar equivalent stress measure  $\tau = \sqrt{\frac{1}{2}\sigma^d : \sigma^d}$ . It is described by the Ellis model, which states

$$\eta(\tau) = \eta_\infty + \frac{\eta_0 - \eta_\infty}{1 + \left(\frac{\tau}{\tau_0}\right)^{n-1}}. \quad (\text{A.19})$$

with subscripts “0” and “ $\infty$ ” denoting the initial and infinite values, respectively. The initial value for viscosity is defined as  $\eta_0 = G\lambda$ , whereas the infinite viscosity is written as  $\eta_\infty = k\eta_0$ . For viscoelastic parameters  $G$  and  $\lambda$  see Table 5.1.

## A.2 Numerical implementation

For the computation of the Cauchy stress (Equation (A.1) for a given deformation  $F(t)$  at the end of an increment from  $t - \Delta t$  to  $t$ , several steps are taken (see Figure A.3). The elastic stresses  $\sigma_e^h(t)$  and  $\sigma_e^d(t)$  can be computed directly. For the time integration of the viscoelastic stress modes, the Heun’s method, also known as the improved Euler’s method, is used [82]. This involves an explicit time integration scheme for Equation (A.14). First, a prediction (indicated by the superscript “\*”) of the time derivatives of the viscous right Cauchy-Green deformation tensors  $C_{v_i}^*(t)$  are computed using the Euler forward method. These are used to calculate  $\sigma_{ve_i}^{*d}(t)$  and  $\dot{C}_{v_i}^*(t)$ . After that, the tensors  $C_{v_i}(t)$  are more accurately determined by applying the trapezoidal rule, after which  $\sigma_{ve_i}^d(t)$  and subsequently  $\sigma$  are calculated. For each time step, the values of tensors  $C_{v_i}(t)$  and  $\dot{C}_{v_i}(t)$ , are stored for the next time increment. For the initial values, no deformation is assumed, which yields  $F(0) = I$ ,  $C_{v_i}(0) = I$ , and  $\dot{C}_{v_i}(0) = O$ . These steps are implemented in the usersubroutine USRMVITNO of the explicit FE code Madymo, version 6.3.2, according to the following scheme:

1. Compute the deformation  $F(t)$  from the nodal displacements.
2. Compute  $\sigma_e^h(t) = K(J(t) - 1)I$
3. Compute  $\sigma_e^d(t) = \frac{G_\infty}{\sqrt{I_3(t)}} \left[ (1-A) \exp\left(-C\sqrt{b\tilde{I}_1(t) + (1-b)\tilde{I}_2(t) - 3}\right) + A \right] \left[ b\tilde{B}^d(t) - (1-b)(\tilde{B}^{-1}(t))^d \right]$

4. (a) Retrieve  $\mathbf{C}_{v_i}(t - \Delta t)$  and  $\dot{\mathbf{C}}_{v_i}(t - \Delta t)$  from the previous time increment for each mode  $i = 1$  to  $N$ .

- (b) For mode  $i = 1$  to  $N$ , predict  $\mathbf{C}_{v_i}(t)$ ,  $\mathbf{B}_{e_i}(t)$ , and  $\boldsymbol{\sigma}_{ve_i}^d(t)$

$$\mathbf{C}_{v_i}^*(t) = \mathbf{C}_{v_i}(t - \Delta t) + \dot{\mathbf{C}}_{v_i}(t - \Delta t)\Delta t$$

$$\mathbf{B}_{e_i}^*(t) = \mathbf{F}(t) \cdot \mathbf{C}_{v_i}^{*-1}(t) \cdot \mathbf{F}^T(t)$$

$$\boldsymbol{\sigma}_{ve_i}^{*d}(t) = \frac{G_i}{\sqrt{I_3(t)}} \left[ a\tilde{\mathbf{B}}_{e_i}^{*d}(t) - (1 - a)(\tilde{\mathbf{B}}_{e_i}^{*-1}(t))^d \right]$$

- (c) Predict  $\boldsymbol{\sigma}^d(t)$  and  $\tau(t)$

$$\boldsymbol{\sigma}^{*d}(t) = \boldsymbol{\sigma}_e^d(t) + \sum_{i=1}^N \boldsymbol{\sigma}_{ve_i}^{*d}(t)$$

$$\tau^*(t) = \sqrt{\frac{1}{2}\boldsymbol{\sigma}^{*d}(t) : \boldsymbol{\sigma}^{*d}(t)}$$

- (d) For mode  $i = 1$  to  $N$ , predict  $\eta_i(t)$ ,  $\mathbf{D}_{v_i}(t)$ , and  $\dot{\mathbf{C}}_{v_i}(t)$

$$\eta_i^*(t) = \eta_{\infty_i} + \frac{\eta_{0_i} - \eta_{\infty_i}}{1 + \left(\frac{\tau^*(t)}{\tau_0}\right)^{(n_i-1)}}$$

$$\mathbf{D}_{v_i}^*(t) = \frac{\boldsymbol{\sigma}_{ve_i}^{*d}(t)}{2\eta_i^*(t)}$$

$$\dot{\mathbf{C}}_{v_i}^*(t) = 2 \cdot \mathbf{F}^T(t) \cdot \mathbf{B}_{e_i}^{*-1}(t) \cdot \mathbf{D}_{v_i}^*(t) \cdot \mathbf{F}(t)$$

and determine

$$\mathbf{C}_{v_i}(t) = \mathbf{C}_{v_i}(t - \Delta t) + \frac{1}{2}(\dot{\mathbf{C}}_{v_i}(t - \Delta t) + \dot{\mathbf{C}}_{v_i}^*(t))\Delta t$$

$$\mathbf{B}_{e_i}(t) = \mathbf{F}(t) \cdot \mathbf{C}_{v_i}^{-1}(t) \cdot \mathbf{F}^T(t)$$

$$\boldsymbol{\sigma}_{ve_i}^d(t) = \frac{G_i}{\sqrt{I_3(t)}} \left[ a\tilde{\mathbf{B}}_{e_i}^d(t) - (1 - a)(\tilde{\mathbf{B}}_{e_i}^{-1}(t))^d \right]$$

and store  $\mathbf{C}_{v_i}(t)$  for the next time increment.

- (e) Determine

$$\boldsymbol{\sigma}^d(t) = \boldsymbol{\sigma}_e^d(t) + \sum_{i=1}^N \boldsymbol{\sigma}_{ve_i}^d(t)$$

$$\tau(t) = \sqrt{\frac{1}{2}\boldsymbol{\sigma}^d(t) : \boldsymbol{\sigma}^d(t)}$$

- (f) For mode  $i = 1$  to  $N$ , determine

$$\eta_i(t) = \eta_{\infty_i} + \frac{\eta_{0_i} - \eta_{\infty_i}}{1 + \left(\frac{\tau(t)}{\tau_0}\right)^{n_i-1}}$$

$$D_{v_i}(t) = \frac{\sigma_{ve_i}^d(t)}{2\eta_i(t)}$$

$$\dot{C}_{v_i}(t) = 2 \cdot F^T(t) \cdot B_{e_i}^{-1}(t) \cdot D_{v_i}(t) \cdot F(t)$$

and store  $\dot{C}_{v_i}(t)$  for the next time increment.

5. Compute  $\sigma(t) = \sigma_e^h(t) + \sigma^d(t)$

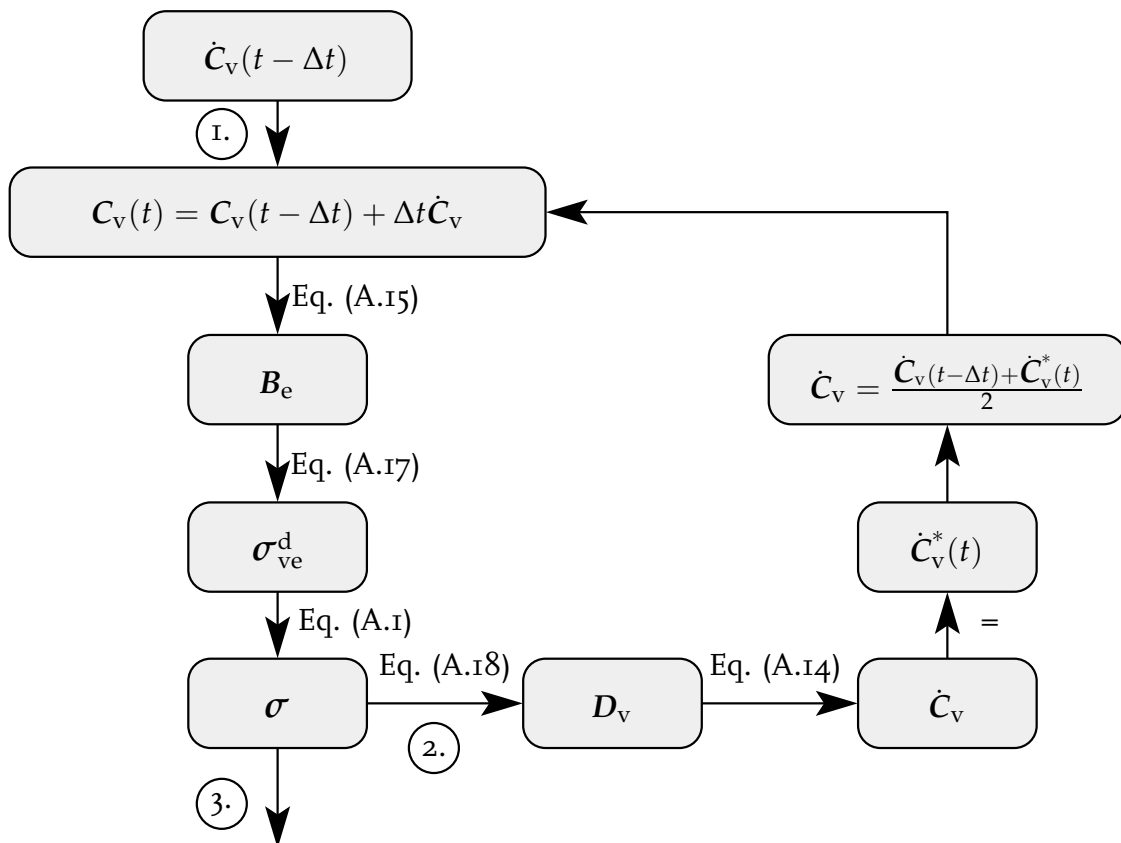


**Figure A.3:** Flow diagram of integration scheme. Each increment starts at (1). Subsequently, routes (2) and (3) are followed.



# Bibliography

---

- [1] Peden, M., Scurfield, R., Sleet, D., Mohan, D., Hyder, A. A., Jarawan, E., and Mathers, C., 2004. World report on road traffic injury prevention. Tech. rep., World Health Organization.
- [2] Langlois, J. A., Rutland-Brown, W., and Thomas, K. E., 2004. Traumatic brain injury in the united states: Emergency department visits, hospitalizations, and deaths. Tech. rep., Centers for Disease Control and Prevention, National Center for Injury Prevention and Control.
- [3] Iwata, A., Stys, P. K., Wolf, J. A., Chen, X. H., Taylor, A. G., Meaney, D. F., and Smith, D. H., 2004. “Traumatic axonal injury induces proteolytic cleavage of the voltage-gated sodium channels modulated by tetrodotoxin and protease inhibitors”. *The Journal of Neuroscience*, **24**(19), pp. 4605–4613.
- [4] The American Society of Clinical Oncology, 2008. <http://www.asco.org>.
- [5] Drake, R. L., Vogl, W., and Mitchell, A. W. M., 2005. *Gray’s Anathomy for students*. Elsevier Inc.
- [6] Linder, C. R., Wikipedia, 2008. <http://en.wikipedia.org/wiki/fmri>.
- [7] Versace, J., 1971. “A review of the severity index”. In Proceedings of the 15<sup>th</sup> Stapp Car Crash Conference, no. SAE 710881, pp. 771–796.
- [8] Gurdjian, E. S., Lissner, H. R., and Patrick, L. M., 1962. “Protection of the head and neck in sports”. *The Journal of the American Medical Association*, **182**, pp. 502–512.
- [9] Newman, J. A., 1980. “A generalized acceleration model for brain injury threshold”. In Proceedings of the IRCOBI Conference, pp. 121–131.
- [10] Newman, J. A., Barr, C., Beusenberg, M., Fiurnier, E., Shewchenko, N., Welbourne, E., and Withnall, C., 2000. “A new biomechanical assessment of mild traumatic brain injury part 2: results and conclusions”. In Proceedings of the IRCOBI Conference, pp. 223–233.



- [11] Newman, J. A., Shewchenko, N., and Welbourne, E., 2000. "A proposed new biomechanical head injury assessment function - the maximum power index". In Proceedings of the 44<sup>th</sup> Stapp Car Crash Conference, no. SAE 2000-01-SC16.
- [12] Brands, D. W. A., Peters, G. W. M., and Bovendeerd, P. H. M., 2004. "Design and numerical implementation of a 3-d non-linear viscoelastic constitutive model for brain tissue during impact". *Journal of Biomechanics*, 37(1), pp. 127-134.
- [13] ETSC, 1993. Report in motorcycle safety, european experimental vehicles committee ad-hoc group. Tech. rep., European Transport Safety Council, Brussels, Belgium.
- [14] Ommaya, A. K., 1968. "Mechanical properties of tissue of the nervous system". *Journal of Biomechanics*, 1(2), pp. 127-138.
- [15] Goldsmith, W., 1972. "Biomechanics of head injury". In Biomechanics - Its Foundation and Objectives, Y. C. Fund, N. Perrone, and M. Anliker, eds., Prentice-Hall Inc., pp. 585-634.
- [16] Thibault, L. E., and Gennarelli, T. A., 1985. "Biomechanics and craniocerebral trauma". In Central Nervous System Trauma Status Report, National Institutes of Health, pp. 379-389.
- [17] Donnelly, B. R., 1998. "Brain tissue material properties: A comparison of results". In Biomechanical Research: Experimental and Computational, Proceedings of the 26<sup>th</sup> International Workshop, pp. 47-57.
- [18] Kruse, S. A., Dresner, M. A., Rossman, P. J., Felmlee, J. P., Jack, C. R., and Ehman, R. L., 1999. "Palpation of the brain using magnetic resonance elastography". In Proceedings of the 7<sup>th</sup> Annual Meeting of ISMRM, p. 258.
- [19] Manduca, A., Oliphant, T. E., Dresner, M. A., Mahowald, J. L., Kruse, S. A., Amromin, E., Felmlee, J. P., Greenleaf, J. F., and Ehman, R. L., 2001. "Magnetic resonance elastography: Non-invasive mapping of tissue elasticity". *Medical Image Analysis*, 5(4), pp. 237-254.
- [20] Manduca, A., Lake, D. S., Kruse, S. A., and Ehman, R. L., 2003. "Spatio-temporal directional filtering for improved inversion of MR elastography images". *Medical Image Analysis*, 7(4), pp. 465-473.
- [21] McCracken, P. J., Manduca, A., Felmlee, J., and Ehman, R. L., 2005. "Mechanical transient-based magnetic resonance elastography". *Magnetic Resonance in Medicine*, 53(1), pp. 628-639.
- [22] Hamhaber, U., Sack, I., Papazoglou, S., Rump, J., Klatt, D., and Braun, J., 2007. "Three-dimensional analysis of shear wave propagation observed by in vivo magnetic resonance elastography of the brain". *Acta Biomaterialia*, 3(1), pp. 127-137.

- [23] Etoh, A., Mitaku, S., Yamamoto, J., and Okano, K., 1994. "Ultrasonic absorption anomaly of brain tissue". *Japanese Journal of Applied Physics*, **33**, pp. 2874–2879.
- [24] Lin, S., Shieh, S., and Grimm, M. J., 1997. "Ultrasonic measurements of brain tissue properties". In Proceedings of the 7<sup>th</sup> Injury Prevention through Biomechanics Symposium, Centers for Disease Control, Wayne State University, pp. 27–31.
- [25] Lin, S., and Grimm, M. J., 1998. "Characterization of the mechanical properties of brain tissue using ultrasound". In Proceedings of the 8<sup>th</sup> Injury Prevention through Biomechanics Symposium, Centers for Disease Control, Wayne State University, pp. 59–64.
- [26] Lippert, S. A., Rang, E. M., and Grimm, M. J., 2003. "The wave-in-a-tube method for estimation of mechanical properties of viscoelastic materials using ultrasound". *Journal of Testing and Evaluation*, **31**(1), pp. 73–78.
- [27] Lippert, S. A., Rang, E. M., and Grimm, M. J., 2004. "The high frequency properties of brain tissue". *Biorheology*, **41**(6), pp. 681–691.
- [28] Fallenstein, G. T., Hulce, V. D., and Melvin, J. W., 1969. "Dynamic mechanical properties of human brain tissue". *Journal of Biomechanics*, **2**(3), pp. 217–226.
- [29] McElhaney, J. H., Melvin, J. W., Roberts, V. L., and Portnoy, H. D., 1973. "Dynamic characteristics of the tissues of the head". In Perspectives in Biomedical Engineering, R. M. Kenedi, ed., MacMillan Press, pp. 215–222.
- [30] Wang, H. C., and Wineman, A. S., 1972. "A mathematical model for the determination of viscoelastic behavior of brain in vivo". *Journal of Biomechanics*, **5**(5), pp. 431–446.
- [31] Arbogast, K. B., Meaney, D. F., and Thibault, L. E., 1995. "Biomechanical characterization of the constitutive relationship for the brainstem". In Proceedings of the 39<sup>th</sup> Stapp Car Crash Conference, no. SAE 952716, pp. 153–159.
- [32] Arbogast, K. B., and Margulies, S. S., 1997. "Regional differences in mechanical properties of the porcine central nervous system". In Proceedings of the 41<sup>st</sup> Stapp Car Crash Conference, no. SAE 973336, pp. 293–300.
- [33] Arbogast, K. B., Prange, M. T., Meaney, D. F., and Margulies, S. S., 1997. "Properties of cerebral gray and white matter undergoing large deformation". In Proceedings of the 7<sup>th</sup> Injury Prevention through Biomechanics Symposium, Centers for Disease Control, Wayne State University, pp. 33–39.
- [34] Arbogast, K. B., and Margulies, S. S., 1998. "Material characterization of the brainstem from oscillatory shear tests". *Journal of Biomechanics*, **31**(9), pp. 801–807.
- [35] Bilston, L. E., Liu, Z., and Phan-Thien, N., 1997. "Linear viscoelastic properties of bovine brain tissue in shear". *Biorheology*, **34**(6), pp. 377–385.



- [36] Bilston, L. E., Liu, Z., and Phan-Thien, N., 2001. "Large strain behavior of brain tissue in shear: Some experimental data and differential constitutive model". *Biorheology*, **38**(3), pp. 335–345.
- [37] Brands, D. W. A., Bovendeerd, P. H. M., Peters, G. W. M., Wismans, J. S. H. M., Paas, M. H. J. W., and van Bree, J. L. M. J., 1999. "Comparison of the dynamic behavior of the brain tissue and two model materials". In Proceedings of the 43<sup>rd</sup> Stapp Car Crash Conference, no. SAE 99SC21, pp. 57–64.
- [38] Brands, D. W. A., Bovendeerd, P. H. M., Peters, G. W. M., and Wismans, J. S. H. M., 2000. "The large shear strain dynamic behavior of in-vitro porcine brain tissue and the silicone gel model material". In Proceedings of the 44<sup>th</sup> Stapp Car Crash Conference, no. SAE 2000-01-SC17, pp. 249–260.
- [39] Cheng, S., and Bilston, L. E., 2007. "Unconfined compression of white matter". *Journal of Biomechanics*, **40**(1), pp. 117–124.
- [40] Darvish, K. K., and Crandall, J. R., 2001. "Nonlinear viscoelastic effects in oscillatory shear deformation of brain tissue". *Medical Engineering & Physics*, **23**(9), pp. 633–645.
- [41] Dodgson, M. C. H., 1962. "Colloidal structures of brain". *Biorheology*, **1**(1), pp. 21–30.
- [42] Donnelly, B. R., and Medige, J., 1997. "Shear properties of human brain tissue". *Journal of Biomechanical Engineering - Transactions of the ASME*, **119**(4), pp. 423–432.
- [43] Estes, M. S., and McElhaney, J. H., 1970. "Response of brain tissue of compressive loading". In Proceedings of the 4<sup>th</sup> ASME Biomechanics Conference, no. 70-BHF-13.
- [44] Franceschini, G., Bigoni, D., Regitnig, P., and Holzapfel, G. A., 2006. "Brain tissue deforms similarly to filled elastomers and follows consolidation theory". *Journal of the Mechanics and Physics of Solids*, **54**(12), pp. 2592–2620.
- [45] Galford, J. E., and McElhaney, J. H., 1970. "A viscoelastic study of scalp, brain, and dura". *Journal of Biomechanics*, **3**(2), pp. 211–221.
- [46] Garo, A., Hrapko, M., van Dommelen, J. A. W., and Peters, G. W. M., 2007. "Towards a reliable characterisation of the mechanical behaviour of brain tissue: the effects of post-mortem time and sample preparation". *Biorheology*, **44**(1), pp. 51–58.
- [47] Gefen, A., Gefen, N., Zhu, Q., Raghupathi, R., and Margulies, S. S., 2003. "Age-dependent changes in material properties of the brain and braincase of the rat". *Journal of Neurotrauma*, **20**(11), pp. 1163–1177.
- [48] Gefen, A., and Margulies, S. S., 2004. "Are in vivo and in situ brain tissues mechanically similar?". *Journal of Biomechanics*, **37**(9), pp. 1339–1352.

- [49] Hrapko, M., van Dommelen, J. A. W., Peters, G. W. M., and Wismans, J. S. H. M., 2006. "The mechanical behaviour of brain tissue: large strain response and constitutive modelling". *Biorheology*, **43**(5), pp. 623–636.
- [50] Hrapko, M., van Dommelen, J. A. W., Peters, G. W. M., and Wismans, J. S. H. M., 2008. "Characterisation of the mechanical behaviour of brain tissue in compression and shear". *Journal of Biomechanical Engineering - Transactions of the ASME*, *submitted*.
- [51] Koeneman, J. B., 1966. Viscoelastic properties of brain tissue. M.S. Thesis, Case Institute of Technology, USA.
- [52] Metz, H., McElhaney, J., and Ommaya, A. K., 1970. "A comparison of the elasticity of live, dead, and fixed brain tissue". *Journal of Biomechanics*, **3**(4), pp. 453–458.
- [53] Miller, K., and Chinzei, K., 1997. "Constitutive modeling of brain tissue: Experiment and theory". *Journal of Biomechanics*, **30**(11-12), pp. 1115–1121.
- [54] Miller, K., Chinzei, K., Orssengo, G., and Bednarz, P., 2000. "Mechanical properties of brain tissue in-vivo: experiment and computer simulation". *Journal of Biomechanics*, **33**(11), pp. 1369–1376.
- [55] Miller, K., and Chinzei, K., 2002. "Mechanical properties of brain tissue in tension". *Journal of Biomechanics*, **35**(4), pp. 483–490.
- [56] Nicolle, S., Lounis, M., and Willinger, R., 2004. "Shear properties of brain tissue over a frequency range relevant for automotive impact situations: New experimental results". *Stapp Car Crash Journal*, **48**, no. SAE 2004-22-0011, pp. 239–258.
- [57] Nicolle, S., Lounis, M., Willinger, R., and Palierne, J. F., 2005. "Shear linear behaviour of brain tissue over a large frequency range". *Biorheology*, **42**(3), pp. 209–223.
- [58] Ning, X., Zhu, Q., Lanir, Y., and Margulies, S. S., 2006. "A transversely isotropic viscoelastic constitutive equation for brainstem undergoing finite deformation". *Journal of Biomechanical Engineering - Transactions of the ASME*, **128**(6), pp. 925–933.
- [59] Peters, G. W. M., Meulman, J. H., and Sauren, A. H. J., 1997. "The applicability of the time/temperature superposition principle to brain tissue". *Biorheology*, **34**(2), pp. 127–138.
- [60] Prange, M. T., Meaney, D. F., and Margulies, S. S., 1998. "Directional properties of gray and white brain tissue". In *Proceedings of the Eight Injury Prevention through Biomechanics Symposium*, Centers for Disease Control, Wayne State University, pp. 65–71.

- [61] Prange, M. T., and Margulies, S. S., 1999. "Anisotropy and inhomogeneity of the mechanical properties of brain tissue at large deformation". In Proceedings of the 9<sup>th</sup> Injury Prevention through Biomechanics Symposium, Centers for Disease Control, Wayne State University, pp. 95–100.
- [62] Prange, M. T., Meaney, D. F., and Margulies, S. S., 2000. "Defining brain mechanical properties: Effects of region, direction, and species". In Proceedings of the 44<sup>th</sup> Stapp Car Crash Conference, no. SAE 2000-01-SC15, pp. 205–213.
- [63] Prange, M. T., and Margulies, S. S., 2002. "Regional, directional, and age-dependent properties of the brain undergoing large deformation". *Journal of Biomechanical Engineering - Transactions of the ASME*, **124**(2), pp. 244–252.
- [64] Shen, F., Tay, T. E., Li, J. Z., Nigen, S., Lee, P. V. S., and Chan, H. K., 2006. "Modified bilston nonlinear viscoelastic model for finite element head injury studies". *Journal of Biomechanical Engineering - Transactions of the ASME*, **128**(5), pp. 797–801.
- [65] Shuck, L. Z., and Advani, S. H., 1972. "Rheological response of human brain tissue in shear". *Journal of Basic Engineering - Transactions of the ASME*, **94**, pp. 905–911.
- [66] Velardi, F., Fraternali, F., and Angelillo, M., 2006. "Anisotropic constitutive equations and experimental tensile behavior of brain tissue". *Biomechanics and Modeling in Mechanobiology*, **5**(1), pp. 53–61.
- [67] Takhounts, E. G., Crandall, J. R., and Matthews, B. T., 1999. "Shear properties of brain tissue using non-linear Green-Rivlin viscoelastic constitutive equation". In Injury Biomechanics Research, Proceedings of the 27<sup>th</sup> International Workshop, pp. 141–156.
- [68] Takhounts, E. G., Crandall, J. R., and Darvish, K. K., 2003. "On the importance of nonlinearity of brain tissue under large deformations". *Stapp Car Crash Journal*, **47**, no. SAE 2003-22-0005, pp. 107–134.
- [69] Thibault, K. L., and Margulies, S. S., 1996. "Material properties of the developing porcine brain". In Proceedings of the IRCOBI Conference, pp. 75–85.
- [70] Thibault, K. L., and Margulies, S. S., 1998. "Age-dependent material properties of the porcine cerebrum: Effect on pediatric inertial head injury criteria". *Journal of Biomechanics*, **31**(12), pp. 1119–1126.
- [71] van Turnhout, M., Oomens, C., Peters, G., and Stekelenburg, A., 2005. "Passive transverse mechanical properties as a function of temperature of rat skeletal muscle in vitro". *Biorheology*, **42**(3), pp. 193–207.
- [72] Ferry, J. D., 1980. *Viscoelastic Properties of Polymers; Third Edition*. John Wiley & Sons.

- [73] Arbogast, K. B., Thibault, K. L., Pinheiro, B. S., Winey, K. I., and Margulies, S. S., 1997. "A high-frequency shear device for testing soft biological tissues". *Journal of Biomechanics*, **30**(7), pp. 775–759.
- [74] Dobbing, J., 1974. "The later development of the brain and its vulnerability". In *Scientific foundation of Paediatrics*, J. A. Davis and J. Dobbing, eds., Heinemann Medical, London, Great Britain.
- [75] ETSC, 2003. Transport safety performance in the EU - a statistical overview. Tech. rep., European Transport Safety Council, Brussels, Belgium.
- [76] Mendis, K. K., Stalnaker, R. L., and Advani, S. H., 1995. "A constitutive relationship for large deformation finite element modeling of brain tissue". *Journal of Biomechanical Engineering - Transactions of the ASME*, **117**(3), pp. 279–285.
- [77] Miller, K., 1999. "Constitutive model of brain tissue suitable for finite element analysis of surgical procedures". *Journal of Biomechanics*, **32**(5), pp. 531–537.
- [78] Brain Museum, 2008. <http://www.brainmuseum.org>.
- [79] Peters, G. W. M., and Baaijens, F., 1997. "Modelling of non-isothermal viscoelastic flows". *Journal of Non-Newtonian Fluid Mechanics*, **68**(2-3), pp. 205–224.
- [80] Bain, A. C., and Meaney, D. F., 2000. "Tissue-level thresholds for axonal damage in an experimental model of cerebral nervous system white matter injury". *Journal of Biomechanical Engineering - Transactions of the ASME*, **122**(6), pp. 615–622.
- [81] Morrison III, B., Cater, H. L., Wang, C. C.-B., Thomas, F. C., Hung, C. T., Ateshian, G. A., and Sundstrom, L. E., 2003. "A tissue level tolerance criterion for living brain developed with an in vitro model of traumatic mechanical loading". *Stapp Car Crash Journal*, **47**, no. SAE 2003-22-0006, pp. 93–106.
- [82] Brands, D. W. A., Bovendeerd, P. H. M., and Wismans, J. S. H. M., 2002. "On the potential importance of non-linear viscoelastic material modelling for numerical prediction of the tissue response: test and application". *Stapp Car Crash Journal*, **46**, no. SAE 2002-22-0006, pp. 103–121.
- [83] Franke, E. K., 1954. The response of human skull to mechanical vibrations. Tech. Rep. WADC Tech. Rept. 54-24, Wright-Patterson Air Force Base, Ohio.
- [84] Miller, K., 2005. "Method of testing very soft biological tissues in compression". *Journal of Biomechanics*, **38**(1), pp. 153–158.
- [85] Hrapko, M., van Dommelen, J. A. W., Peters, G. W. M., and Wismans, J. S. H. M., 2008. "The influence of test conditions on characterization of the mechanical properties of brain tissue". *Journal of Biomechanical Engineering - Transactions of the ASME*, **130**(3).

- [86] Wu, J. Z., Gong, R. G., and Schopper, A. W., 2004. "Analysis of effects of friction on the deformation behaviour of soft tissues in unconfined compression tests". *Journal of Biomechanics*, 37(1), pp. 147–155.
- [87] Claessens, M. H. A., Sauren, F., and Wismans, J. S. H. M., 1997. "Modelling of the human head under impact conditions: A parametric study". In Proceedings of the 41<sup>th</sup> Stapp Car Crash Conference, no. SAE 973338, pp. 315–328.
- [88] Kleiven, S., and von Holst, H., 2002. "Consequences of reduced brain volume following impact in prediction of subdural hematoma evaluated with numerical techniques". *Traffic Injury Prevention*, 3(4), pp. 303–310.
- [89] Kleiven, S., and Hardy, W. N., 2002. "Correlation of an FE model of the human head with experiments on localized motion of the brain – consequences for injury prediction". In Proceedings of the 46<sup>th</sup> Stapp Car Crash Conference, Vol. 46.
- [90] Al-Bsharat, A. S., Hardy, W. N., Yang, K. H., Khalil, T. B., Tashman, S., and King, A. I., 1999. "Brain skull relative displacement magnitude due to blunt head impact: New experimental data and model". In Proceedings of the 43<sup>rd</sup> Stapp Car Crash Conference, no. SAE 99SC22, pp. 321–332.
- [91] Nahum, A. M., Smith, R. W., and Ward, C. C., 1977. "Intracranial pressure dynamics during head impact". In Proceedings of the 21<sup>st</sup> Stapp Car Crash Conference, no. SAE 770922, pp. 339–366.
- [92] Bradshaw, D. R. S., and Morfey, C. L., 2001. "Pressure and shear response in brain injury models". In Proceedings of the 17<sup>th</sup> International Technical Conference on the Enhanced Safety of Vehicles, US Department of Transportation: National Highway Traffic Safety Administration.
- [93] Brands, D. W. A., 2002. Implementation of sliding interface in the TU/e FE head model. Tech. rep., TNO Automotive, The Netherlands.
- [94] Moerman, K., and Herlaar, K., 2006. Finite element modelling of the human head to predict and analyse brain injury due to blast induced acceleration. Tech. Rep. TNO-DV2 2005 IN017, TNO Defense, Security and Safety, The Netherlands.
- [95] Willinger, R., Kang, H., and Diaw, B., 1999. "Three-dimensional human head finite-element model validation against two experimental impacts". *Annals of Biomedical Engineering*, 27(3), pp. 403–410.
- [96] Zhang, L., Yang, K. H., and King, A., 2001. "Comparison of brain responses between frontal and lateral impacts by finite element modelling". *Journal of Neurotrauma*, 18(1), pp. 21–30.
- [97] Kleiven, S., and von Holst, H., 2001. "Consequences of brain size following impact in prediction of subdural hematoma with numerical techniques". In Proceedings of the International Conference on the Biomechanics of Impact, IRCOBI, pp. 161–172.

- [98] Pudenz, R. H., and Shelden, C. H., 1946. "The lucite calvarium: a method for direct observation of the brain". *Journal of neurosurgery*, 3(6), pp. 487–505.
- [99] Ivarsson, J., Viano, D. C., Lövsund, P., and Aldman, B., 2000. "Strain relief from the cerebral ventricles during head impact: experimental studies on natural protection of the brain". *Journal of Biomechanics*, 33(2), pp. 181–189.
- [100] Ivarsson, J., Viano, D. C., and Lövsund, P., 2002. "Influence of the lateral ventricles and irregular skull base on brain kinematics due to sagittal plane head rotations". *Journal of Biomechanical Engineering - Transactions of the ASME*, 124(4), pp. 422–431.
- [101] Margulies, S. S., Thibault, L. E., and Gennarelli, T. A., 1990. "Physical model simulations of brain injury in the primate". *Journal of Biomechanics*, 23(8), pp. 823–836.
- [102] Meaney, D. F., Smith, D. H., Schreiber, D. I., Bain, A. C., Miler, R. T., Ross, D. T., and Gennarelli, T. A., 1995. "Biomechanical analysis of experimental diffuse axonal injury". *Journal of Neurotrauma*, 12(4), pp. 689–694.
- [103] Hardy, W. N., Foster, C. D., King, A. I., and Tashman, S., 1997. "Investigation of brain injury kinematics: introduction of a new technique". *Crashworthiness, Occupant Protection and Biomechanics in Transportation Systems AMD*, 225, pp. 241–254.
- [104] Hardy, W. N., Foster, C. D., Mason, J., Yang, K. H., King, A., and Tashman, S., 2001. "Investigation of head injury mechanisms using neutral density technology and high-speed biplanar x-ray". *Stapp Car Crash Journal*, 45, no. SAE 2001-22-0016, pp. 337–368.
- [105] Bayly, P. V., Cohen, T. S., Leister, E. P., Ajo, D., Leuthardt, E. C., and Genin, G. M., 2005. "Deformation of the human brain induced by mild acceleration". *Journal of Neurotrauma*, 22(8), pp. 845–856.
- [106] Bayly, P. V., Ji, S., Song, S. K., Okamoto, R. J., Massouros, P., and Genin, G. M., 2004. "Measurement of strain in physical models of brain injury: a method based on harp analysis of tagged magnetic resonance images (mri)". *Journal of Biomechanical Engineering - Transactions of the ASME*, 126(4), pp. 523–528.
- [107] Bayly, P. V., Black, E. E., Pedersen, R. C., Leister, E. P., and Genin, G. M., 2006. "In vivo imaging of rapid deformation and strain in an animal model of traumatic brain injury". *Journal of Biomechanics*, 39(6), pp. 1086–1095.
- [108] Heinritzi, K., and Schillinger, S., 1996. "Untersuchung des liquor cerebrospinalis bei gesunden und zentralnervös erkrankten schweinen". *Tierärztl Prax*, 24, pp. 359–367.
- [109] Welker, W., Johnson, J. I., and Noe, A., 2007. Comparative mammalian brain collections, [www.brainmuseum.org](http://www.brainmuseum.org). Tech. rep., University of Wisconsin, Michigan State and National Museum of Health and Medicine.

- [II0] Gonzalez, R. C., and Wintz, P., 1983. *Digital image processing*. Addison-Wesley Publishing Company, Amsterdam.
- [II1] Chu, T. C., Ranson, W. F., Sutton, M. A., and Peters, W. H., 1985. "Applications of digital-image-correlation techniques to experimental mechanics". *Experimental Mechanics*, 25, pp. 232–244.
- [II2] Sutton, M. A., Cheng, M., Peters, W. H., Chao, Y. J., and McNeill, S. R., 1986. "Application of an optimized digital correlation method to planar deformation analysis". *Image and Vision Computing*, 4, pp. 143–150.
- [II3] GOM, 2005. *Aramis user manual v5.4.0*.
- [II4] Cloots, R. J. H., Gervaise, H. M. T., van Dommelen, J. A. W., and Geers, M. G. D., 2008. "Biomechanics of traumatic brain injury: Influences of the morphologic heterogeneities of the cerebral cortex". *Annals of Biomedical Engineering*, submitted.
- [II5] Graham, D. I., Adams, J. H., Nicolle, J. A. R., Maxwell, W. L., and Gennarelli, T. A., 1995. "The nature, distribution and causes of traumatic brain injury". *Brain Pathology*, 5(4), pp. 397–406.
- [II6] Narmoneva, D. A., Wang, J. Y., and Setton, L. A., 1999. "Nonuniform swelling-induced residual strains in articular cartilage". *Journal of Biomechanics*, 32(4), pp. 401–408.
- [II7] McElhaney, J. H., Roberts, V. L., and Hilyard, J. F., 1976. *Handbook of human tolerance*. Automobile Research Institute Inc., Tokyo, Japan.
- [II8] McIlwain, H., and Bachelard, H. S., 1966. *Biochemistry and the central nervous system, 3rd Edition*. J. & A. Churchill Ltd., London, Great Britain.
- [II9] Sherwooda, C. C., Stimpsona, C. D., Raghantia, M. A., Wildmand, D. E., Uddind, M., Grossmand, L. I., Goodmanb, M., Redmondh, J. C., Bonari, C. J., Erwinj, J. M., and Hof, P. R., 2006. "Evolution of increased glianeuron ratios in the human frontal cortex". *Proceedings of the National Academy of Sciences of the United States of America*, 103(37), pp. 13606–13611.
- [I20] Lind, N. M., Moustgaard, A., Jelsing, J., Vajta, G., Cumming, P., and Hansen, A. K., 2007. "The use of pigs in neuroscience: Modeling brain disorders". *Neuroscience and Biobehavioral Reviews*, 31(5-6), pp. 728–751.
- [I21] Vappou, J., Breton, E., Choquet, P., Goetz, C., Willinger, R., and Constantinesco, A., 2007. "Magnetic resonance elastography compared with rotational rheometry for in vitro brain tissue viscoelasticity measurement". *Magnetic Resonance Materials in Physics Biology and Medicine*, 20(5-6), pp. 273–278.

# Samenvatting

---

Bij botsingen is het hoofd het meest kwetsbare deel van het menselijk lichaam en het loopt daarbij vaak levensbedreigend letsel op. Om inzicht te verwerven in de vervormingen die aan de basis van dit letsel liggen, en deze te kunnen voorspellen voor een gegeven uitwendige belasting op het hoofd, is het noodzakelijk om het mechanisch gedrag van hersenweefsel te kennen. Deze kennis kan vervolgens, in de vorm van een wiskundige beschrijving van het mechanische gedrag, worden gebruikt in een eindige elementen model van het hoofd, waarmee zulke voorspellingen kunnen worden gedaan. Ondanks dat de mechanische eigenschappen van hersenweefsel al worden bestudeerd sinds de jaren zestig van de vorige eeuw, zijn ze tot nu toe niet binnen redelijke marges vastgelegd; de resultaten van verschillende studies liggen soms decades uit elkaar.

De hoofddoelen van deze studie zijn het vaststellen van het mechanisch gedrag van hersenweefsel onder invloed van grote rekken bij verschillende typen vervormingen, zoals afschuiving en compressie, het vastleggen van dit gedrag in een constitutief model, en gebruiken van deze beschrijving in een numeriek model dat de respons van de hersenen kan voorspellen tijdens botsingen. Een dergelijk model geeft bovendien de mogelijkheid om de invloed van structurele veranderingen in de constitutieve vergelijking te onderzoeken, in het bijzonder veranderingen van de niet-lineaire termen die het gedrag bij grote vervormingen beschrijven.

Het mechanisch gedrag van hersenweefsel kenmerkt zich als viscoelastisch. Voor de karakterisering van dit viscoelastisch gedrag zijn zowel lineaire en niet-lineaire metingen gedaan aan weefsel van varkenshersenen. Varkenshersenen zijn gekozen vanwege beschikbaarheid en de mogelijkheid om de post-mortem tijd gedurende de metingen te minimaliseren. Afschuif- en compressiemetingen zijn uitgevoerd op een ARES-II rotatiereometer, gebruik makend van een plaat-plaat geometrie. Bij de afschuifmetingen werd het monster excentrisch geplaatst om zodoende de signaal-ruis verhouding te verbeteren en een nagenoeg homogene deformatie in het monster te bewerkstelligen.

De effecten van verschillende testomstandigheden zijn onderzocht voor afschuifproeven; in het bijzonder de procedure voor monsterpreparatie, post-mortem tijd, testtemperatuur, precompressie en eventueel aanwezige anisotropie in relatie tot de afschuifrichting. Voor de compressieproeven is aangetoond dat zowel de, altijd op het weefsel aanwezige, vloeïstoflaag en de wrijving tussen weefsel en omgeving een belangrijke rol spelen in de





uiteindelijke respons van het monster.

Vervolgens is de weefselrespons voor grote afschuifrekken onderzocht. Tot rekken van 0.45 is geen directe mechanische schade, dat wil zeggen een substantiële verandering van de mechanische respons, gevonden en dus kon met deze proeven het materiaalgedrag voor complexe deformatie geschiedenissen worden bepaald. Op basis van de resultaten is een nieuwe constitutieve vergelijking van het differentiaal type opgesteld die vervolgens is gevalideerd in gecombineerde afschuif- en compressiemetingen aan dezelfde monsters.

Een compressibele versie van dit model, gecombineerd met een expliciet tijdsintegratie schema, is geïmplementeerd in het botssimulatie software pakket MADYMO. Resultaten van simulaties met dit constitutieve model, toegepast in een 3-dimensionaal eindige elementen hoofdmodel, zijn vergeleken met simulatie resultaten op basis van een vereenvoudigde versie van het model en met die van een niet-lineair model uit de literatuur. Hiermee is de gevoeligheid van de resultaten voor niet-lineariteiten in de constitutieve modelvorming van hersenweefsel onderzocht.

Verder zijn experimenten uitgevoerd aan plakken hersenweefsel, gebruik makend van beeldcorrelatie technieken, die bedoeld zijn als de opstap naar experimenten die toegankelijk zijn voor het meten van grote vervormingen onder botsingcondities. Aangetoond is dat geometrische en materiaal heterogeniteiten een belangrijke rol spelen in de locale respons van hersenweefsel en dus voor de mechanismen die ten grondslag liggen aan traumatisch hersenletsel. Het inbouwen van zulke heterogeniteiten in de volgende generatie letselanalyse gereedschappen is dan ook aan te bevelen.

# Acknowledgements

---

There are no words to express my gratitude to those who have contributed to my work and to this thesis. The thesis would have never been completed without your help.

First, I would like to thank the European Integrated Project on Advanced Passive Safety – APROSYS and the European Commission for their support. Second, I would like to thank my promotor Jac Wismans, for making me a part of this tiny subproject of APROSYS and supporting me during my studies. I would also like to thank my copromotors Gerrit Peters and Hans van Dommelen for their everyday support. I really enjoyed your friendly attitude, pragmatic and educational approach, drive to work and solve problems. I believe, you three have formed the perfect team in guiding me during these four years.

I am also grateful to the committee members prof. dr. ir. Marc Geers, prof. dr. ir. Jos Van der Sloten and dr. Svein Kleiven for their valuable comments on this thesis and their attendance in my defence; the Dean of our department prof. dr. ir. René de Borst for being the chairman during my defence.

I would also like to thank all the students who have contributed to this project, René Benders, Norman Delhey, Anais Garo, H el ene Gervaise, Lisa Tang, Caroline Lauret, Jan Neggens, Joost Velterop, Marc Haring and Tom van der Sande, your work is appreciated; TNO and particularly Marike van der Horst for her support and for providing the numerical head model; Marc, for the help with Aramis; Sjoerd, for delivering all the lunch meat; guys from the workshop, GTD and especially Sjef, for machining all the weird parts we needed; Leon, for support during our squeezing measurements; Jos, for support with culturing and staining of brain tissue; Patrick & Leo, for all the hardware & software support, especially Linux tips & tricks are highly appreciated; and Alice, Marleen and Yvon, for your kindness and for the great support during my studies.

Furthermore, I would like to acknowledge all the MaTe students and staff, particularly Alexei, Anish, Anita, Cem, Evelyne, Gabriel, Gwen, Hamid, Hanna, Ihor,  sa,  zzet, Jan-Willem, Jesus, Johan, Kang Yuen, Linda, Luigi, Marcel, Marco, Martijn, MK, Mohammad, M uge, Murthy, Piet, Roel, Ron, Rudi, Tom, Tuncay, Varya, Viny and Yvonne; and especially my current – former roommates Roy, Frederico, Yuriy, Lambert, Pieter, Gaetano, Rudy and Arash. I have really appreciated the international environment.

Special thanks to all of my Dutch, Slovak and the rest of international friends, who helped



me to relax, Arno & Agnieszka, Juraj & Miška, Ivan & Dadka & Zuzka, Barny & Rachel, Marcel & Raluca, Marcel & Janka, Milan & Eva, Milan, Miro, Tomáš, Jan, Jorge, Panos & Mihaela, Daniel & Delia, Chris & Danielle, Jannie & Lambèr & Ramona, Martijn, Tom & Shirley, etc.

Last but not least, many thanks to my family and friends back in Slovakia and especially to my wife, Lucka, you have always been a great support to me.

*Thank you, Hartelijk bedankt, Ďakujem!*  
*Matej*

Eindhoven, April 2008.

# Curriculum Vitae

---

- 23.5.1979 Born in Bratislava, Czechoslovakia.
- 1985–1997 Primary, secondary school in Bratislava, Slovakia.
- 1997–2003 Master's Degree under supervision of prof. L. Starek, Research topic: 'Solute Finite Element Model of Magnetic Bearings', Department of Technical Mechanics, Faculty of Mechanical Engineering, Slovak University of Technology in Bratislava, Slovakia.
- 2004–2008 PhD, under supervision of prof.dr.ir. J. S. H. M. Wismans, Research topic: 'Mechanical behaviour of brain tissue for injury prediction: characterisation and modelling', Department of Mechanical Engineering, Materials Technology Institute, Eindhoven University of Technology, The Netherlands.